Enhancing indoor location fingerprinting using channel state information

Luan Chen

le cnam

École Doctorale Informatique, Télécommunications et Électronique (EDITE)

Centre d'Études et De Recherche en Informatique et Communications (CEDRIC)

THÈSE DE DOCTORAT

présentée par : **Luan CHEN**

soutenue le : **15 Avril 2020**

pour obtenir le grade de : **Docteur du Conservatoire National des Arts et Métiers**

Discipline : **Génie Informatique, Automatique et Traitement du Signal**

Spécialité : **Radiocommunications**

Enhancing Indoor Location Fingerprinting using Channel State Information

THÈSE dirigée par

M. LE RUYET Didier — *Professeur des Universités, CNAM*

ET co-encadrée par

Mme. AHRIZ Iness — *Maître de conférences, CNAM*

RAPPORTEURS

M. BOYER Rémy — *Professeur des Universités, Université de Lille*
M. CANCES Jean-Pierre — *Professeur des Universités, Université de Limoges*

PRÉSIDENT DU JURY

M. DENBY Bruce — *Professeur des Universités, Sorbonne Université*

EXAMINATEURS

Mme. BAUDOIN Geneviève — *Professeur, ESIEE Paris*
Mme. SUN Hong — *Professeur, Université de Wuhan*

Acknowledgements

The whole journey of my Ph.D. study would not have been accomplished without the supports from lots of amazing people.

First and foremost, I would like to express my greatest gratitude to my thesis supervisors Prof. Didier Le Ruyet and Dr. Iness Ahriz. They have guided me throughout the research process, taught me how to frame problems and analyze them, inspired me to conquer all the tough challenges. Beyond this, Didier's unfailingly positive attitude and his excellent advice can always help me walk out of our meeting with a newfound vigor and enthusiasm for my coming works. In addition, Iness's ability to get to the heart of the issue incredibly facilitated my research and I really appreciate her thoughtful caring to my daily life in Paris. I have benefited tremendously from both relationships and fell extremely privileged to have worked with them in the past three years.

I am immensely grateful to my former supervisor Prof. Hong Sun. Without her recommendation, I would not have this opportunity to study in CNAM and finally obtain the doctoral degree. I also greatly appreciate Dr. Haijian Zhang's research guidance before my Ph.D. study in Wuhan University. Besides, Mr. Christophe Alexandre had done a great contribution in the hardware part of my thesis and I will be always thankful for that.

I thank my fellow lab mates Wafa Njima, Stanley Smith, Bastien Ligneul, Chaima Zammali, Xinying Cheng, Xiaotian Fu, Bruno Fontana da Silva, Yang Wu, Yi Yu, etc.. This wonderful experience we have shared in the lab will always be kept in my mind. I also cherish the enjoyable memories in Paris with my friends Gang Liu, Chenguang Liu

and Xiangli Yang.

Meanwhile, I would also like to send heartfelt thanks to my thesis jury members for their valuable and constructive suggestions, which further help to improve my research work towards perfection.

My graduate work was fully supported by the China Scholarship Council (CSC). I will bear in mind with enduring appreciations.

Last but not least, I thank my parents and my girlfriend Qian Zhang for their unconditional love and endless support at any time. Hereby, I wish all the beloved ones to enjoy a happy and healthy life in the years to come.

Abstract

The expeditious development of wireless communications and ubiquitous deployment of Wi-Fi systems indoors have nurtured considerable commercial and industrial indoor Location based Services (LBSs) in the field of Internet of Things (IoT). The most fundamental functionality is to pinpoint the location of the target via wireless devices. To this end, the pattern-matching based Location Fingerprinting (LF) stands out as a promising technique which can return the best-fitted location estimation among a set of geo-tagged Reference Points (RPs), enabling accurate position determination even in the complex multipath-rich environments. For the existing indoor LF solutions, most previous works appeal to the simple and easily-accessible Received Signal Strength (RSS) fingerprint as the indicator of Medium Access Control (MAC) layer's link quality. However, RSS suffers from dramatic performance degradation due to sophisticated environmental dynamics. In contrast, the fine-grained Physical (PHY) layer Channel State Information (CSI) characterizes the channel qualities on the level of multiple orthogonal subcarriers, thus capable of bringing richer location-specific information for indoor fingerprinting. Meanwhile, this intricate structure of CSI inevitably leads to an increased computational complexity for the practical localization implementation. In addition, the harsh indoor environment can also breed similar radio signatures among certain predefined reference points, which may be randomly distributed in the area of interest, thus mightily tampering the location mapping accuracy.

To work out these dilemmas, in this thesis, we design and implement two CSI-based indoor location fingerprinting systems, namely EntLoc and AngLoc. For EntLoc, a power-based tap filtering scheme is first proposed to remove the noisy component in raw CSI measurements. To capture the most informative statistical channel information while

maintaining the structural simplicity, we adopt the Autoregressive (AR) modeling based entropy of CSI amplitude as the location fingerprint to construct a robust offline radio map. In the online phase, we employ the succinct Manhattan distance as similarity metric and resort to the flexible kernel regression approach to accurately figure out the target's position. As an upgraded version of EntLoc, AngLoc system leverages the well-known Angle of Arrival (AoA) as an additional fingerprint, which can be accurately retrieved from CSI phase through an enhanced subspace based algorithm. This dedicated mechanism serves to further eliminate the error-prone RP candidates, thus fertilizing the opportunity to achieve the decimeter-level positioning accuracy. Specifically, apart from the AR entropy-based fingerprint generating for CSI amplitude in the offline phase, we also study some deep-rooted phase errors in the raw CSIs and utilize several phase calibration algorithms to mitigate them, which guarantees a reliable angular fingerprint estimation. In the online phase, by exploiting both CSI amplitude and phase information, a novel bivariate kernel regression scheme is proposed to precisely infer the target's location. Furthermore, the entire indoor experiments are conducted on the lightweight HummingBoard platform, which tremendously facilitates the time-consuming and labor-intensive fingerprinting implementation. Besides, the results from extensive indoor experiments validate the superior localization performance of our proposed systems over previous approaches.

Keywords: Indoor localization, channel state information, entropy, array signal processing, kernel regression.

Résumé

Le développement rapide des communications sans fil et le déploiement omniprésent des systèmes Wi-Fi ont nourri des services commerciaux et industriels de géolocalisation (LBS) dans le domaine de l'Internet des objets (IoT). La fonctionnalité la plus fondamentale consiste à localiser l'emplacement de la cible via des appareils sans fil. À cette fin, la localisation par empreinte radio (LF) basée sur la correspondance de motifs se distingue comme une technique prometteuse qui peut renvoyer l'estimation de l'emplacement la plus fine à partir d'un ensemble de points de référence (RP) géolocalisés, permettant une détermination précise de la position, même dans les environnement complexes riches en trajets multiples. Pour les solutions LF d'intérieur existantes, la plupart des travaux précédents font appel à l'empreinte RSS (Received Signal Strength) simple et facilement accessible comme indicateur de la qualité de liaison de la couche MAC (Medium Access Control). Cependant, RSS souffre d'une dégradation spectaculaire des performances due à une dynamique environnementale importante. L'information sur l'état du canal (CSI) de la couche physique indique la qualité du canal au niveau de plusieurs sous-porteuses orthogonales, donc capable d'apporter des informations spécifiques à l'emplacement plus riches pour les empreintes digitales en intérieur. Cette structure complexe de CSI conduit inévitablement à une complexité de calcul accrue pour la mise en œuvre pratique de la localisation. En outre, l'environnement intérieur hostile peut également générer des signatures radio similaires parmi certains points de référence prédéfinis, qui peuvent être distribués de manière aléatoire dans la zone d'intérêt, altérant ainsi la précision de la cartographie de localisation.

Pour résoudre ces dilemmes, dans cette thèse, nous concevons et mettons en œuvre

deux systèmes d'empreintes de localisation en intérieur basés sur CSI, à savoir EntLoc et AngLoc. Pour EntLoc, un schéma de filtrage des mesures basé sur la puissance est d'abord proposé pour supprimer la composante bruyante dans les mesures CSI brutes. Pour capturer les informations de canal statistique les plus informatives tout en partageant la simplicité structurelle du RSS, nous adoptons l'entropie basée sur la modélisation autorégressive (AR) de l'amplitude CSI comme empreinte de l'emplacement pour construire une carte radio hors ligne robuste. Dans la phase en ligne, nous utilisons la distance de Manhattan comme métrique de similarité et avons recouru au schéma de régression par noyaux pour déterminer avec précision la position de la cible. En tant que version améliorée d'EntLoc, le système AngLoc exploite l'angle d'arrivée bien connu (AoA) comme empreinte supplémentaire, qui peut être récupérée avec précision à partir de la phase CSI grâce à un algorithme par sous-espace. Ce mécanisme dédié sert à éliminer davantage les candidats RP sujets aux erreurs, permettant ainsi d'atteindre la précision au niveau du décimètre. Plus précisément, en plus de la génération d'empreintes digitales basée sur l'entropie AR pour l'amplitude CSI dans la phase hors ligne, nous étudions également certaines erreurs de phase profondément enracinées dans les CSI bruts et utilisons plusieurs algorithmes d'étalonnage de phase pour les atténuer et garantir une estimation d'empreinte angulaire fiable. Dans la phase en ligne, en exploitant à la fois les informations d'amplitude et de phase CSI, un nouveau schéma de régression par noyaux bivarié est proposé pour déduire précisément l'emplacement de la cible. En outre, toutes les expériences en intérieur sont menées sur la plate-forme légère HummingBoard, ce qui facilite considérablement la mise en œuvre des empreintes digitales chronophages et laborieuses. En outre, les résultats d'expériences montrent les meilleures performances de localisation de nos systèmes proposés par rapport aux approches précédentes.

Mots clés: Localisation indoor, informations des canaux, entropie, traitement du signal du réseau, régression par noyaux.

Résumé de la Thèse en Français

Chapitre 1: Introduction

Avec la prolifération à grande échelle des communications sans fil et de l'informatique omniprésente, le service basé sur la localisation (LBS) est devenu un catalyseur clé pour une myriade d'applications de pointe dans le domaine de l'Internet des objets (IoT). Malgré cela, le système mondial de navigation par satellite (GNSS) peut déjà offrir une localisation extérieure réussie et précise. Cependant, il souffre d'une dégradation spectaculaire des performances dans l'environnement intérieur complexe en raison du blocage des signaux satellites. Grâce à la disponibilité omniprésente et au déploiement à faible coût, la connaissance de la localisation intérieure basée sur le Wi-Fi se distingue comme l'une des solutions les plus attrayantes vis à vis des autres techniques de communication sans fil. Parmi les solutions émergentes pour le positionnement intérieur basé sur le Wi-Fi, l'empreinte digitale de localisation (LF) bénéficie d'un mécanisme de correspondance de modèle, qui comprend une phase de formation hors ligne et une phase d'estimation de localisation en ligne. Plus précisément, dans la phase hors ligne, les signatures sans fil sont collectées sur un ensemble de points de référence (RP) géolocalisés dans la zone d'intérêt pour construire la base de données d'empreintes digitales (carte radio par exemple). Pendant la phase en ligne, la signature mesurée à une position inconnue est associée à la carte radio hors ligne pour renvoyer l'estimation de l'emplacement la mieux adaptée.

Comparé à la puissance du signal reçu (RSS) qui souffre d'une dégradation spectaculaire des performances due à la décoloration par trajets multiples à petite échelle et à la

dynamique temporelle à l'intérieur, les informations d'état de canal (CSI) de couche PHY sont capables de caractériser le canal pour chaque paire d'antennes d'émission-réception au niveau de plusieurs sous-porteuses orthogonales. Ainsi, il peut servir de géo-signature préférable pour apporter des informations spécifiques à l'emplacement plus riche.

Dans cette thèse, nous proposons d'abord EntLoc, un système d'empreinte digitale de localisation probabiliste basé sur le Wi-Fi utilisant des informations d'amplitude CSI. Il recourt à la métrique entropique basée sur la modélisation autorégressive (AR), qui équivaut à une transformation directe à partir de la PDF d'origine des amplitudes CSI sous forme de densité spectrale de puissance (PSD). Grâce à des expériences approfondies menées dans des bancs d'essai réalistes, nous démontrons que notre métrique entropique AR proposée surpasse son empreinte digitale CSI ou RSS d'origine. Comment exploiter correctement les informations de phase CSI dans notre système d'empreintes digitales de localisation basé sur l'entropie reste ouvert.

Inspiré par les récents progrès du traitement du signal en réseau phasé, l'exploitation de l'AoA comme empreinte digitale supplémentaire nous permet de revisiter l'exploitation de la phase CSI avec un nouvel horizon. Étant donné qu'il peut exister des candidats RP distants dont les lectures AoA diffèrent beaucoup de celles de la cible en ligne, ces faux RP hors ligne peuvent être exclus pour affiner davantage la précision de la prise d'empreintes digitales de l'emplacement. Sur cette base, nous concevons plus avant AngLoc, un système de localisation intérieure probabiliste compatible AoA utilisant un appareil Wi-Fi standard. Toutes les expériences sont menées sur la plate-forme légère HummingBoard, ce qui facilite considérablement la mise en œuvre des empreintes digitales chronophages et laborieuses. Les résultats expérimentaux valident les performances supérieures de notre système proposé par rapport aux approches d'empreintes digitales de localisation précédentes.

Chapitre 2: Préliminaires

Dans ce chapitre, nous examinerons l'empreinte digitale du signal sans fil de base de cette thèse, c'est-à-dire les informations sur l'état des canaux.

Dans les systèmes de communication sans fil, le récepteur de signaux opère une estimation de canal grâce au mécanisme de sondage de canal. Plus précisément, pour le système IEEE 802.11n basé sur les paquets, l'émetteur envoie des séquences d'information, y compris la trame à haut débit (HT-LTF) dans le préambule. Une fois que le récepteur détecte la position de départ du premier HT-LTF, il commence à dériver immédiatement les informations sur l'état du canal. Plus précisément, CSI décrit les propriétés des canaux de la couche PHY dans le domaine fréquentiel et révèle les effets combinés de la propagation par trajets multiples du signal qui inclut l'atténuation d'amplitude et le décalage de phase. La réponse en fréquence du canal (CFR) est représentée par chaque entrée CSI. Il peut être exprimé par

$$H(f) = |H(f)|e^{j\angle H(f)} \tag{1}$$

ici $H(f)$ est la valeur complexe de CFR à la sous-porteuse avec une fréquence centrale de f. $|H(f)|$ et $\angle H(f)$ désignent respectivement son amplitude et sa phase. De plus, le domaine fréquentiel CFR se compose d'une réponse amplitude-fréquence et d'une réponse phase-fréquence, caractérisant l'évanouissement sélectif en fréquence provoqué par les phases constructives et destructrices dans l'environnement riche en trajets multiples. Il contient ainsi plus d'informations sur les canaux que la mesure RSS basée sur la puissance.

Chapitre 3: Empreinte radio de localisation basée sur l'entropie AR en utilisant l'amplitude CSI

Dans ce chapitre, nous proposons EntLoc, un système d'empreinte digitale de localisation intérieure basé sur CSI utilisant l'empreinte entropique AR structurellement simple et spatialement informative. La conception détaillée de la majeure partie d'EntLoc sera présentée. De plus, nous mettons en œuvre des expériences en intérieur approfondies et dédiées pour évaluer les performances du système proposé.

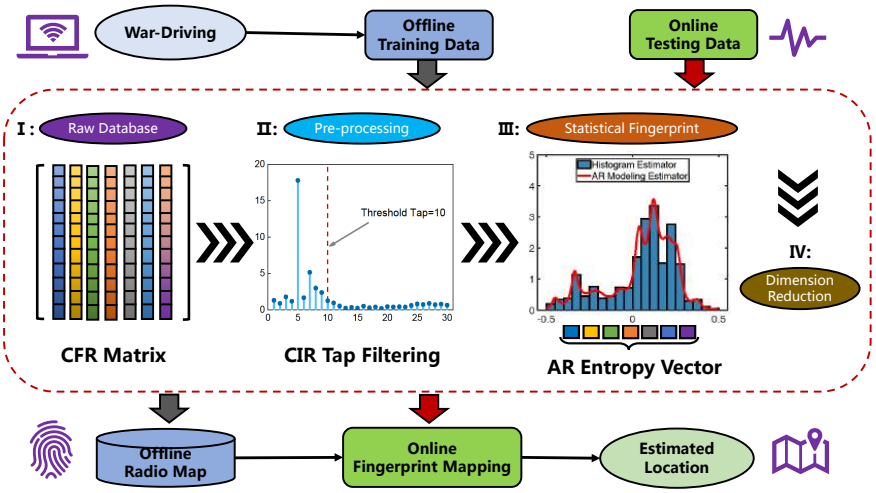

Figure 1: L'architecture du système EntLoc.

L'architecture du Système EntLoc

L'architecture globale du système proposé est illustrée sur la Figure 1. En général, il se compose de deux composants principaux: la construction de la carte radio des empreintes digitales hors ligne et l'estimation de la position de la cible en ligne. Pour la construction de la base de données d'empreintes digitales CSI, une fois que les paquets CFR bruts reçus ont été transmis on utilise d'abord un schéma de prétraitement basé sur le filtrage des données pour extraire les composants les plus informatifs et les plus dépendants de l'emplacement dans le scénario d'intérieur riche en trajets multiples. Par la suite, nous modélisons les caractéristiques statistiques de l'amplitude CFR filtrée en calculant une métrique entropique basée sur la modélisation AR, puis construisons une

carte radio d'empreintes digitales représentative après avoir supprimé les sous-porteuses ambiguës. Ensuite, pour le processus d'estimation d'emplacement en ligne, lorsqu'une cible mobile arrive dans la zone d'intérêt, elle exécute les mêmes procédures pour acquérir le vecteur d'entropie et les compare aux attributs hors ligne appris. Enfin, l'approche de régression du noyau basée sur la distance de Manhattan peut être pleinement exploitée pour accomplir l'estimation de la position physique de la cible mobile.

Dans ce qui suit, nous décrirons les empreintes digitales plus basées sur l'entropie générées dans le système EntLoc.

Estimation des empreintes digitales d'entropie AR

Rappelons que la métrique d'entropie est considérée comme une empreinte digitale de localisation souhaitée en raison de sa simplicité structurelle ainsi que de son mode de réalisation statistique d'informations riches spécifiques à la localisation. En réalité, il est impossible de dériver directement l'entropie de Shannon à partir de données réelles. La raison de ce dilemme est double: (i) Étant donné que le vrai PDF est normalement inconnu, l'approximation d'entropie n'est accessible qu'à partir des simples échantillons de données. (ii) Le calcul conventionnel de l'entropie de Shannon nécessite une intégration numérique lourde car il n'existe pas de substitut de forme fermée.

Pour relever les défis ci-dessus, dans cette thèse, nous proposons d'estimer avec précision l'entropie en s'appuyant sur l'approche de modélisation AR, dont le principe de base est d'estimer la PSD équivalente au PDF d'un processus AR de variance unitaire. Cette contrainte de variance unitaire est importée pour répondre aux exigences de base du PDF (c'est-à-dire une fonction positive unitaire). Plus précisément, nous définissons une notation générale de l'amplitude CSI β d'une sous-porteuse et l'ensemble des relations PDF-PSD est présenté par

$$p(\beta) = S_W(\beta) = \frac{\sigma_\epsilon^2}{\left|1 + \sum_{i=1}^{p} a_i e^{-j2\pi i\beta}\right|^2}, \beta \in [-0.5, 0.5] \tag{2}$$

ici $p(\beta)$ et $S_W(\beta)$ sont respectivement le PDF et le PSD d'amplitude β. L'ensemble de $\{a_i\}_{1\leq i\leq p}$ sont les coefficients AR d'un processus AR d'ordre p et σ_ϵ^2 est l'erreur de

prédiction du modèle qui est choisi de telle sorte que $\int_{-0.5}^{0.5} S_W(\beta)d\beta = 1$. Il est à noter que puisque la loi est modélisée comme la restriction du spectre sur l'intervalle de $[-0.5, +0.5]$, les données d'amplitude doivent d'abord être redimensionnées sur cet intervalle.

Pour résoudre l'équation (2), un ordre de modèle approprié p doit d'abord être choisi car un ordre faible conduit à une résolution inadéquate et un ordre élevé entraîne des pics parasites (variance excessive). Nous adoptons ainsi la technique de la famille exponentiellement intégrée (EEF) pour déterminer l'ordre du modèle AR en raison de ses performances supérieures grâce à nos expériences approfondies. Par la suite, les coefficients AR et son erreur de prédiction de modèle correspondante peuvent être estimés en résolvant les équations de Yule-Walker bien connues en utilisant la récursion de Levinson-Durbin. Une fois que l'AR PDF est déterminé à partir de (2), le calcul d'entropie peut alors être exprimé par la forme suivante:

$$\begin{aligned} \widehat{\phi}_\beta &= -\int_{-0.5}^{0.5} \widehat{p}(\beta) \log \widehat{p}(\beta) d\beta \\ &= -\int_{-0.5}^{0.5} \widehat{S}_W(\beta) \log \widehat{S}_W(\beta) d\beta \end{aligned} \tag{3}$$

En outre, en appliquant la formule de Plancherel-Parseval sur le côté droit de (3), une alternative de forme fermée réalisable sans aucune intégration numérique peut être obtenue comme

$$\widehat{\phi}_\beta = -\sum_{i=-\infty}^{\infty} R_W(i) Z_W^*(i) \tag{4}$$

ici $(\cdot)^*$ est l'opérateur conjugué et $Z_W(i)$ désigne la composante i^{th} du cepstrum du processus AR, qui peut être obtenue en appliquant l'IFFT à $\log \widehat{S}_W(\beta)$. $R_W(i)$ représente la fonction d'autocorrélation des données d'amplitude.

Résultats Expérimentaux

La figure 2 montre le plan d'étage du laboratoire de $15m \times 15m$ avec un couloir principal le long de plusieurs bureaux et salles de réunion. L'ordinateur portable HP servant d'émetteur de signal est fixé sur la table du bureau central. En mode injection, il est conçu pour transmettre par intermittence à raison de 100 paquets par seconde en utilisant une seule antenne d'émission. Il convient de mentionner qu'un réglage de l'émetteur est

hautement suffisant et bien exécuté dans ce scénario de laboratoire. Si nécessaire, nous pouvons recourir à plusieurs émetteurs pour le futur banc d'essai plus grand. Les points bleus représentés sur la Figure 2 désignent les 70 points de référence d'entraînement avec un espacement d'un mètre et les 30 emplacements de test sont marqués comme des étoiles rouges. Dans la phase de formation hors ligne, les mesures CSI sont collectées par le HMB léger à ces points de référence pour construire la carte radio brute. À chaque point, environ 5000 paquets CSI sont stockés sous forme de signatures RF dans le micrologiciel. Dans la phase en ligne, nous déplaçons ensuite le récepteur HMB parmi 30 emplacements de test pour obtenir la même taille de paquets CSI. De plus, toutes les extrémités du récepteur sont placées à la même hauteur, construisant une plate-forme 2-D simple pour l'estimation précise de la position intérieure.

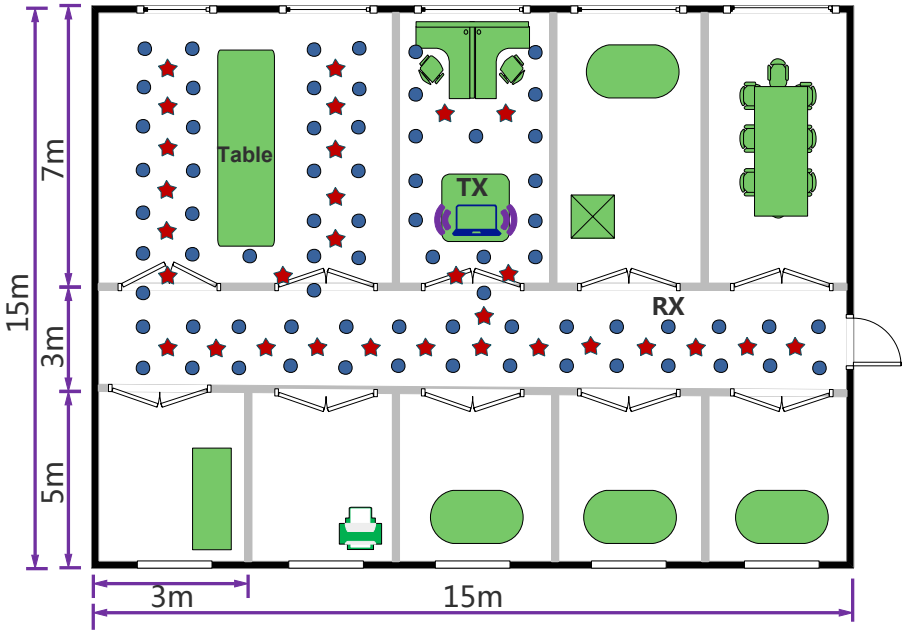

Figure 2: Le plan d'étage de notre laboratoire.

En termes de précision de localisation, notre système EntLoc est alors prêt à défier d'autres systèmes d'empreintes digitales de localisation existants. Plus spécifiquement, comme mentionné dans la section précédente, nous concevons un cadre équitable pour comparer notre approche de localisation basée sur l'entropie AR proposée avec les systèmes de type PinLoc, FIFS et Horus, respectivement. Comme on peut le voir dans la

Figure 3, notre système proposé atteint l'erreur au 90e centile de 2.69m, ce qui surpasse l'approche de type PinLoc, FIFS et Horus avec le même niveau d'erreur de 63%, 57% et 28%, respectivement.

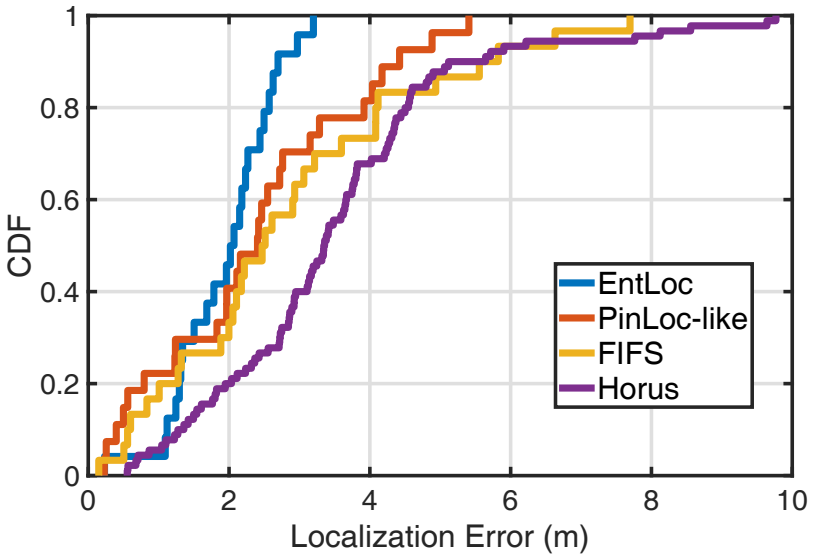

Figure 3: Précision de la localisation de l'EntLoc proposé par rapport à l'état de l'art.

Chapitre 4: Amélioration de la localisation d'empreintes radio assistée par AoA impliquant la phase CSI

Dans ce chapitre, nous présentons AngLoc, un système amélioré d'empreinte digitale de localisation intérieure basé sur l'entropie AR impliquant une empreinte AoA supplémentaire. La précision de localisation résultante a été améliorée par rapport à EntLoc.

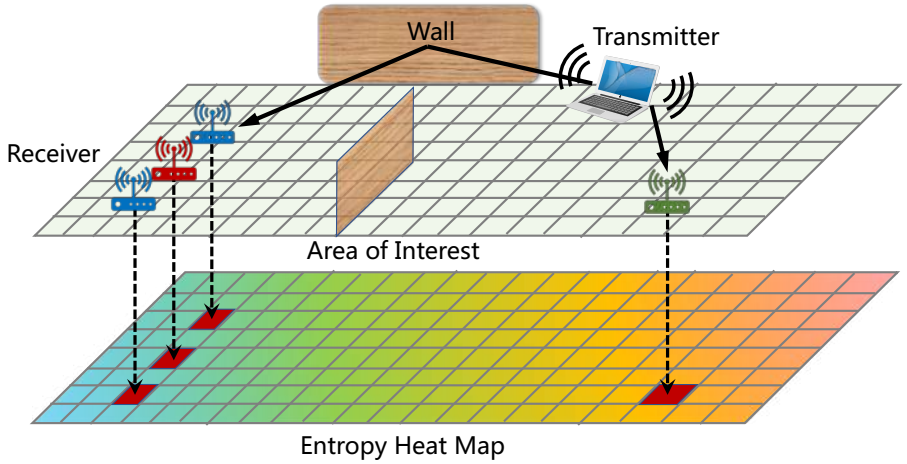

Figure 4: Un exemple illustratif du mécanisme du système AngLoc.

Avant d'énumérer les contributions de ce chapitre, en comparaison avec le système EntLoc susmentionné, nous élaborons d'abord le concept de base et la mise à niveau majeure de notre système de positionnement AngLoc proposé. Comme illustré dans la Figure 4, notre solution intégrée AoA adopte le concept méthodologique de la technique bien connue des k-voisins les plus proches (kNN) et dévoile deux informations heuristiques:

(i) Pour certains récepteurs de surveillance hors ligne aux positions RP correspondantes, qu'ils soient à proximité (en bleu) du récepteur en ligne (en rouge) ou à distance (en vert), leurs mesures CSI peuvent partager les mêmes valeurs d'entropie.

(ii) Ces récepteurs voisins enregistrent également les AoA similaires des chemins incidents parallèles avec ce récepteur en ligne, que ce soit pour les chemins directs dans le scénario LoS ou les chemins réfléchis dans la condition NLoS. Par conséquent, le récepteur distant peut être exclu de manière sélective conformément à la différence AoA distincte, ce qui améliore encore la précision d'estimation de l'emplacement.

En conséquence, en adoptant l'approche de raffinage RP assistée par AoA ci-dessus, notre système de positionnement AngLoc hérité est capable d'atteindre des performances de localisation supérieures à son système EntLoc prédécesseur.

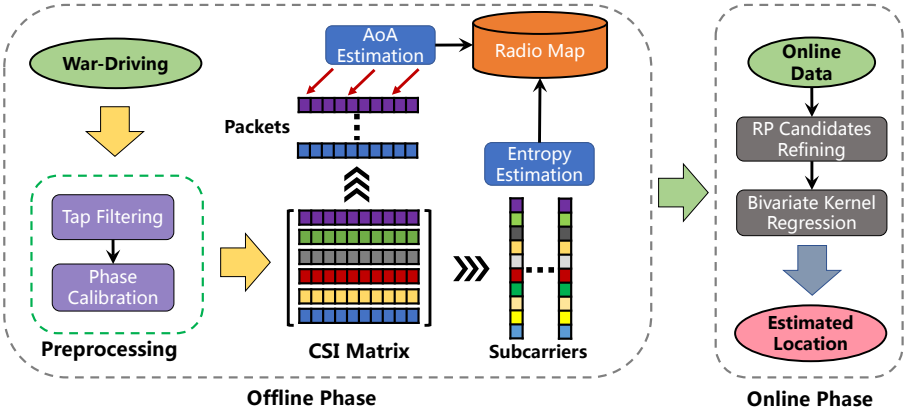

Figure 5: L'architecture globale du système AngLoc.

L'architecture du Système AngLoc

Comme illustré dans la Figure 5, l'architecture globale de notre système AngLoc proposé a une conception par blocs. Pour être précis, dans le bloc de construction de carte radio hors ligne, une fois que les mesures CSI brutes ont été enregistrées, nous introduisons d'abord un schéma de filtrage des données pour extraire le composant le plus informatif spécifique à l'emplacement des CSI bruyants. Dans le but d'une estimation précise de l'AoA, plusieurs techniques d'étalonnage de phase sont ensuite exploitées pour compenser les décalages de phase correspondants, qui existent dans les appareils WiFi courants. Par la suite, pour les amplitudes CSI, nous les modélisons statistiquement comme la métrique d'entropie AR simplement structurelle. L'algorithme JADE-MUSIC est ensuite adopté pour les phases CSI pour déduire les estimations angulaires. Par conséquent, l'intégralité de la base de données hors ligne peut être pleinement réalisée par l'intégration des empreintes entropiques et AoA, en utilisant pleinement les informations d'amplitude et de phase CSI. Pour le bloc d'estimation d'emplacement en ligne, lorsqu'une cible mobile entre dans la zone d'intérêt, elle exécute les mêmes protocoles de prétraitement pour obtenir les estimations d'entropie et d'AoA. La tâche d'estimation d'emplacement suivante comprend

alors deux étapes principales:

(i) Le vecteur d'entropie en ligne est d'abord associé à une base de données hors ligne pour trouver les candidats les plus probables parmi les postes RP les plus proches.

(ii) Parmi ces emplacements candidats, un nouveau schéma de régression par noyau bivarié est proposé pour réduire davantage le nombre de RP sujets aux erreurs, abordant ainsi la détermination de l'emplacement de la cible avec une précision améliorée.

Résultats Expérimentaux

La Figure 6 affiche le plan détaillé de la salle de classe utilisée pour les tests. Tout d'abord, l'ordinateur portable sert d'émetteur de signal dont le placement est fixé sur la table et connu a priori. En mode d'injection de paquets, il est conçu pour envoyer par intermittence à raison de 100 paquets par seconde en utilisant une seule antenne d'émission. Il est à noter qu'un tel réglage d'antenne répond à l'exigence d'une cartographie spatiale directe, qui peut produire des données CSI sans CSD. Pendant ce temps, la précision de localisation peut également être garantie avec le coût de calcul le plus bas. Pour la disposition expérimentale, les points bleus montrés sur la figure 6 indiquent les 40 emplacements RP d'entraînement avec un espacement d'un mètre et les 28 positions de test sont marquées comme des étoiles rouges. Pendant la phase de formation hors ligne, environ 5000 paquets CSI sont collectés et stockés par le HMB léger à chaque point de référence pour créer la carte radio CSI brute. Dans la phase en ligne, nous déplaçons ce récepteur HMB parmi tous les emplacements de test pour acquérir la même taille de paquets CSI à des fins de localisation. De plus, chaque extrémité du récepteur fonctionne à la même hauteur, construisant une plate-forme 2-D simple pour l'estimation précise de la position intérieure.

En vertu de la fonction de distribution cumulative (CDF), nous évaluons d'abord la précision de localisation de notre système AngLoc proposé par rapport à l'état de l'art. Comme on peut l'observer dans la Figure 7, pour l'environnement de laboratoire, notre

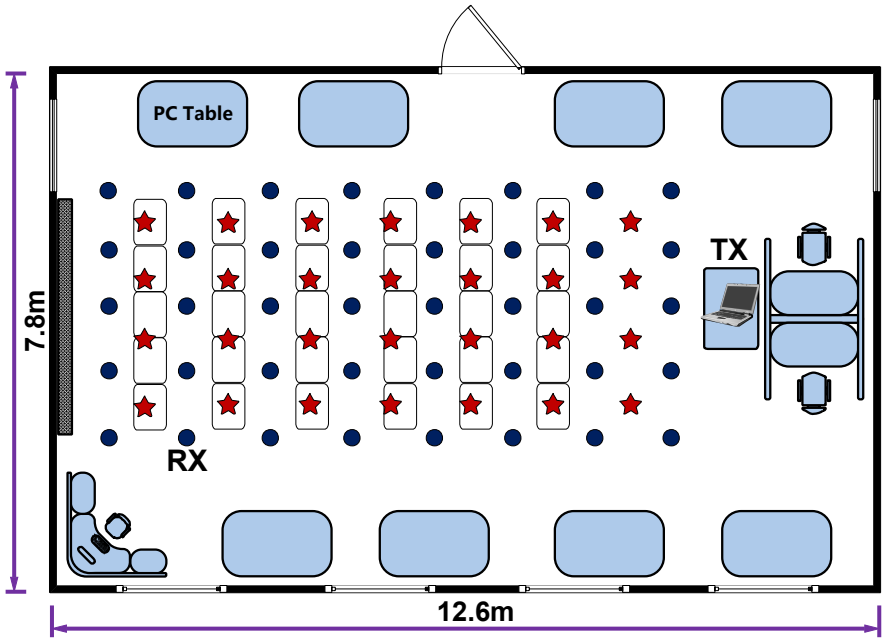

Figure 6: Le plan d'étage de notre salle de classe.

système proposé est capable d'atteindre l'erreur du 90e centile de 2.27 m, ce qui surpasse les systèmes EntLoc, PinLoc-like, FIFS et Horus avec la même erreur niveau de 2.69 m, 4.15 m, 5.56 m et 5.64 m, respectivement. De même, dans le scénario de la salle de classe, nous pouvons remarquer dans la Figure 8 que AngLoc précède toujours les autres rivaux en termes d'erreur du 90e centile. Concrètement, il peut garantir que 90% des emplacements de test ont une erreur de positionnement inférieure à 1.99 m, dépassant les systèmes EntLoc, PinLoc-like, FIFS et Horus avec le même pourcentage d'erreur de 82.1%, 64.3%, 57.1% et 28.6%, respectivement.

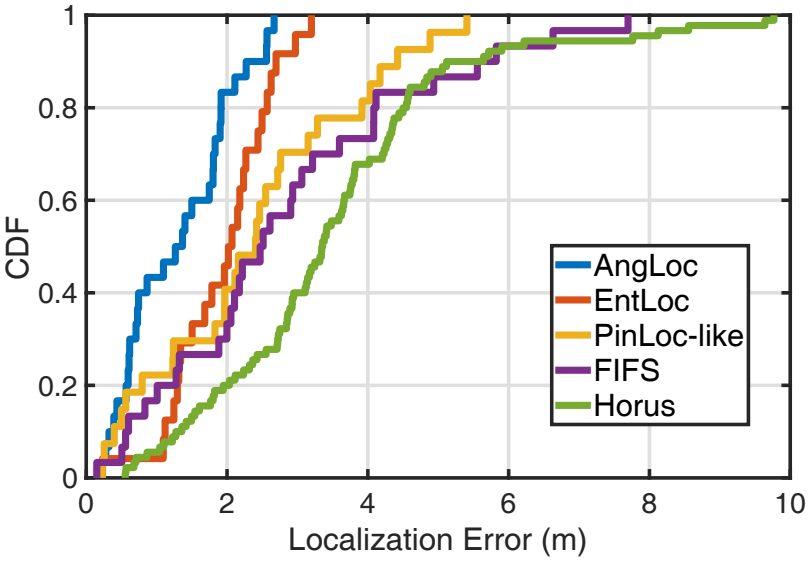

Figure 7: Précision de localisation pour le laboratoire.

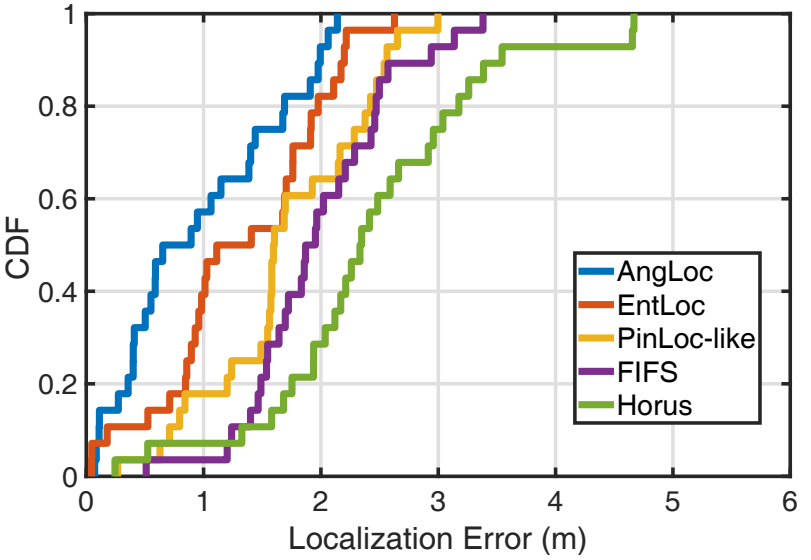

Figure 8: Précision de localisation pour la salle de classe.

Chapitre 5: Conclusion

Sur la base de la conception de systèmes d'empreintes digitales de localisation efficaces, nous résumons cette thèse dans ce qui suit.

Premièrement, en raison de la présence d'une limitation de la bande passante du canal et du bruit non intentionnel des appareils, nous concevons un schéma de filtrage des données basé sur la puissance pour atténuer largement le bruit de mesure CSI. De plus, nous nous penchons également sur certains problèmes d'erreur de phase CSI profondément enracinés et réussissons à tirer parti de plusieurs techniques d'étalonnage de phase pour acquérir des mesures CSI adéquates et fiables.

Deuxièmement, afin d'exploiter l'inférence probabiliste des propriétés complexes des canaux sans fil intérieurs, nous avons recours à la métrique d'entropie basée sur la modélisation AR, qui partage la simplicité structurelle avec RSS tout en exploitant les riches informations statistiques sur les canaux. Sur cette base, nous avons proposé EntLoc, un système de localisation d'empreintes digitales basé sur l'amplitude CSI utilisant un appareil Wi-Fi commercial.

Troisièmement, au-dessus du système de positionnement EntLoc, qui exploite uniquement les informations d'amplitude CSI, nous développons un prototype d'AngLoc, un système amélioré d'empreinte digitale de localisation impliquant des informations de phase CSI. Il est capable de libérer tous les potentiels liés à la localisation en utilisant des empreintes digitales supplémentaires basées sur l'AoA.

Enfin et surtout, tout au long de l'étude pratique du positionnement intérieur basé sur CSI, nous parvenons progressivement à développer la plate-forme d'acquisition de données CSI plus légère et réalisable basée sur le système embarqué HummingBoard Pro. Il facilite considérablement notre processus d'enquête sur les sites de localisation.

Table of Contents

List of Figures

List of Tables

Abbreviations

LBS	Location-Based Service
IoT	Internet of Things
GNSS	Global Navigation Satellite System
GPS	Global Positioning System
WLAN	Wireless Local Area Network
RFID	Radio Frequency Identification
UWB	Ultra Wideband
IPS	Indoor Positioning System
LF	Location Fingerprinting
ToF	Time of Flight
AoA	Angle of Arrival
LoS	Line-of-Sight
RP	Reference Point
RSS	Received Signal Strength
MAC	Medium Access Control
IEEE	Institute of Electrical and Electronics Engineers
MIMO	Multiple-Input Mulitiple-Output
OFDM	Orthogonal Frequency Division Multiplexing
NIC	Network Interface Card
CSI	Channel State Information
PDF	Probability Distribution Function

PSD	Power Spectral Density
JADE	Joint Angle and Delay Estimation
MUSIC	Multiple Signal Classification
FEC	Forward Error Correction
MCS	Modulation and Coding Scheme
QAM	Quadrature Amplitude Modulation
STBC	Space-Time Block Coding
CSD	Cyclic Shift Diversity
SMM	Spatial Mapping Matrix
IFFT	Inverse Fast Fourier Transform
DAC	Digital-to-Analog Converting
HT-LTF	High Throughput-Long Training Fields
CFR	Channel Frequency Response
CIR	Channel Impulse Response
kNN	k-Nearest Neighbors
KLD	Kullback-Leibler Divergence
MAP	Maximum A Posteriori
AP	Access Point
SNR	Signal-to-Noise Ratio
AWGN	Additive White Gaussian Noise
EEF	Exponentially Embedded Family
GLRT	Generalized Likelihood Ratio Test
RBF	Radial Basis Function
SFO	Sampling Frequency Offset
STO	Symbol Timing Offset
CFO	Carrier Frequency Offset
CPO	Carrier Phase Offset
PDP	Power Delay Profile
PLL	Phase Locked Loop

Symbols

$(\cdot)^\top$	The transpose operator
$(\cdot)^*$	The conjugate operator
$(\cdot)^H$	The Hermitian transpose operator
$\mathbb{E}\{\cdot\}$	The expectation operator
$\delta(\cdot)$	The Dirac delta function
$\|\cdot\|_1$	The ℓ_1 norm operator
$\circ$	The Hadamard product operator
$\otimes$	The Kronecker product operator
$\boldsymbol{\ell}_m$	The coordinates of the m^{th} RP
$\boldsymbol{\ell}_o$	The coordinates of the online unknown target
$\widehat{\boldsymbol{\ell}}_o$	The estimated coordinates of the online unknown target
N_{ss}	The number of spatial streams
N_{sts}	The number of space-time streams
N_t	The number of transmit antennas
N_r	The number of receive antennas
M	The number of reference points
S	The number of access points
K	The number of OFDM subcarriers of one CSI packet
R	The dimensionality of one CSI packet measured at one RP location from a single AP
N	The number of CSI packets
L	The number of multipaths

$\mathbf{H}_m^s$	The $N \times R$ dimensional CSI matrix which are acquired at the m^{th} RP from the s^{th} AP
$\boldsymbol{\mathcal{H}}_m$	The $N \times SR$ dimensional CSI signature set which are acquired at the m^{th} RP
$\mathbf{G}_o^s$	The $N \times R$ dimensional CSI matrix which are acquired at the target's unknown location from the s^{th} AP
$\boldsymbol{\mathcal{G}}_o$	The $N \times SR$ dimensional CSI signature set which are acquired at the target's unknown location
$\widehat{\boldsymbol{\Phi}}_{\mathbf{H}_m^s}$	The AR entropy vector of CSI amplitudes at the m^{th} RP from the s^{th} AP
$\widehat{\boldsymbol{\Phi}}_{\mathbf{G}_o^s}$	The AR entropy vector of CSI amplitudes at the target's unknown location from the s^{th} AP
$\widehat{\theta}_m^s$	The AoA estimate at the m^{th} RP location from the s^{th} AP
$\widehat{\tau}_m^s$	The ToF estimate at the m^{th} RP location from the s^{th} AP
$\widehat{\theta}_o^s$	The AoA estimate at the target's unknown location from the s^{th} AP
$\widehat{\tau}_o^s$	The ToF estimate at the target's unknown location from the s^{th} AP
$\mathcal{K}$	The probability kernel function
$\mathscr{D}_m$	The Manhattan distance of AR entropy between the online fingerprints at target's unknown location and the offline fingerprints at the m^{th} RP
$\mathcal{D}_m$	The Edclidean distance of AoA-ToF between the online fingerprints at target's unknown location and the offline fingerprints at the m^{th} RP
w_e	The weighting factor for AR entropy based kernel function
w_a	The weighting factor for AoA based kernel function
ρ_e	The AR entropy based kernel coefficient
ρ_a	The AoA based kernel coefficient

Chapter 1

Introduction

Contents

1.1 Motivation

With the wide-scale proliferation of wireless communication and ubiquitous computing, Location-Based Service (LBS) has emerged as a key enabler for myriad cutting-edge applications in the domain of Internet of Things (IoT) [1, 2, 3]. Examples of such widespread LBSs can be categorized into a number of groups. To name a few, for visually-impaired individuals, it is imperative for them to receive autonomous and accurate navigation services in the complicated surroundings. In the modern mega warehouse, by leveraging the logistic tracing and monitoring, staff can detect the goods and inventory in real time, which enormously facilitates the operation efficiency. The consumers in the fancy commercial mall usually desire the dedicated product information through the proximity-based marketing advertisements. For some sensitive facilities like banking systems, the topic of intruder tracking is also of great significance in order to guarantee a round-the-clock security level and so forth. Accordingly, in order to meet the pressing need of human social activities, the most fundamental common ground for these LBS applications is to precisely and effectively pinpoint the location of the target in a wireless manner.

To this end, the well-known Global Navigation Satellite System (GNSS) such as Global Positioning System (GPS) from the U.S. can already offer successful and accurate localization in the outdoor space. However, it suffers dramatic performance degradation in the complex indoor environment due to the blockage of satellite signals. Moreover, the location resolution demand for indoor positioning schemes is generally higher than that in the outdoor scenarios. Consequently, in addition to providing the seamless and ubiquitous location-aware services indoors, it brings us new challenges for designing indoor localization systems which are capable of covering the requirements of high accuracy, time-critical constraints and energy efficiency. As illustrated in Figure 1.1, we further present a wide variety of LBS applications from outdoor to indoor situations.

In light of the continuous mobile technique innovation and its hardware upgrading, accurate, reliable and ubiquitous indoor localization solutions have been extensively studied in recent years [4, 5, 6]. Such examples comprise not only well-known Wireless Local Area Network (WLAN) based technologies like Wi-Fi [7, 8, 9], Bluetooth [10], Radio Fre-

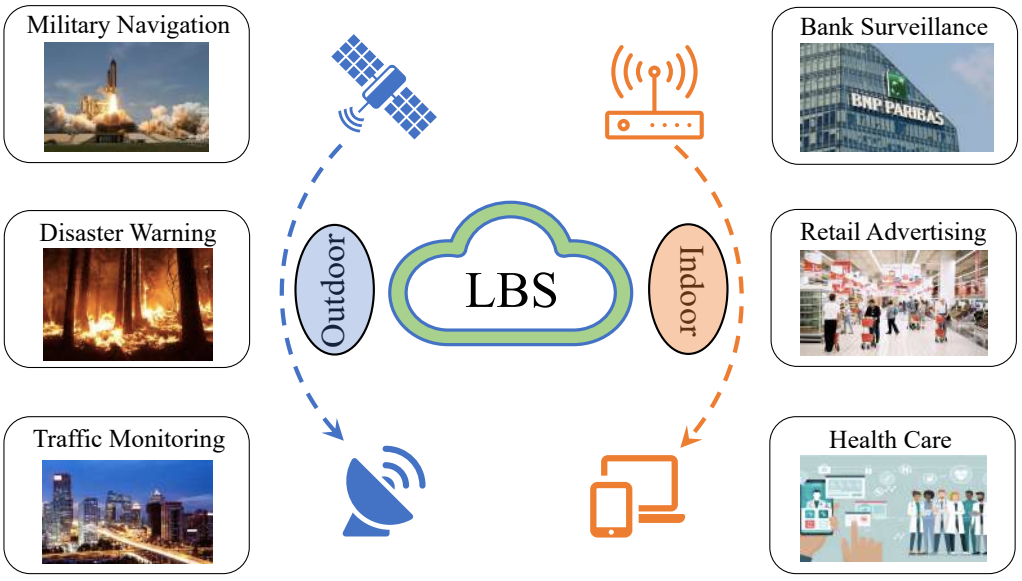

Figure 1.1: Different applications of location based services.

quency Identification (RFID) [11], Ultra Wideband (UWB) [12], but also some emerging areas such as infrared [13], visible light [14, 15], ultrasound [16], geomagnetic field [17] and so forth. Among these techniques, the Wi-Fi based positioning is probably of the greatest popularity, mainly owing to the pervasive availability of the high-throughput and low-cost Wi-Fi technology. Thereupon, indoor position determination can be then operated in Wi-Fi based communication systems through firmware upgrades and software implementations.

In general, conventional Wi-Fi based Indoor Positioning Systems (IPSs) either adopt geometric mapping approach or resort to the Location Fingerprinting (LF) [18]. For geometric mapping, intermediate spatial parameters like distance or direction are first derived from certain physical measurements. Typical parameters include Time of Flight (ToF) [19] and Angle of Arrival (AoA) [20]. Then, target's physical location can be further inferred by using geometric algorithms (e.g., trilateration or triangulation). Nevertheless, the performance of geometric mapping approach heavily relies on the Line-of-Sight (LoS) condition. In wireless communications, when a signal emitted from a transmitter is reflected or scattered by a scatterer, an attenuated copy of the original signal is generated and reaches the receiver through a different path. The phenomenon that a signal is received by two

or more paths is known as multipath propagation [21]. Figure 1.2 displays a typical indoor multipath propagation scenario. The rich indoor multipath and shadowing effects, to a great extent, blur the monotonous relation between physical measurements and distances, complicate RF propagation modeling, and thus degenerate positioning accuracy. This makes geometric mapping less eligible for the sophisticated indoor environment with rich hindrances and room partitions. As an emerging alternative for indoor positioning,

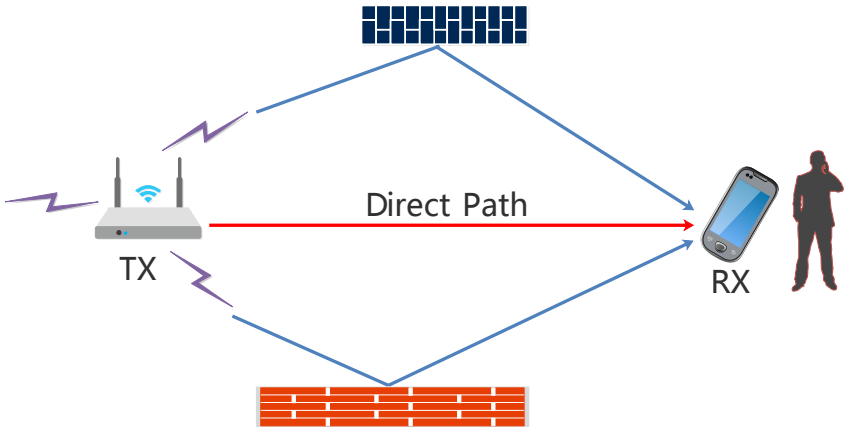

Figure 1.2: Diagram for typical indoor multipath propagation.

location fingerprinting benefits from a pattern-matching mechanism, which comprises offline training phase and online location estimation phase. Specifically, in the offline phase, wireless signatures are collected at a set of geo-tagged Reference Points (RPs) in the area of interest to construct the fingerprint database (a.k.a. radio map). During the online phase, the measured signature at an unknown position is matched with the offline radio map to return the best-fitted location estimation.

Although the mainstream Wi-Fi fingerprinting systems take the simple Received Signal Strength (RSS) as the indicator of Medium Access Control (MAC) layer's link quality, it suffers dramatic performance degradation due to small-scale multipath fading and temporal dynamics indoors. In Institute of Electrical and Electronics Engineers (IEEE) 802.11 n/ac standard, Wi-Fi networks use Multiple-Input Mulitiple-Output (MIMO) [22, 23] and Orthogonal Frequency Division Multiplexing (OFDM) [24] techniques to modulate data on different orthogonal sub-channels and transmit them over multiple transmit-receive

(TX-RX) antenna pairs simultaneously. Therefore, it can reflect the fine-grained channel feature known as channel response, which can be partially extracted from many commercial off-the-shelf Wi-Fi Network Interface Cards (NICs) [25, 26] in the format of Channel State Information (CSI). Specifically, CSI is aggregated by a set of channel estimations depicting the amplitude and phase information of each OFDM subcarrier. Different from coarse-grained RSS, the Physical (PHY) layer CSI measurement can serve as a preferable location signature characterized by the small-scale multipath fading, which significantly deteriorates the quality of its RSS counterpart. Furthermore, CSI indicates channel qualities in the level of multiple subcarriers and thus provides richer location-specific information than RSS-based localization schemes.

In principle, Wi-Fi fingerprinting algorithms can be categorized into deterministic and probabilistic ones [8]. Deterministic approaches enjoy the easy implementation but fail to fully exploit environmental fluctuations, which consequently renders the location estimation error-prone. In contrast, probabilistic methods embrace the channel variation by inferring a signal distribution based statistical model, thus obtaining more robust and accurate positioning performance than its deterministic adversary. Nevertheless, there still exists three underlying challenges for probabilistic Wi-Fi fingerprinting systems:

(i) The accurate approximation of Probability Distribution Function (PDF) is largely driven by massive storage of signal measurements [27], which in turn brings huge system burden and computational requirement.

(ii) Most probabilistic location-aware solutions are well established on the assumption of Gaussian-distributed measurements [28, 29]. However, due to the complex nature of indoor environment and the imperfection of wireless devices, some practical measurements appear to be non-Gaussian distributed or even do not fit any known distribution [30, 31, 32]. This then complicates the fingerprinting process and incurs severe ambiguity for location estimation.

(iii) When it comes to multivariate fingerprint structure (e.g. multi-subcarrier CSI), traditional probabilistic methods turn powerless since existing statistical tools only work for measurements with identifiable distributions [33].

Therefore, it would be highly desirable for a fingerprint which shares the simplicity of RSS (scalar) and meanwhile conserves rich statistical location-specific information.

To address the aforementioned substantial challenges, in this thesis, we first propose EntLoc [34], a Wi-Fi based probabilistic indoor location fingerprinting system using CSI amplitude information. It resorts to the Autoregressive (AR) modeling based Shannon entropy metric [35, 36], which equals a direct transformation from the original PDF of CSI amplitudes. Unlike traditional data-adaptive histogram estimator which entails a slow convergence rate, AR modeling approach provides a feasible parametric workaround to accurately infer the PDF in the form of Power Spectral Density (PSD) [37, 38]. Despite its structural simplicity, this novel entropy fingerprint embodies the whole statistical information of CSI amplitudes. Through extensive experiments conducted in realistic testbeds, we demonstrate that our proposed AR entropy metric outperforms its original CSI or RSS fingerprint [34]. However, since CSI phases of one subcarrier are generally uniformly distributed [39], this quantifies each RP location with an equally maximized entropy value (a.k.a. Gibbs' inequality [40]), thereby hampering the location distinction to a great extend. How to properly exploit CSI phase information in our entropy-based location fingerprinting system still remains open.

Inspired by the recent advancement of phased array signal processing [20], leveraging AoA as supplementary fingerprint enables us to revisit CSI phase exploitation with a fresh horizon. Given the fact that there may exist some remote RP candidates whose AoA readings differ a lot with those around the online target, these false offline RPs can be ruled out to further refine the location fingerprinting accuracy. On this basis, we design AngLoc [41], an AoA-aware probabilistic indoor localization system using commercial off-the-shelf Wi-Fi device. To remove the noisy component from the raw CSI measurements, we first introduce a power-based tap filtering scheme to preserve the most informative CSI signatures. For the purpose of precise AoA estimation, a set of phase calibration techniques are then employed to mitigate dramatic phase drifts. Subsequently, for the offline radio map construction, the pre-processed CSIs are simultaneously fed to two independent fingerprint generators, namely AR modeling based entropy estimator for CSI amplitude and the enhanced AoA-ToF estimator driven by Joint Angle and Delay Estimation (JADE)

Multiple Signal Classification (MUSIC) algorithm [42, 43, 44]. It is worth noting that ToF is utilized here to create measurable phase shift across subcarriers, by which realizes virtual antenna extension to overcome the antenna number restriction for classical MUSIC algorithm [20]. The other trick of ToF here is to identify the first incoming path (not necessarily the direct path) as the angular fingerprint benchmark, which serves to guarantee similar AoA recordings around closely-spaced RPs. Moreover, in the online phase, due to the simple structure of the radio map, the succinct Manhattan distance and Euclidean distance can be fully competent as the similarity metrics for AR entropy and AoA fingerprints, respectively. Afterwards, we propose an optimal bivariate kernel regression scheme to accurately infer the target's physical location. The entire experiments are conducted on the lightweight HummingBoard platform [45], which tremendously facilitates the time-consuming and labor-intensive fingerprinting implementation. Experimental results validate the superior performance of our proposed system over previous location fingerprinting approaches.

1.2 Contributions

In a nutshell, the major contributions of this thesis can be summarized and laid out below:

- The first contribution of this dissertation is that we design an AR entropy based indoor location fingerprinting system using fine-grained channel state information, namely EntLoc. As far as we are aware of, this is the first work to statistically study the AR modeling based entropy signature in CSI fingerprint localization system. This simple fingerprint structure helps decrease the pattern-matching complexity and its informative statistical embodiment also facilitates the location estimation accuracy.

- As an upgraded version of EntLoc, the pioneering AngLoc system is further proposed as the second main contribution of this thesis. Specifically, in AngLoc, we constructively incorporate the angular signature (AoA information) in CSI entropy based indoor location fingerprinting system, which manages to narrow down the

error-prone RP candidates and further improves the positioning accuracy. It even fertilizes the opportunity to achieve a decimeter-level localization precision in our indoor experimental testbed.

- Since the raw CSI measurements retrieved from commercial Wi-Fi NICs contain various noises, which may severely jeopardize the localization performance, such noises have to be first removed before proceeding to conduct the location fingerprinting process. Accordingly, we propose a power-based tap-filtering program alongwith several CSI phase calibration pre-processing techniques to effectively mitigate CSI noisy component and sanitize CSI phase errors, respectively.

- Recall that for the part of the aforementioned AngLoc system, we fully exploit both CSI amplitude and phase information to pinpoint the online target's physical position. The respective AR entropy and AoA information are designated as dual location fingerprints in AngLoc. On this basis, we design a feasible bivariate kernel regression scheme for the online location estimation stage, which organically combines the weighting factors for both amplitude based entropy and phase-based AoA fingerprints.

- Last but not least, in view of the cumbersome laboring process for the traditional offline fingerprint database construction, based on the Linux CSI tool with a modified firmware, we build and implement extensive experiments on the lightweight HummingBoard Pro device for different indoor testbeds. In addition to the superior localization performance, our mobile CSI receiver prototype remarkably enhances the location fingerprinting efficiency.

1.3 Structure of the Thesis

This thesis focuses on the problem of Wi-Fi based indoor fingerprint localization using channel state information. We successfully and effectively design the whole framework of two location fingerprinting systems which leverage the AR entropy and enhanced AoA estimates as their location signatures, achieving a superior localization performance over

the previous approaches. The remainder of this dissertation is organized as follows:

Chapter 2 reviews the overall technical background which is closely related to the domain of Wi-Fi based indoor localization. To be specific, we first introduce some Wi-Fi based physical measurements, which are extremely crucial to the localization performance, and discuss their respective strength and weakness in a comparative manner. Next, we dive into the two basic categories of the localization algorithms and present the relevant examples for both indoor location-aware techniques.

Chapter 3 lays out the in-depth structural presentation of our proposed EntLoc system. First of all, we investigate several representative literature reviews to reach an overview understanding for the state-of-the-art. The overall EntLoc system architecture is then given in the sequel. In the offline phase, we introduce the tap filtering pre-processing scheme and the detailed fingerprint generation process of the CSI amplitude based AR entropy. As for the online stage, the distance-based proximity comparison is carried out and then fed to the kernel regression algorithm to estimate the target's position. Subsequently, we evaluate the EntLoc's localization performance in comparison with the state-of-the-art. In addition, the impacts of some defining experimental factors are also discussed in this chapter.

Chapter 4 further proceeds to illustrate the updated design of the AngLoc system. Specifically, compared with aforementioned EntLoc system, there are three significant upgrades in the AngLoc system. Firstly, since the raw CSI measurements are full of phase errors and ineligible for the accurate AoA estimation, we employ a set of phase calibration techniques for the CSI pre-processing to effectively mitigate these phase offsets. Secondly, after acquiring the AR entropy fingerprint, we leverage an enhanced subspace based algorithm to estimate the AoA information, which serves as an additional fingerprint to further improve the location fingerprinting accuracy. Thirdly, in view of the AngLoc's dual-fingerprint structure, we propose a novel bivariate kernel regression scheme to precisely infer the final location. In addition to providing the experimental evaluations for AngLoc, we also discuss some unsolved issues which may further increase the efficiency and accuracy of our AngLoc system.

Chapter 5 draws the conclusions of this thesis by briefly reviewing our main contributions. Moreover, we highlight some potential research directions that can be further explored in our future works.

1.4 Related Publications

The content of this dissertation is mainly based on the following publications:

- **Luan Chen**, Iness Ahriz and Didier Le Ruyet. "AoA-aware Probabilistic Indoor Location Fingerprinting using Channel State Information", IEEE Internet of Things Journal, 2020. (IF: 9.515)
- **Luan Chen**, Iness Ahriz and Didier Le Ruyet. "CSI-based Probabilistic Indoor Position Determination: An Entropy Solution", IEEE Access, 2019. (IF: 4.098)
- **Luan Chen**, Iness Ahriz, Didier Le Ruyet and Hong Sun. "Probabilistic Indoor Position Determination via Channel Impulse Response", in Proceedings of the 29th Annual IEEE International Symposium on Personal, Indoor, and Mobile Radio Communications (PIMRC), 2018.
- **Luan Chen**, Iness Ahriz, Hong Sun and Didier Le Ruyet. "Source Position Estimation via Subspace based Joint Sparse Recovery", in Proceedings of the 13th IEEE International Conference on Signal Processing (ICSP), 2016.

Chapter 2

Technical Background

Contents

2.1 Introduction

In this chapter, we will review some technical backgrounds of Wi-Fi based indoor localization, whose methodological concepts are widely covered throughout this dissertation. Since the radio measurement lays the firm foundation for a decent wireless positioning system, we first study some typical WLAN measurements according to the wireless signal characteristics, such as signal transmission power decay, transmission time delay, transceiver spatial relations and the channel properties, etc.. Both the advantages and weaknesses for each signal measurement will be also discussed in particular.

In addition, by focusing on the Wi-Fi based indoor position determination, we will elucidate the principle of two conventional wireless localization algorithms, i.e., the geometric mapping approach and the location fingerprinting method. Some well-known localization methodologies for both algorithms will be also introduced, respectively.

2.2 Wi-Fi based Physical Measurements

For Wi-Fi based indoor location-aware solutions, acquiring an appropriate kind of physical measurement is of great importance for the accurate indoor position determination. There are many factors or properties which need to be considered when it comes to determine a good candidate. Such properties include the signal accessibility, the structure complexity, location dependency, power consumption and the robustness against environmental dynamics, etc.. In this section, we will present some popular physical measurements in the domain of indoor localization and compare them on the basis of these signal properties.

2.2.1 Power based Measurement

Signal power is widely used in both geometric mapping (especially in ranging) and location fingerprinting due to its handy accessibility from myriad commercial off-the-shelf wireless devices. Particularly, the MAC layer power signature, namely RSS, is one of the most prevalent power features, which attracts extensive popularities in the wireless

techniques ranging from UWB, ZigBee [46], Wi-Fi to cellular networks [47].

In order to conduct indoor location determination, the intermediate power measurement is closely related to signal transmission distance due to the wireless signal's natural attenuation over physical distance. Therefore, a proper pass loss model should be first determined for the purpose of accurate indoor positioning. Consider a signal transmitted through free space to a receiver located at distance d from the transmitter. Assume there are no obstructions between the transmitter and receiver and the signal propagates along a straight line between the two. The simplest free-space power-distance relationship can be characterized as [48]

$$P_r = \frac{P_t G_t G_r \lambda^2}{(4\pi d)^n} \tag{2.1}$$

where P_r and P_t are the received and transmitted signal power, respectively. G_r and G_t denote the antenna gains at the receiver and transmitter, respectively. λ is the wavelength of the transmitted signal and n is the environmental attenuation factor.

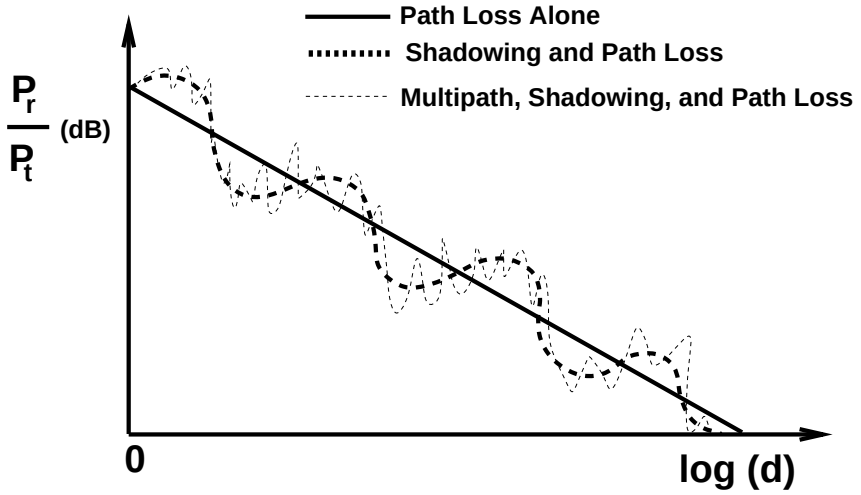

Figure 2.1: Path loss, shadowing and multipath versus distance [49].

Nevertheless, the practical wireless radio channel poses a severe challenge as a medium for reliable high-speed communication. It is not only susceptible to noise, interference, and other channel impediments, but these impediments change over time in an unpredictable

manner due to user movement. As shown in Figure 2.1, the combined effects of path loss, shadowing and multipath contribute to significant variations of the ratio between the received power P_r and the transmitted power P_t in dB with regard to distance d in logarithm. Hence, when coping with power-based ranging, RSS can be mapped into the distance from the transmitter by a more realistic and prevalent path loss model, which is known as the Log-normal Distance Path Loss (LDPL) model [50]

$$PL(d)[dB] = \overline{PL\,(d_0)} + 10n \lg\left(\frac{d}{d_0}\right) + X_\sigma \tag{2.2}$$

where $PL(d)$ denotes the measured path loss at distance d. $\overline{PL(d_0)}$ is the average path loss at reference point d_0 and n is the path loss exponent. X_σ is a zero-mean normal random variable reflecting the attenuation in decibel caused by shadowing.

In conclusion, RSS benefits well from its easy accessibility and low-cost deployment. However, the main drawback of RSS lies in its temporal fluctuations in complex indoor environments, making it a volatile and coarse-grained feature. The multipath-rich indoor environment complicates the wireless propagation and derails RSS-based ranging technique. Thus, more accurate power-based ranging then requires better characterizing and modeling of the small-scale multipath effects [51].

2.2.2 Temporal Measurement

The typical time features extracted from wireless signals include Time Of Arrival (TOA) and Time Difference Of Arrival (TDOA). Similar with RSS, they are commonly employed in the distance based ranging. In general, time-based ranging is impressively accurate under LoS condition. Unlike power-based schemes, the accuracy of time-based ranging improves with signal bandwidth. The UWB radio therefore enjoys sheer prevalence due to its high time resolution and extremely large bandwidth [52].

Specifically, for the TOA ranging technique, also known as Time of Flight (ToF) estimation method, the distance between two nodes is obtained by measuring the propagation time of the RF signal and then multiplying it with the speed of the electromagnetic waves, i.e., the speed of light $c = 3 \times 10^8 m/s$. The TOA technique measures the transmitting

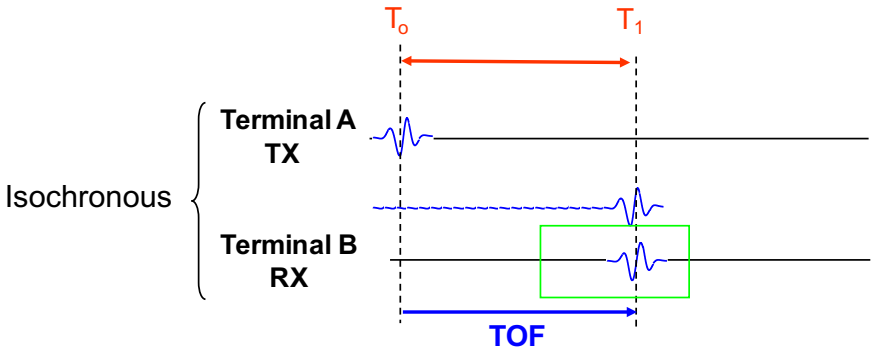

Figure 2.2: The diagram of the TOA technique.

time from transmitter to the receiver by following the procedure depicted in Figure 2.2. Terminal A sends to terminal B a ranging message at time T_0 and it includes the time stamp T_0 in this message. Terminal B then receives the message at time T_1 and estimates the propagation time as $TOF = T_1 - T_0$.

For the TDOA based method, it is typically employed when some anchor nodes are synchronized among them to a common clock while the mobile node, whose position is unknown, is not synchronized with the anchors. In particular, this scheme consists of measuring the difference of ToF between the mobile node with respect to two anchors. Figure 2.3 shows the procedure related to the TDOA method. At time T_0, the mobile

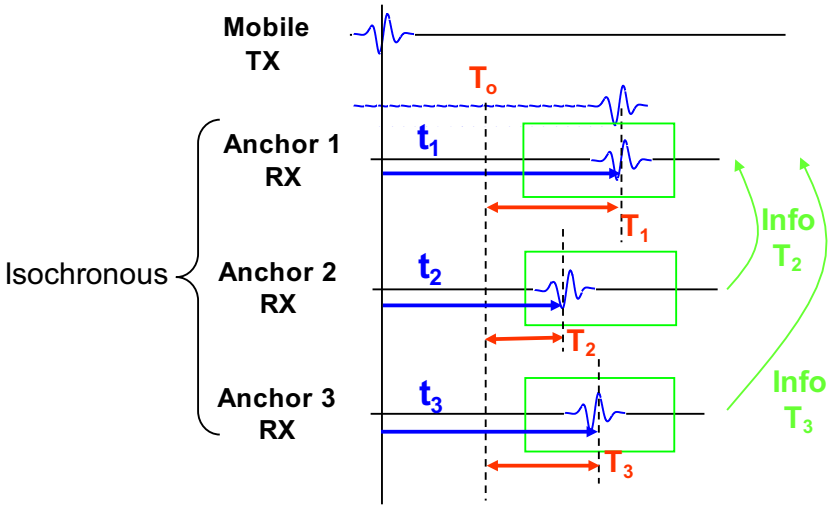

Figure 2.3: The diagram of the TDOA technique.

node broadcasts a ranging message. Since the mobile node is not synchronized with the anchors' clock, the anchors do not know the exact sending time. However, the anchor nodes are able to use the corresponding arrival times (T_1, T_2 and T_3) and calculate the TOA (t_1, t_2, t_3) with respect to an initial time that is different from T_0. Next, the TDOA can be calculated as $t_{12} = t_1 - t_2$ and $t_{23} = t_2 - t_3$. Finally, given the two independent TDOA estimations, the location of the mobile node is calculated as the intersection of two hyperbolas with foci at the three anchor nodes.

To summarize, a striking advantage of time based wireless technique lies in its superior ranging accuracy. But the greatest weakness of this method is that it requires an accurate time synchronization, either between the transmitter and receiver for TOA or among the anchor nodes for TDOA. For example, just a synchronization error of 10 ns will lead to a ranging error of around 3 meters.

2.2.3 Angular Measurement

Angular information provides an orthogonal dimension with regard to the distance for geometric mapping. Angle can be combined with distance estimates to enable single-anchored localization. In comparison with distance based estimation, the cost of angle measurements is generally higher. Technically, angle-based techniques estimate the position of a mobile node by measuring the Angle of Arrival (AoA) of signals arriving at the measuring node. With perfect physical measurements, the positioning problem can be geometrically solved by finding the intersection of a number of straight lines representing the signal AoAs (e.g. triangulation). In 2-D scenarios, two AoA recordings are just sufficient.

To this end, directional antennas are often capable of obtaining both angle and distance estimates while avoiding interferences from other directions, yet at the cost of dedicated infrastructure. Recently, antenna arrays have also attracted increasing interests with the rapid development of MIMO technology [22], which sets a handy path to achieve a desired AoA estimation performance. However, the environmental noise, the limited number of array antennas and the small-scale multipath propagation might drastically impact the accuracy of the final position estimation. In the later part of this thesis, we will explore the

problem of accurate AoA estimation in Chapter 4 and provide some insightful discussions for our future work.

2.2.4 Channel Response based Measurement

Recall that RSS is merely an indicator of the MAC layer' link quality, it suffers from severe variation due to the constructive and destructive superposition of multipath signal components. On the contrary, the finer-grained PHY layer channel response based measurements characterize the channel properties and embrace the channel diversity, thus providing richer location-dependent information and achieving superior localization performance over its RSS counterpart. In this section, we begin with the introduction of MIMO-OFDM mechanism and then elaborate the technical background of the PHY layer channel state information.

2.2.4.1 MIMO-OFDM Mechanism

In general, without properly compensating for the wireless signal propagation and the asynchronization effects, the receiver has no way of detecting what has been transmitted [19]. To this end, through a mechanism named *channel sounding*, the receiver obtains an estimate of wireless channel. This is accomplished by sending a training sequence which is known to both transmitter and receiver. For a wideband MIMO-OFDM system, the estimate of the channel is a collection of complex matrices for each OFDM subcarrier. In this part, we present the detailed mechanism of this MIMO-OFDM technology under the framework of IEEE 802.11 n/ac standard [53, 54].

Figure 2.4 depicts the holistic structure of the end-to-end MIMO-OFDM wireless transceiver. It consists of two major functionality blocks: signal transmitter block and RF receiver block. In the transmitter block, the scrambler and Forward Error Correction (FEC) encoder first convert the input data into high-rate bit stream(s). The stream parser is then applied on bit stream(s) to generate N_{ss} spatial streams, whose number is determined by the parameter of Modulation and Coding Scheme (MCS). After interleaving and constellation mapping (e.g. Quadrature Amplitude Modulation (QAM)), N_{ss} spatial

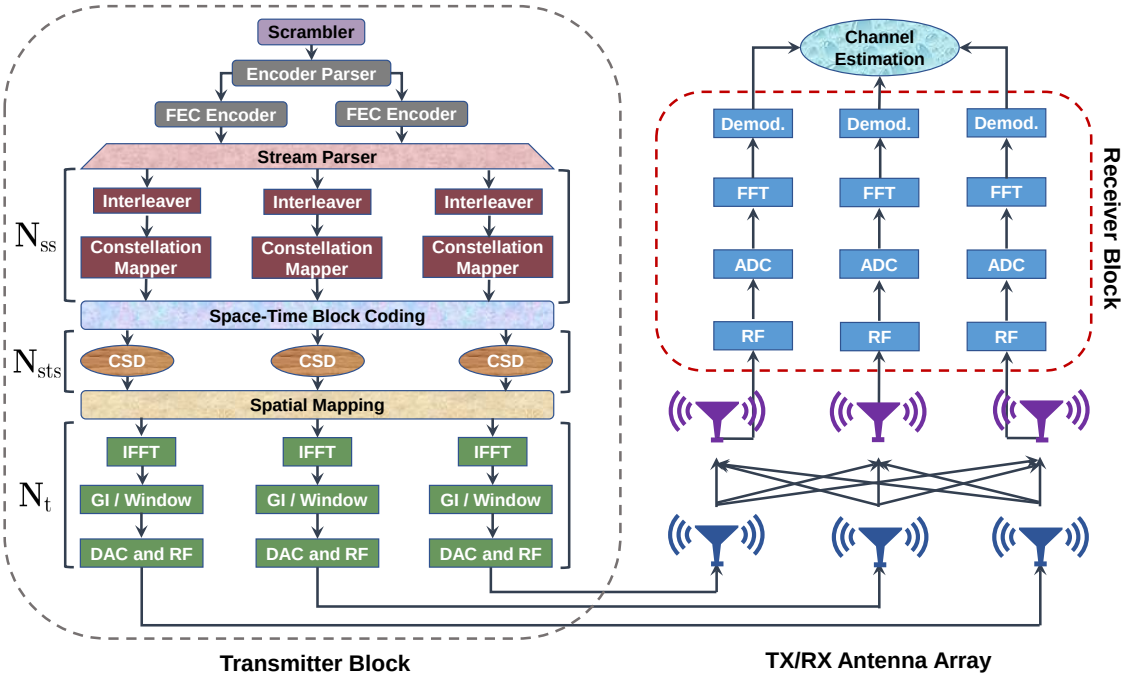

Figure 2.4: MIMO-OFDM transceiver architecture.

streams are modulated as stream of symbols, which may be spread into N_{sts} space-time streams in the sequel when Space-Time Block Coding (STBC) is used. Next, a mechanism named Cyclic Shift Diversity (CSD) is applied to insert cyclic shifts into space-time streams, thus creating extra frequency diversity to avoid unintentional beamforming. Spatial mapping then proceeds to map fewer number of N_{sts} space-time streams into larger number of N_t transmit chains through Spatial Mapping Matrix (SMM). Afterwards, the frequency domain samples are converted into time domain ones by the Inverse Fast Fourier Transform (IFFT). The RF signals are then simultaneously sent from all transmit antennas after the insertion of guard interval (GI), windowing operation and Digital-to-Analog Converting (DAC).

In reverse, upon receiving the signals, the receiver block first samples them and digitizes them through analog-to-digital converters (ADCs). Subsequently, a forward FFT procedure is conducted to convert the data samples back to the frequency domain. The desired channel estimation then becomes achievable after the signal demodulation process.

2.2.4.2 Channel State Information

In wireless communication systems, the signal receiver operates channel estimation by virtue of channel sounding mechanism. Specifically, for the packet-based IEEE 802.11n system, the transmitter sends training sequences, including High Throughput-Long Training Fields (HT-LTF) in the preamble. Once receiver detects the starting position of the first HT-LTF, it commences to derive channel state information immediately. As aforementioned in Chapter 1, CSI portrays the PHY layer channel properties in the frequency domain and reveals the combined effects of signal multipath propagation which includes the amplitude attenuation and phase shift. The Channel Frequency Response (CFR) is represented by each CSI entry. It can be expressed by

$$H(f) = |H(f)|e^{j\angle H(f)} \tag{2.3}$$

where $H(f)$ is the complex value of CFR at the subcarrier with central frequency of f. $|H(f)|$ and $\angle H(f)$ denote its amplitude and phase, respectively. Moreover, the frequency domain CFR consists of amplitude-frequency response and phase-frequency response, characterizing the frequency-selective fading caused by the constructive and destructive phases in the multipath-rich environment [18]. It thus contains more channel information than the power based RSS measurement.

Additionally, in order to fully characterize the indoor multipaths, the time domain counterpart of CFR, also termed as Channel Impulse Response (CIR), is able to model the wireless propagation channel as a temporal linear filter. Mathematically, it can be denoted as

$$h(\tau) = \sum_{i=1}^{L} \alpha_i e^{-j\varphi_i} \delta(\tau - \tau_i) \tag{2.4}$$

where α_i, φ_i and τ_i are the amplitude, phase and time delay spread of the i^{th} path, respectively. L is the total number of multipaths and $\delta(\cdot)$ is the Dirac delta function. Each impulse represents a delayed multipath component, multiplied by the corresponding amplitude and phase. As depicted in Figure 2.5, by focusing on the amplitude response of CIR, the first appearing path normally represents the LoS direct path, which is followed by several resolvable time delayed NLoS paths.

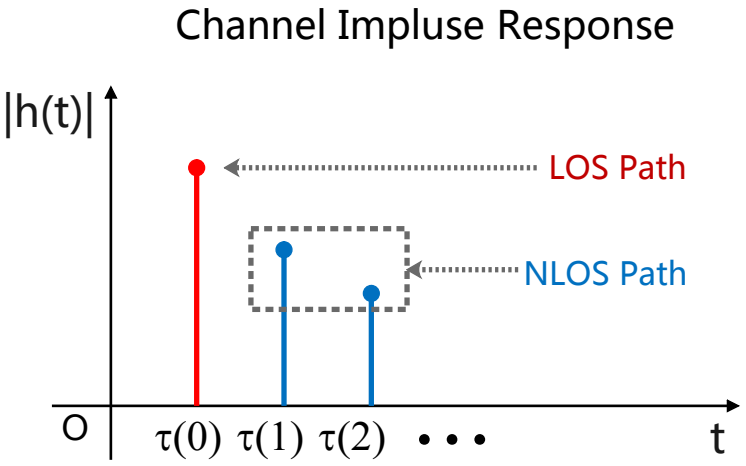

Figure 2.5: A simple diagram of the channel impulse response.

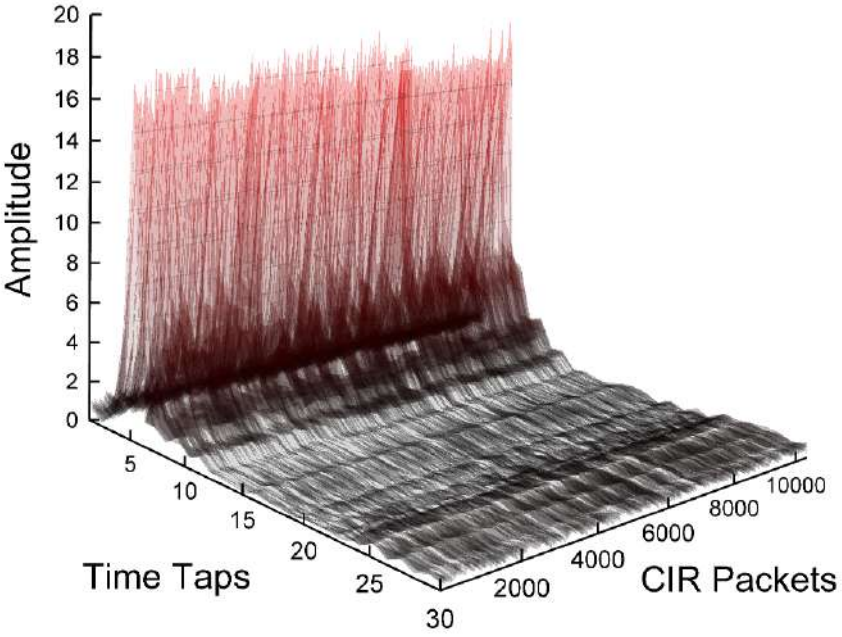

Figure 2.6: An example of CIR time samples with 20 MHz bandwidth

Given infinite bandwidth, CIR is equivalent to CFR. And CFR is the Fourier transform of CIR. Both CIR and CFR depict the small-scale multipath effect and are also widely used for channel measurement. In practice, it is worth mentioning that, all of our experiments are implemented on the basis of Linux CSI tool [25], whose off-the-shelf Intel 5300 network interface card reports 30 out of 56 OFDM subcarriers for the 20 MHz bandwidth CFR. After applying IFFT on the recorded CFR, we can acquire the time domain CIR with an equivalent number of 30 channel filter taps. As further observed in Figure 2.6, we display an example of 100 CIR time samples with 20 MHz bandwidth in the LoS dominant indoor scenario. Similar with Figure 2.5, the front CIR time taps appear with stronger amplitudes than their tail taps, revealing the distinct indoor multipath propagation of wireless signals.

2.3 Wi-Fi based Localization Algorithms

The previous section discussed some commonly adopted Wi-Fi signal patterns, which settle the precondition for accurate Wi-Fi based indoor position determination. In this section, we proceed to lay out the concepts of some popular Wi-Fi based localization algorithms. Since the traditional Wi-Fi based positioning approaches can be classified into two categories: geometric mapping and location fingerprinting. We then roll out this section by presenting these two parts respectively.

2.3.1 Geometric Mapping

In geometric mapping, intermediate geometric parameters such as distance or direction with regard to the reference points are first derived from certain physical measurements. These relative parameters are then converted into locations by applying geometric algorithms. There are generally two sorts of geometric mapping methods, namely trilateration and triangulation. The former one corresponding to the distance-based mapping, in particular, is often termed as ranging, which involves power or time based physical measurements. The latter one is related to direction-based mapping, whose angular measurement is less popular than the ranging technique due to its cumbersome acquisition from pervasive devices. However, direction information is directly measurable at the receiver, while

the derivation of distance involves the complex wireless propagation rules.

In this part, we will briefly introduce the typical trilateration and triangulation algorithms as follows.

2.3.1.1 Trilateration

Trilateration is the process of determining absolute or relative locations of points by measurement of distances, using the geometry of the environment. In addition to its interest as a geometric problem, trilateration has practical applications in surveying and navigation, including global positioning systems [55]. For the conciseness of presentation, we model the trilateration process as finding the position of an unknown node based on its distances to three anchors. As shown in Figure. 2.7, assume that the coordinate of an unknown node D is (x, y). The coordinates of three anchor nodes A, B, C are (x_a, y_a), (x_b, y_b) and (x_c, y_c), respectively. The distances between D and A, B, C are d_a, d_b and d_c.

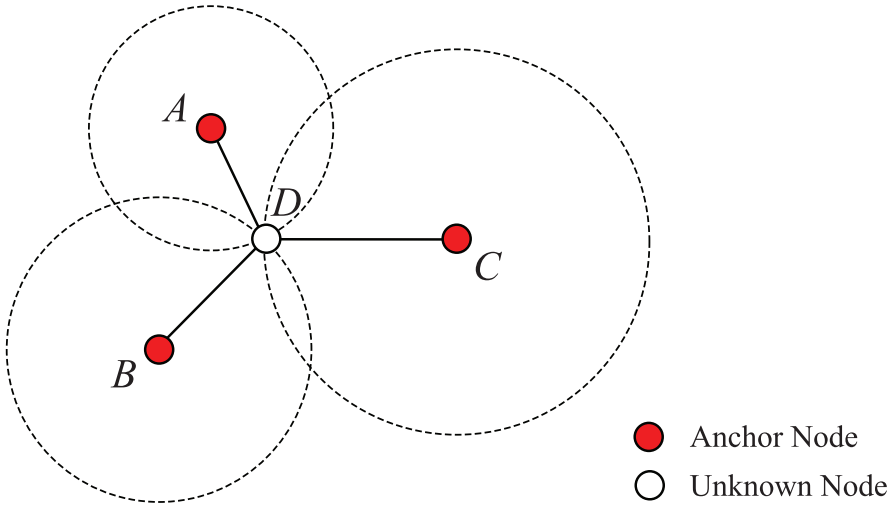

Figure 2.7: An example of the trilateration algorithm [56].

These geometric constraints can be expressed by the following equations.

$$\begin{cases} \sqrt{(x-x_a)^2+(y-y_a)^2} = d_a \\ \sqrt{(x-x_b)^2+(y-y_b)^2} = d_b \\ \sqrt{(x-x_c)^2+(y-y_c)^2} = d_c \end{cases} \tag{2.5}$$

By solving Equation 2.5, we can get the matrix $AX = B$ [57], where

$$
\begin{aligned}
X &= \begin{bmatrix} x & y \end{bmatrix}^T \\
A &= 2 \begin{bmatrix} (x_a - x_c) & (y_a - y_c) \\ (x_b - x_c) & (y_b - y_c) \end{bmatrix} \\
B &= \begin{bmatrix} x_a^2 - x_c^2 + y_a^2 - y_c^2 + d_c^2 - d_a^2 \\ x_b^2 - x_c^2 + y_b^2 - y_c^2 + d_c^2 - d_b^2 \end{bmatrix}
\end{aligned} \tag{2.6}
$$

Thus, the trilateration approach can be accomplished by solving the above liner equation to estimate the coordinate of the unknown node D.

Even though the basic trilateration can be easily implemented and is able to acquire accurate estimations under most conditions, in practice, due to the complex indoor environmental dynamics and the asynchrony of commercial wireless devices, it inevitably suffers a lot from aforementioned power and time based distance miscalculations.

2.3.1.2 Triangulation

Triangulation, unlike trilateration, computes the position of an unknown node based on the angular distance between three different pairs of anchor nodes. Consider the example depicted in Figure 2.8, suppose that the coordinate of an unknown node D is (x, y). The coordinates of three anchor nodes A, B, C are (x_a, y_a), (x_b, y_b) and (x_c, y_c), respectively. If we know the angles between the line segments connecting D and the anchors, then the unknown node's coordinates must be calculated using triangulation instead of trilateration.

Let $\angle ADB$, $\angle ADC$, $\angle BDC$ denote the angles between the line segments connecting D to the anchors, respectively. D is the intersection point of the three circles. If the angular distance between the anchor nodes is known, the centers of the circles can be obtained. For anchor nodes A, C and the angle $\angle ADC$, if the arc AC is within the scope of the $\triangle ABC$, the circle can be uniquely identified. Assume that the center of the circle is $O_1(x_{O_1}, y_{O_1})$, the radius is r_1, thus, $\angle AO_1C = 2(\pi - \angle ADC)$. O_1 and r_1 can be computed

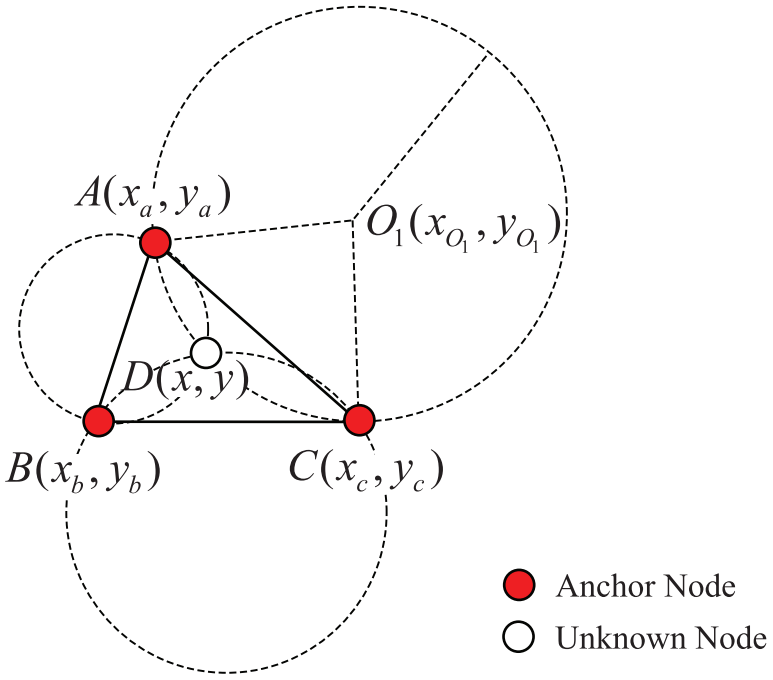

Figure 2.8: An example of the triangulation algorithm [56].

by the following equation as [58]

$$\begin{cases} \sqrt{(x_{O_1} - x_a)^2 + (y_{O_1} - y_a)^2} = r_1 \\ \sqrt{(x_{O_1} - x_b)^2 + (y_{O_1} - y_b)^2} = r_1 \\ (x_a - x_c)^2 + (y_a - y_c)^2 = 2r_1^2 - 2r_1^2 \cos \angle AO_1C \end{cases} \tag{2.7}$$

Similarly, anchor nodes A, B, the angle $\angle ADB$ and anchor nodes B, C, the angle $\angle BDC$ can determine $O_2(x_{O_2}, y_{O_2})$, r_2 and $O_3(x_{O_3}, y_{O_3})$, r_3, respectively. Thus, knowing the coordinates of $O_1(x_{O_1}, y_{O_1})$, $O_2(x_{O_2}, y_{O_2})$ and $O_3(x_{O_3}, y_{O_3})$, the coordinate of $D(x, y)$ can be calculated by applying Equation (2.5).

To conclude, in triangulation, distances are computed from angle observations. This inherently makes the triangulation scheme more expensive than trilateration in terms of deployment and computational cost. Especially for the indoor scenario implementation, the pressing demand of the accurate angular metric estimation renders the triangulation approach even more challenging.

2.3.2 Location Fingerprinting

In addition to geometric mapping, as a promising alternative to analyzing the sophisticated signal propagation, location fingerprinting technique adopts a pattern-matching approach. It roughly consists of two main phases: the offline fingerprint database generating (training) phase and the online location estimation (testing) phase. Figure 2.9 depicts the basic system flow diagram for Wi-Fi based fingerprint localization.

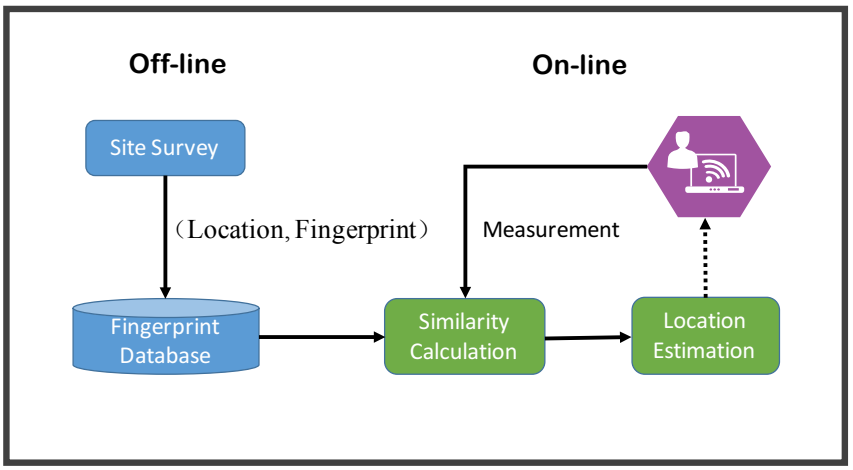

Figure 2.9: The basic system flow diagram for Wi-Fi fingerprint localization.

- **Offline Training Phase**: To be specific, in the offline phase, the area of interest is first divided into a reasonable number of spatial grids, where the reference points are situated at the vertexes and their coordinates are known a priori. Then, a mobile receiver moves around among these predefined reference points to conduct a comprehensive site survey, whose main idea is to collect wireless signal signatures at all reference points to finally construct a fingerprint database.

  Particularly, Sometimes before the process of fingerprint generating, the recorded measurements should be pre-processed in order to refine the measurement quality for further improving the localization performance. Typical Wi-Fi based pre-processing techniques consist of measurement noise reduction, signal transformation and signal

extraction [9, 59]. For noise reduction, the phase offsets removal and outliers removal are the most appealing approaches. In Chapter 4, we will provide an in-depth overview on the CSI phase compensation issue. For signal transformation, techniques like FFT [60], short time Fourier transform [61], discrete Hilbert transform [62] and discrete wavelet transform [63] are widely employed in CSI pre-processing related works. As for the signal extraction, it is for extracting target signals from raw CSI measurements. Sometimes it needs thresholding [64], filtering [65] or signal compression [66] (e.g. Principal Component Analysis (PCA)) to remove unrelated or redundant signals. In some cases, it requires the composition [67] of multiple signal sources and data interpolation to get more location-specific information.

- **Online Testing Phase**: Subsequently, in the online phase, localization is then simply the process of matching the measured fingerprints at an unknown location with those in the database by calculating the similarity and returning the location corresponding to the best-fitted fingerprint by the location estimation algorithms.

Based on the statistical property, conventional indoor localization algorithms comprise deterministic and probabilistic methods. Accordingly, we will present each kind of location-aware methods in the coming part.

2.3.2.1 Deterministic Methods

Deterministic algorithms use a similarity metric to differentiate online signal measurement and the offline fingerprint data. Target is then estimated at the closest fingerprint RP location in signal space [68]. Assume that there are M RPs in the area of interest, whose coordinates are denoted by $\{\boldsymbol{\ell}_m\}_{1\leq m\leq M}$. The basic deterministic target position determination of $\widehat{\boldsymbol{\ell}_o}$ can be expressed by the following equation.

$$\widehat{\boldsymbol{\ell}_o} = \arg\min_{\boldsymbol{\ell}_m} \mathbb{D}[\boldsymbol{\mathcal{H}}_m, \boldsymbol{\mathcal{G}}_o], m = 1, \cdots, M \tag{2.8}$$

where $\boldsymbol{\mathcal{H}}_m$ represents the offline fingerprints at the m^{th} RP location and $\boldsymbol{\mathcal{G}}_o$ denotes the online signal measurements. $\mathbb{D}[\boldsymbol{\mathcal{H}}_m, \boldsymbol{\mathcal{G}}_o]$ is the specific similarity metric between $\boldsymbol{\mathcal{H}}_m$ and $\boldsymbol{\mathcal{G}}_o$. For instance, the Euclidean distance [69], cosine similarity [70], cross correlation [30],

Time Reversal Resonating Strength (TRRS) [71] and fuzzy logic similarity [72] have been prevalently implemented for the signal comparison [73].

The major advantage of the deterministic methods is their ease of implementation. Traditional deterministic methods can be easily implemented based on k-Nearest Neighbors (kNN) and the computational complexity is often low. Some other more advanced deterministic algorithms such as Support Vector Machine (SVM) [74, 66] and Linear Discriminant Analysis (LDA) [75] show better localization accuracy with higher computational cost.

2.3.2.2 Probabilistic Methods

Unlike deterministic approaches, probabilistic algorithms are based on statistical inference between the target signal measurement and stored fingerprint database. Using a training set, these algorithms can be applied to find the target's location with the maximum likelihood, which is inferred by a probabilistic model reflecting the signal distributions. It can represented by

$$\widehat{\boldsymbol{\ell}_o} = \arg\max_{\boldsymbol{\ell}_m} P(\boldsymbol{\ell}_m|\boldsymbol{\mathcal{G}}_o), m = 1, \cdots, M \tag{2.9}$$

where $P(\boldsymbol{\ell}_m|\boldsymbol{\mathcal{G}}_o)$ indicates the probability of the target at location $\boldsymbol{\ell}_m$ given the online measurements $\boldsymbol{\mathcal{G}}_o$.

Other probabilistic algorithms such as Bayesian network [76, 77], expectation maximization [78], Kullback-Leibler Divergence (KLD) [79, 33], Gaussian process [80] and conditional random field [81] can also achieve high localization accuracy through probabilistic inference.

Moreover, for probabilistic algorithms, since each location estimation can be indicated by a confidence interval [82], it is also amendable to fuse different sensors such as motion [83] and sound [77]. For example, the location can be estimated by maximizing the joint probability or likelihood with the sensor measurements. However, these algorithms usually require some probabilistic assumptions (such as Gaussian noise or probabilistic independence [33]). Furthermore, training probabilistic models may be complicated, and require more datasets than traditional deterministic algorithms.

For our Wi-Fi based indoor positioning problem, since probabilistic algorithm embraces the wireless channel variation by inferring a probabilistic model reflected by the signal distribution, it can fully depict the location-specific information, thus capable of achieving better localization performance than its deterministic counterpart. Therefore, we only consider probabilistic based location fingerprinting schemes in this thesis.

Chapter 3

AR Entropy based Location Fingerprinting using CSI Amplitude

Contents

3.1 Introduction

Location fingerprinting technique has drawn tremendous attractions in recent years due to its huge potential values for industrial and commercial applications. The design of an effective and successful indoor location fingerprinting system, which properly addresses the balancing between positioning accuracy and complexity, still remains challenging.

In this chapter, we propose EntLoc, a CSI based indoor location fingerprinting system using the structurally simple and spatially informative AR entropy fingerprint. We first revisit some related works and form a set of comparative candidates. The detailed design for each part of EntLoc will be displayed in the sequel. Moreover, we implement extensive and dedicated indoor experiments to evaluate the performance of the proposed system. Throughout this chapter, some interesting experimental observations will also be identified and discussed.

3.1.1 Literature Review

Prevalent Wi-Fi fingerprint localization approaches mainly exploit two types of wireless signal properties: the received signal strength and the channel response. We present related works in accordance with these two categories.

Fingerprinting via RSS: Due to the easy acquisition of wireless signal power measurements, RSS-based fingerprinting plans have been widely adopted in various mainstream indoor positioning systems. Pioneering works such as RADAR [84] carried out comprehensive site surveys for the first time and generated the RSS based fingerprint radio map. Subsequently, the deterministic kNN algorithm was utilized to determine the target's location with an average precision of 3 meters. Contrastively, in Horus system [28], Youssef et al. resorted to the Bayes based probabilistic method and a joint clustering algorithm to achieve an accuracy improvement of 2.1 m, which outperformed RADAR even with less computational complexity. However, the instability of RSS still remains challenging. More recently, researchers of LiFS [85] brought up a novel fingerprint space by utilizing the spatial relations of RSS measurements, yielding low human cost for site survey and com-

petitive accuracy over RADAR. Khatab et al. [86] used auto-encoder based deep extreme learning machine to extract high level data features from RSS fingerprint, which further improved the localization performance. Moreover, Wu et al. designed DorFin [87], a RSS-based location fingerprinting system which successfully tackled error mitigation problem by quantifying APs' distinction, alleviating RSS outliers and amending transitional RSS recordings. It reduced the mean and 95th percentile errors to respective $2.5m$ and $6.2m$, outperforming both RADAR and Horus by nearly 50% accuracy improvement.

Fingerprinting via Channel Response: In recent years, channel response based fingerprinting approaches have attracted massive attention due to their capability of harnessing the rich multipath information indoors. The authors of FIFS [29] explored the spatial and frequency diversity of CSI for Wi-Fi fingerprinting localization. Additionally, FIFS took the power summation for all independent subcarriers as location fingerprint and adopted Maximum A Posteriori (MAP) approach to yield an improved performance compared with RSS based Horus system. Meanwhile, for PinLoc [30], the whole location-aware platform was established on a set of $1m \times 1m$ spots. The underlying observation of PinLoc was that the CSIs on a single subcarrier were illustrated to be clustered distributed on the complex plane. The Gaussian mixture distribution was then introduced to properly model the channel measurements for the purpose of accurate localization. Experimental result validated PinLoc's impressive performance with an 89% mean accuracy for 100 spots. Furthermore, when it comes to the time domain CIR, authors in [88] proposed to exploit the amplitude of CIR (ACIR) vector to accomplish location estimation through nonparametric kernel regression scheme. Simulation results showed a distinguished performance superiority over the traditional RSS based fingerprinting methods.

3.1.2 Contributions

In summary, our main contributions of this chapter are set out below:

- As far as we are aware of, this is the first work to statistically study AR modeling based entropy signature in CSI fingerprint localization system. This simple fingerprint structure helps decrease the pattern-matching complexity and its informative

statistical embodiment also facilitates the location estimation accuracy.

- We propose a power based pre-processing filtering scheme to mitigate the irrelevant noisy component in CSI measurements, thus further improving the location fingerprinting performance.
- We implement extensive positioning experiments on the lightweight HummingBoard Pro device, which remarkably enhances the experimental efficiency.

3.1.3 Chapter Organization

The rest of this chapter is organized as follows. In Section 3.2, we elaborate the overall architecture design of our proposed EntLoc localization system along with detailed methodology. We present the realistic experimental setup and provide the experimental results in Section 3.3. Conclusions are drawn in Section 3.4.

3.2 Localization Methodology

In this section, we focus on the overall introduction of our proposed EntLoc positioning system, whose theoretical methodology will be revealed in a divide-and-conquer manner.

3.2.1 EntLoc System Architecture

The overall architecture of the proposed system is illustrated in Figure 3.1. In general, it consists of two major functionality components: the offline fingerprint radio map construction and the online target's position estimation. For CSI fingerprint database construction, once getting the received raw CFR packets through signal war-driving, we first employ a tap filtering based pre-processing scheme to extract the most informative and location-dependent components in the multipath-rich indoor scenario. Subsequently, we model the statistical features of filtered CFR amplitude by calculating an AR modeling based entropy metric and then build a representative fingerprint radio map after removing the ambiguous endpoint subcarriers. Afterwards, for online location estimation process, when a mobile target arrives into the area of interest, it executes the same procedures

to acquire the entropy vector and matches against the learned offline attributes. Finally, the simple Manhattan distance based kernel regression approach can be fully leveraged to accomplish the physical position estimation of the mobile target.

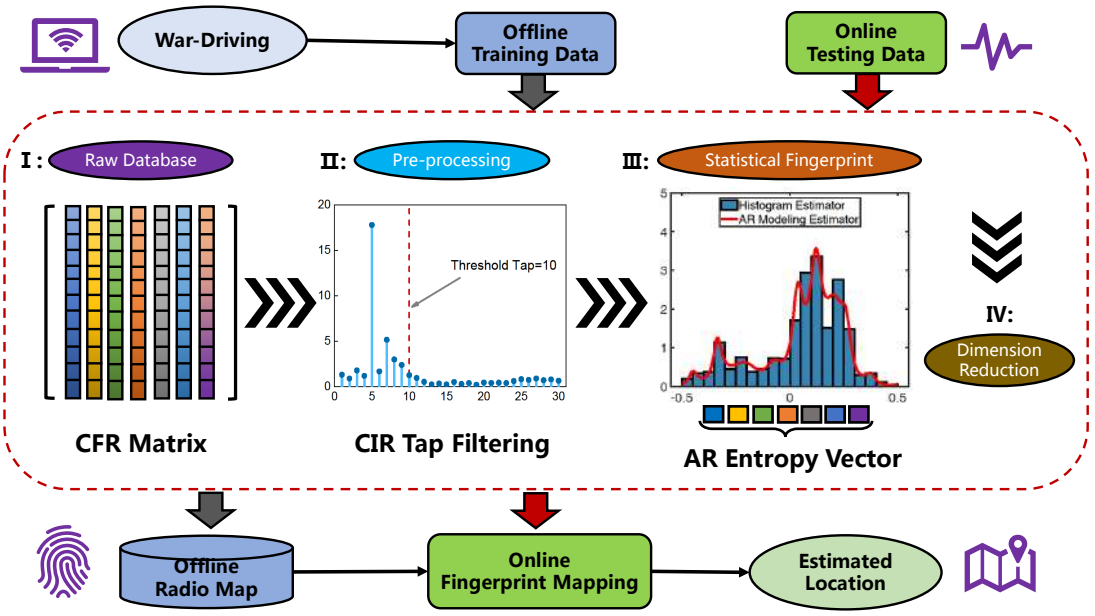

Figure 3.1: The EntLoc system architecture.

In what follows, we will dissect each component of the proposed system in a divide-and-conquer manner.

3.2.2 Offline Radio Map Construction

First of all, we start to elaborate our location fingerprinting methodology with the presentation of the problem formulation. In the offline phase, M reference points are predefined and properly marked in the area of interest. The coordinate of each RP location can be denoted as $\boldsymbol{\ell}_m = (x_m, y_m)$, where x_m and y_m are the respective X- and Y-coordinate of the m^{th} RP, $m \in [1, M]$. Considering that we have S Access Points (APs) as signal transmitters, each of which has N_t TX antennas. One mobile user equipped with N_r RX antennas is regarded as the RF receiver. Thus each TX-RX antenna pair is capable of generating up to $N_t \cdot N_r$ radio links. As for the channel state information, each CSI packet shares the same number of K OFDM subcarriers. So the dimensionality of one CSI packet

measured at one RP location from a single AP can be expressed by $R = N_t \cdot N_r \cdot K$. Moreover, at each RP position, we propose to concatenate CSI packets from S available APs to form the raw CSI signature, whose total dimensionality then extends to be $S \cdot R$. Mathematically, this offline radio signature measured at the m^{th} RP location from all S APs is given by the set $\boldsymbol{\mathcal{H}}_m = \{\mathbf{H}_m^1, \ldots, \mathbf{H}_m^s, \ldots, \mathbf{H}_m^S\}, s \in [1, S]$. Specifically, $\mathbf{H}_m^s \in \mathbb{C}^{N \times R}$ contains N consecutive $1 \times R$ dimensional CSI samples which are adequately acquired at the RP location $\boldsymbol{\ell}_m$ from the s^{th} AP. This CSI matrix can be presented by the following equation.

$$\mathbf{H}_m^s = \begin{bmatrix} H_m^s(1,1) & \cdots & H_m^s(1,r) & \cdots & H_m^s(1,R) \\ \vdots & \ddots & \vdots & \ddots & \vdots \\ H_m^s(n,1) & \cdots & H_m^s(n,r) & \cdots & H_m^s(n,R) \\ \vdots & \ddots & \vdots & \ddots & \vdots \\ H_m^s(N,1) & \cdots & H_m^s(N,r) & \cdots & H_m^s(N,R) \end{bmatrix} \tag{3.1}$$

where $n \in [1, N]$ and $r \in [1, R]$.

During the online stage, the mobile user at an unknown position $\boldsymbol{\ell}_o = (x_o, y_o)$ records the same structural CSI matrix from the s^{th} AP. We denote this matrix as $\mathbf{G}_o^s$, which also shares the same dimension with $\mathbf{H}_m^s$. Likewise, the online measured CSI signature at the location $\boldsymbol{\ell}_o$ can be expressed by the set $\boldsymbol{\mathcal{G}}_o = \{\mathbf{G}_o^1, \ldots, \mathbf{G}_o^s, \ldots, \mathbf{G}_o^S\}$. Accordingly, the mobile user's location can be then estimated as $\widehat{\boldsymbol{\ell}}_o = (\widehat{x}_o, \widehat{y}_o)$ by exploiting these online CSIs and the stored offline database.

3.2.2.1 Tap Filtering Preprocessing Technique

Recall that channel state information completely characterizes the multipath channel and preserves the fine location dependency, which makes it a good choice for location fingerprint. However, it would be fair to state that for the existing Wi-Fi networks, bandwidth limitation introduces severe location ambiguity which leads to limited localization accuracy [89]. By using the commodity Wi-Fi with center frequency of 2.4 GHz, the bandwidth of the system is therefore 20 MHz in this case. Since CFR can be converted into CIR via inverse fast Fourier transform, an estimation of CIR with time resolution of 1/20MHz =50 ns is exposed. Since typical indoor maximum excess delay τ_{max} is smaller than 500 ns [90], given a time resolution of 50 ns, approximately only the first 10 out of

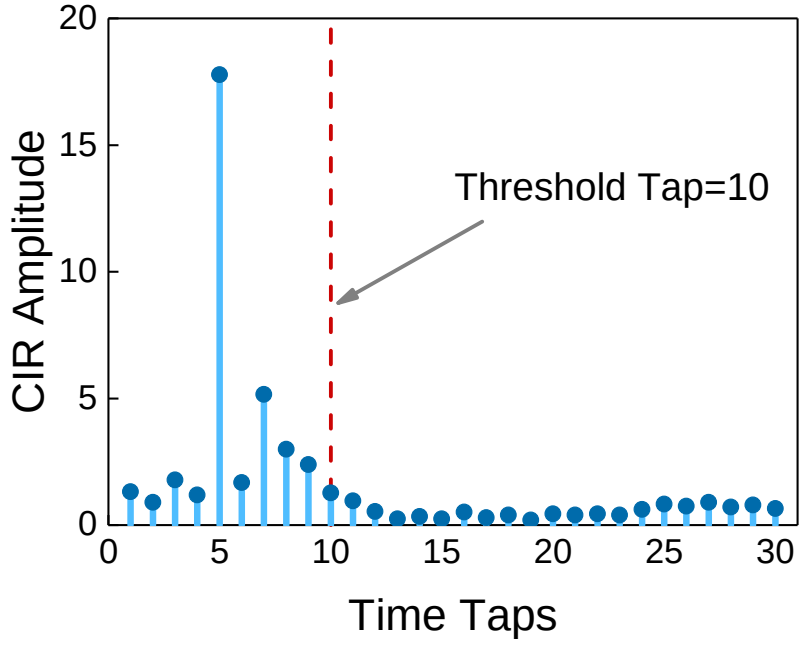

Figure 3.2: Channel impulse response.

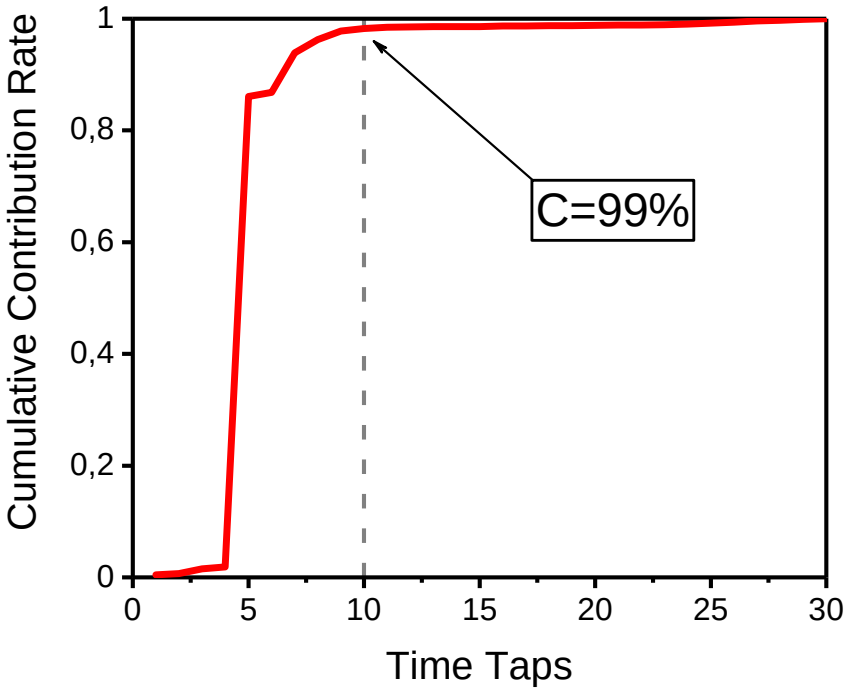

Figure 3.3: Power threshold.

the 30 accessible CIR time taps are relevant to multipath propagation. In other words, the remaining 20 taps are irrelevant for localization purpose. Moreover, when the Signal-to-Noise Ratio (SNR) is not high enough, the receiver's Additive White Gaussian Noise (AWGN) at these time taps will only make the accuracy worse.

Hence, based on the system bandwidth, a reasonable number of relevant time samples should be chosen for the sake of computation efficiency and accuracy. In this research, we design a power-based tap filtering method to preserve the most informative channel features for fingerprinting. Specifically, for the conciseness of expression, we define the individual raw CFR signature as $\mathbf{H} \in \mathbb{C}^{1\times K}$. Through IFFT, we first convert $\mathbf{H}$ into the same dimensional CIR vector $\mathbf{h}$. For each $1 \times K$ CIR packet, we calculate the average channel power for each time tap, denoted by $\mathbf{U} = (u_1, \ldots, u_k, \ldots, u_K), k \in [1, K]$, where $u_k = |\mathrm{h}_k|^2$ and h_k denotes the k^{th} complex tap value of one CIR packet. Then, we define a cumulative contribution rate of the first k taps as

$$C_k = \sum_{i=1}^{k} u_i \Big/ \sum_{i=1}^{K} u_i. \tag{3.2}$$

If the cumulative contribution rate of the first T taps, i.e., C_T, is greater than the predefined threshold C, we then apply a simple rectangular window with length T to truncate the rest $(K-T)$ taps. Next, FFT is further utilized on filtered CIR to yield the smoothed version of CFR. As displayed in Figure 3.2 and Figure 3.3, we define the threshold of the cumulative contribution rate as 99%, the first 10 taps are thereby selected to preserve the most relevant multipath information for localization. Moreover, the differences between the raw CFR measurements and their smoothed versions after filtering processing can be also observed in Figure 3.4 and Figure 3.5.

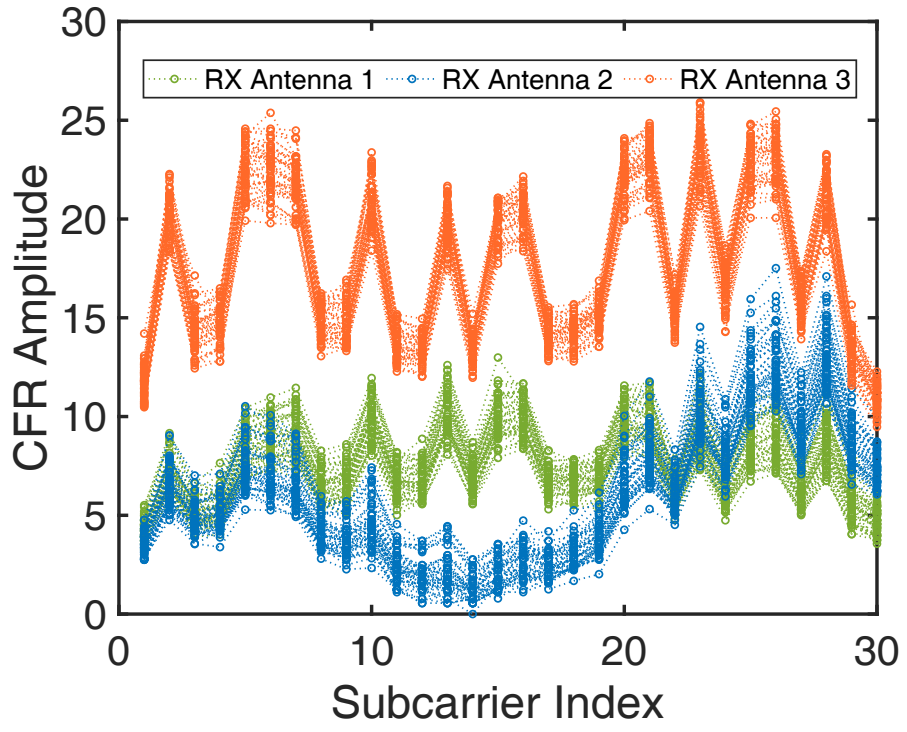

Figure 3.4: The raw CFR.

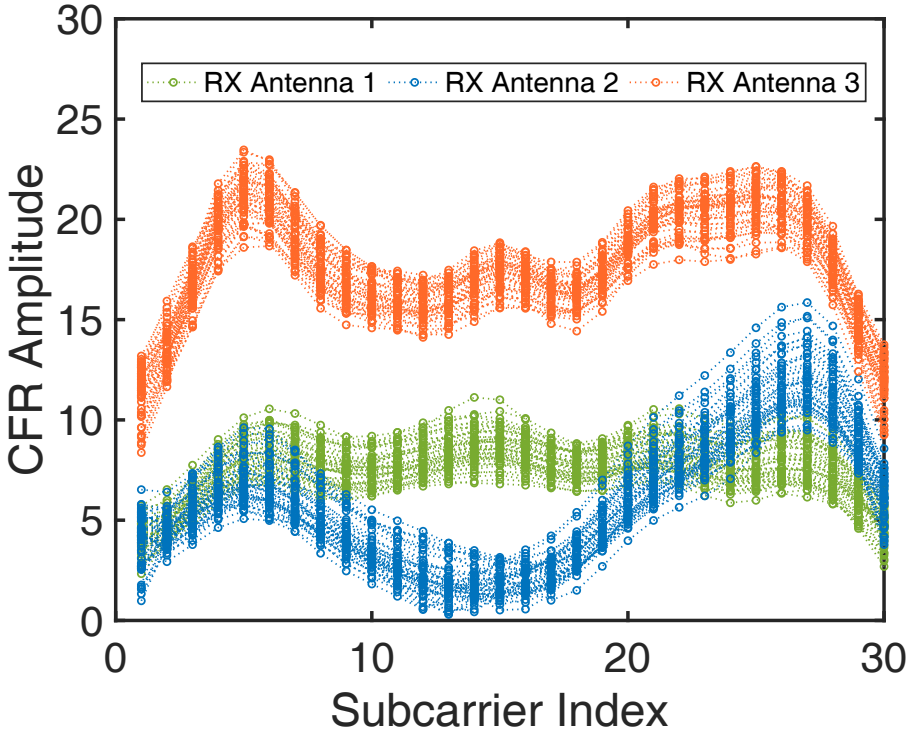

Figure 3.5: CFR after tap filtering.

3.2.2.2 AR Entropy Estimation

As aforementioned in Chapter 2, probabilistic positioning algorithms analytically outperform their deterministic counterparts. Additionally, numerous literature [28, 29, 91] further reveal such superior localization performance of the probabilistic algorithms over their deterministic rivals in the complex indoor environment. Generic probabilistic methods include the Bayesian network [77], KLD [79, 33], Gaussian process [92], etc.. The essential cause resides in the fact that PDF contains the complete statistical characterizations of the complex random variables, which are capable of providing better location-specific RF signatures.

The simplest probabilistic model for CFR is based on the assumption that there are a large number of statistically independent reflected and scattered paths with random amplitudes corresponding to a single subcarrier. By the central limit theorem, it can be reasonably modeled as circularly-symmetric Gaussian (complex Gaussian) random variables [49]. Thus, the amplitudes of the complex Gaussian process are essentially Rayleigh distributed. If the channel has a fixed LoS component, the received signal then equals the superposition of a complex Gaussian component and this LoS component. In this case, the CFR amplitude follows the Rician distribution. However, due to the sophisticated indoor environment and the imperfection of wireless devices, most measured CFR values are non-Gaussian distributed or even do not fit any known distribution [30, 27, 93]. Meanwhile, for multivariate fingerprint structure (e.g., multi-subcarrier CFR in our case), existing statistical tools only work under the condition of identifiably distributed measurements [33]. Besides, most probabilistic approaches require sufficient number of measurements stored in the fingerprint database, which guarantees an accurate PDF estimation but suffers huge system burden.

Therefore, in this thesis, we resort to the well-known Shannon entropy [94] as the fingerprint alternative in our localization system. Given the offline and online CFR amplitude PDF estimates $\hat{p}_{\mathbf{H}_m^s}(\beta; r)$ and $\hat{p}_{\mathbf{G}_o^s}(\beta; r)$, both of which are from the r^{th} subcarrier and the s^{th} AP. For the simplicity of presentation, here we define β as a general expression of CFR amplitude from the same subcarrier. Thus, the offline entropy definition can be

expressed by

$$\hat{\phi}^{r}_{\mathbf{H}^{s}_{m}} = -\int_{-\infty}^{\infty} \hat{p}_{\mathbf{H}^{s}_{m}}(\beta; r) \log \hat{p}_{\mathbf{H}^{s}_{m}}(\beta; r) d\beta \tag{3.3}$$

Similarly, the online CFR entropy $\hat{\phi}^{r}_{\mathbf{G}^{s}_{o}}$ can also be calculated as the fingerprint for the subsequent stage of target's location determination.

In practice, it is a challenging task to implement direct evaluation of the Shannon entropy from real data [95, 36]. The reason behind this dilemma is twofold:

(i) Entropy has to be approximated from the mere sample data due to the fact that probability density function is generally unknown.

(ii) Equation (3.3) requires numerical integration since a closed-form solution of the entropy does not exist.

Typical data-adaptive PDF estimation methods comprise histogram estimator [96], order statistics [97] or kernel method (a.k.a. Parzen method) [98]. However, all of them share the major drawback of slow convergence rate.

In this thesis, we address the entropy estimation problem by leveraging the more accurate and consistent Autoregressive (AR) modeling approach [99]. The basic principle of this approach is to estimate the unknown PDF in the form of Power Spectral Density (PSD) of an unit variance AR process. This unit variance condition ensures that PSD shares the basic requirements of PDF (i.e., positive function that integrates to one).

Given the general expression of amplitude β, we define the input CFR amplitudes from one certain subcarrier as $\boldsymbol{\beta}_I = [\beta(1), \cdots, \beta(n), \cdots, \beta(N)]^{\top}$, where N is the number of CFR packets and $(\cdot)^{\top}$ is the transpose operator. Since the law is modeled as the spectrum restriction on the interval of $[-0.5, +0.5]$, the amplitude data have to be first rescaled on this interval. Meanwhile, an order p AR process $W(n)$ is defined as the output of an all-poles filter driven by a white noise $\epsilon(n)$ with variance δ^2_{ϵ}. It can be mathematically denoted as [99]

$$W(n) = \sum_{i=1}^{p} a_i W(n-i) + \epsilon(n). \tag{3.4}$$

where $\mathbf{a} = \{a_i\}_{1 \leq i \leq p}$ are the AR model parameters.

Since the CFR amplitude PDF $p(\beta)$ can be equivalently depicted by the PSD $S_W(\beta)$ of this AR process which is parameterized by a set of AR parameters, the entire relations can be then presented as [38]

$$p(\beta) = S_W(\beta) = \frac{\sigma_\epsilon^2}{|1 + \sum_{i=1}^{p} a_i e^{-j2\pi i\beta}|^2}, \beta \in [-0.5, 0.5] \tag{3.5}$$

where σ_ϵ^2 is the model prediction error which is chosen so that $\int_{-0.5}^{0.5} S_W(\beta) d\beta = 1$. It is notable that AR model order needs to be chosen appropriately at first since a low order leads to inadequate resolution (estimator bias) while a high order incurs spurious peaks (excessive variance). Through extensive experiments, a well-run model order selection technique known as the Exponentially Embedded Family (EEF) [100] is adopted to select a proper p which maximizes the following criterion.

$$\mathcal{F}(p) = \begin{cases} \xi_p - p(\log(\frac{\xi_p}{p}) + 1), & \text{if } \xi_p \geq p \\ 0, & \text{otherwise} \end{cases} \tag{3.6}$$

Here ξ_p is the Generalized Likelihood Ratio Test (GLRT) statistic which can be asymptotically computed as

$$\xi_p = (N - p) \log \left(\frac{\boldsymbol{\lambda}_p^\top \boldsymbol{\lambda}_p}{\boldsymbol{\lambda}_p^\top (\mathbf{I} - \boldsymbol{\Lambda}_p \left(\boldsymbol{\Lambda}_p^\top \boldsymbol{\Lambda}_p \right)^{-1} \boldsymbol{\Lambda}_p^\top) \boldsymbol{\lambda}_p} \right) \tag{3.7}$$

where $\boldsymbol{\lambda}_p = [\beta(p+1), \beta(p+2), \cdots, \beta(N)]^\top$ and $\boldsymbol{\Lambda}_p = [\boldsymbol{\lambda}_{p-1}, \boldsymbol{\lambda}_{p-2}, \cdots, \boldsymbol{\lambda}_0]$. The detailed procedures are explicitly described in Algorithm 1.

Thereby, the succeeding task of estimating the AR parameters consists of two major steps [38]:

(i) We first estimate the autocorrelation function of the CFR amplitude data sequence $\boldsymbol{\beta}_I$ by applying the sample moment estimator, which is the statistical average correlation estimate:

$$R_W(i) = \frac{1}{N} \sum_{n=1}^{N} e^{j2\pi i\beta(n)}, i \in [0, p] \tag{3.8}$$

Algorithm 1 Model Order Selection using EEF

Input:
N-dimensional CFR amplitude sample vector $\boldsymbol{\beta}_I$ of one certain subcarrier;
Predefined maximum AR model order p_{max}

Output:
Selected AR model order p

Rescale the input vector $\boldsymbol{\beta}_I$ into $[-0.5, +0.5]$;
for each $i \in [1, p_{max}]$ **do**
  Calculate the GLRT statistic ξ_i by (3.7);
  if $\xi_i \geq i$ **then**
    Obtain $\mathcal{F}(i) = \xi_i - i(\log(\frac{\xi_i}{i}) + 1)$ by using EEF criterion in (3.6);
  else
    Make $\mathcal{F}(i)$ be zero;
  end if
end for
Execute $p = \underset{i \in [1, p_{max}]}{\arg\max}\, \mathcal{F}(i)$;
Return p;

(ii) AR coefficient estimation is then achieved by solving the Yule-Walker equations using the Levinson-Durbin recursion [101, 102]:

$$\mathbf{R}_W \mathbf{a} = -\mathbf{r}_W(0) \tag{3.9}$$

where $\mathbf{R}_W = [\mathbf{r}_W(1), \mathbf{r}_W(2), \cdots, \mathbf{r}_W(p)]$ and $\mathbf{r}_W(i) = [R_W(1-i), R_W(2-i), \cdots, R_W(p-i)]^\top$. Once the AR parameters have been estimated, say $\hat{\mathbf{a}} = [\hat{a}_1, \hat{a}_2, \cdots, \hat{a}_p]^\top$, the AR model prediction error can be then computed by

$$\hat{\sigma}_\epsilon^2 = R_W(0) + \sum_{i=1}^{p} \hat{a}_i R_W(-i) \tag{3.10}$$

When AR PSD is determined, according to (3.5), the entropy estimation can be then converted to the following form:

$$\begin{aligned} \hat{\phi}_\beta &= -\int_{-0.5}^{0.5} \hat{p}(\beta) \log \hat{p}(\beta) d\beta \\ &= -\int_{-0.5}^{0.5} \hat{S}_W(\beta) \log \hat{S}_W(\beta) d\beta \end{aligned} \tag{3.11}$$

Additionally, a more feasible closed-form expression without any numerical integration can be obtained by applying Plancherel-Parseval formula to the right hand side of Equation

(3.11) [36] and yielding

$$\hat{\phi}_\beta = -\sum_{i=-\infty}^{\infty} R_W(i) Z_W^*(i) \tag{3.12}$$

where $(\cdot)^*$ is the conjugate operator and $Z_W(i)$ denotes the i^{th} component of the AR process's cepstrum, which can be calculated by proceeding the inverse Fourier transform of $\log \hat{S}_W(\beta)$. The whole entropy estimation process can be presented in Algorithm 2.

Algorithm 2 AR Modeling based Entropy Estimation

Input:

N-dimensional CFR amplitude sample vector $\boldsymbol{\beta}_I$ of one certain subcarrier;
Selected AR model order p from Algorithm 1

Output:

Estimated CFR amplitude entropy $\hat{\phi}_\beta$

1: Rescale the input vector $\boldsymbol{\beta}_I$ into $[-0.5, +0.5]$;
2: Compute the autocorrelation function $\{R_W(i)\}_{0 \le i \le p}$ of the rescaled data via (3.8);
3: Calculate AR model parameters $\hat{\mathbf{a}}$ and prediction error $\hat{\sigma}_\epsilon^2$ by solving Yule-Walker equations in (3.9) and (3.10);
4: Estimate AR model PSD $\hat{S}_W(\beta)$ by applying (3.5);
5: Calculate AR entropy $\hat{\phi}_\beta$ using (3.12);
6: **Return** $\hat{\phi}_\beta$;

In addition, Figure 3.6 and Figure 3.7 illustrates the AR modeling based PDF estimates of CFR amplitude samples at two sample locations. Both of the estimated PDFs (Gaussian-like and non-Gaussian distributions) show good fit to the histograms which further justifies the AR-modeling scheme in practical work. Moreover, some shining points of AR modeling based entropy as location fingerprint will also be experimentally discussed in the performance evaluation section of this chapter.

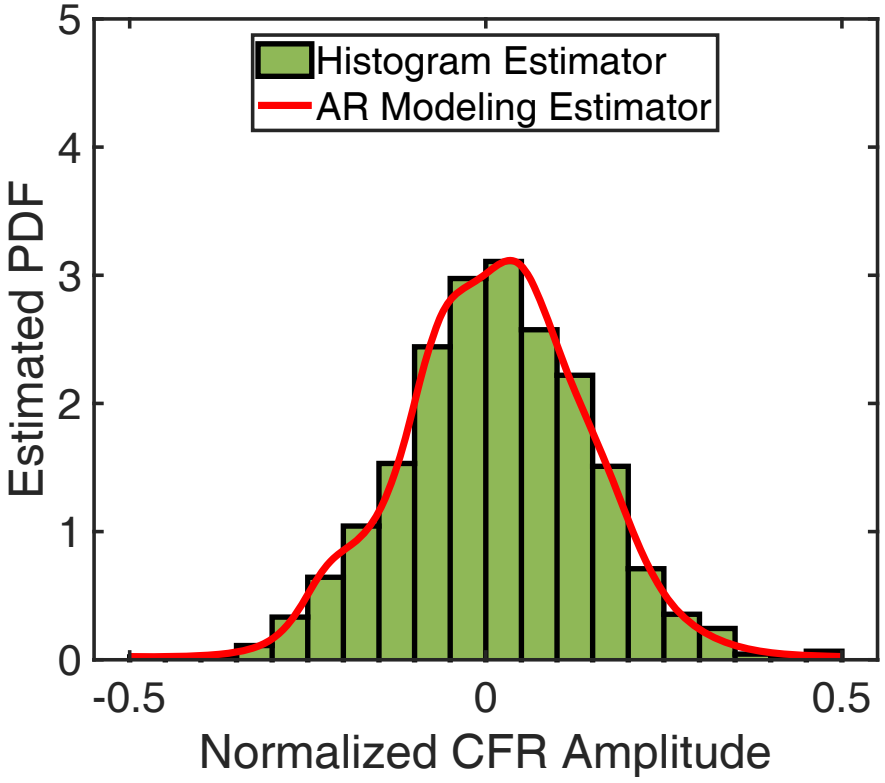

Figure 3.6: AR modeling based PDF estimation at location #1.

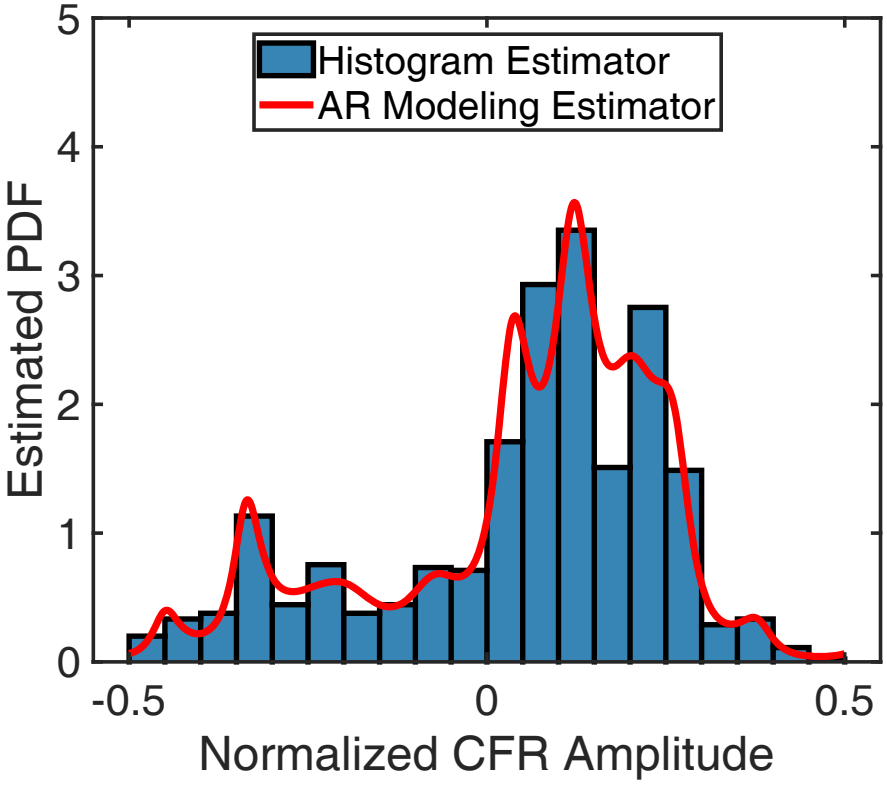

Figure 3.7: AR modeling based PDF estimation at location #2.

Endpoint Subcarrier Removal In this part, we continue to exploit the AR modeling based entropy and shed light on some interesting observations in the sequel.

For location fingerprinting, the spatial resolvability is a key performance indicator for the proposed location fingerprint. In order to validate such property of our AR entropy-based fingerprint, a simple test was taken in our lab corridor. Concretely, we linearly selected 15 sample locations with $1m$ spacing. A RF transmitter was placed at one end of the corridor, sending wireless packets continuously. In the meantime, we moved a mobile receiver in sequence at these sample locations. Around 500 CFR measurements were collected at each location. After calculating the AR entropies of all subcarriers at each position, we applied confusion matrix to portray the entropy differences among these 15 locations for each CFR subcarrier. In Figure 3.8, for the visual clarity, we only exhibit subcarrier index 1, 10, 20, 30 and experimentally observe that the endpoint subcarriers #1 and #30 show a clear ambiguity in terms of location differentiation.

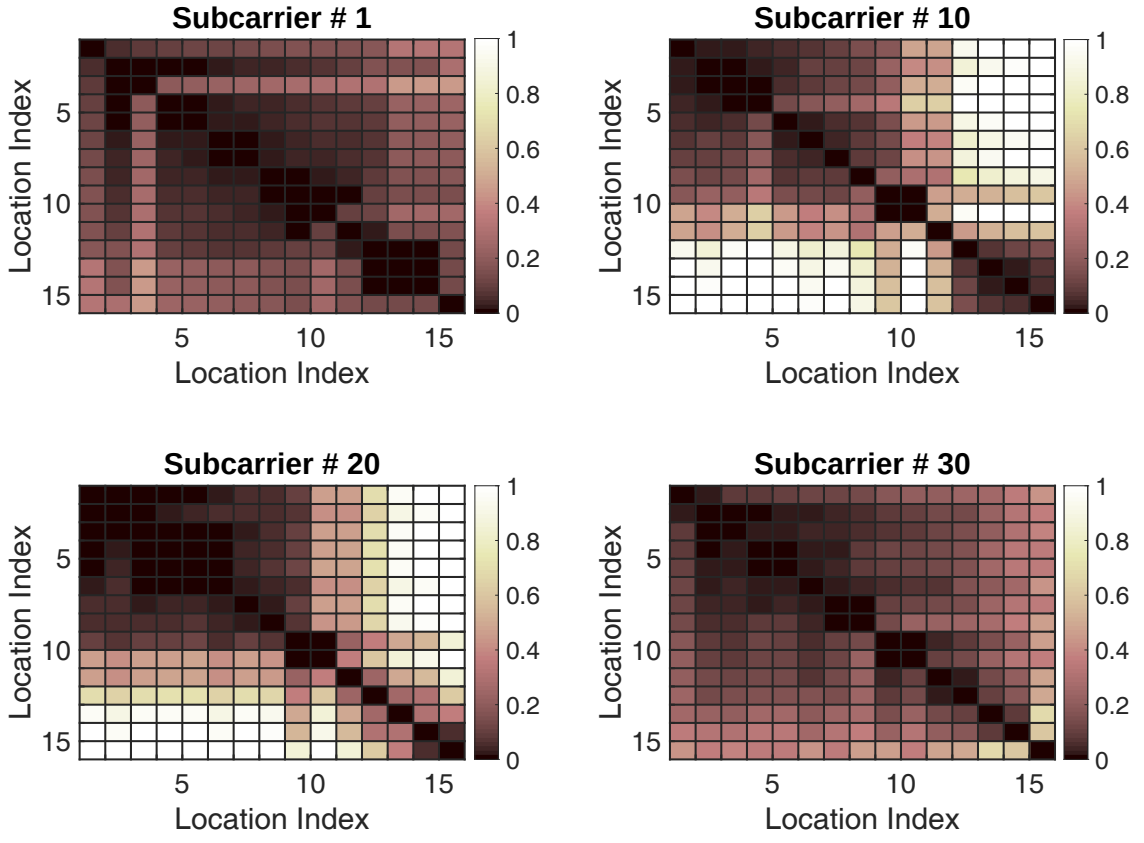

Figure 3.8: Ambiguity test for 4 subcarriers, namely #1, #10, #20 and #30.

Given that this is only a visual indication, we then utilize the statistical Cumulative Distribution Function (CDF) to carefully study the behavior of these entropy differences. As depicted in Figure 3.9, most subcarriers display an obvious entropy differences for different locations while the endpoint subcarrier #1 and #30 still show the opposite, inducing potential location differentiation errors in the next online pattern-matching stage.

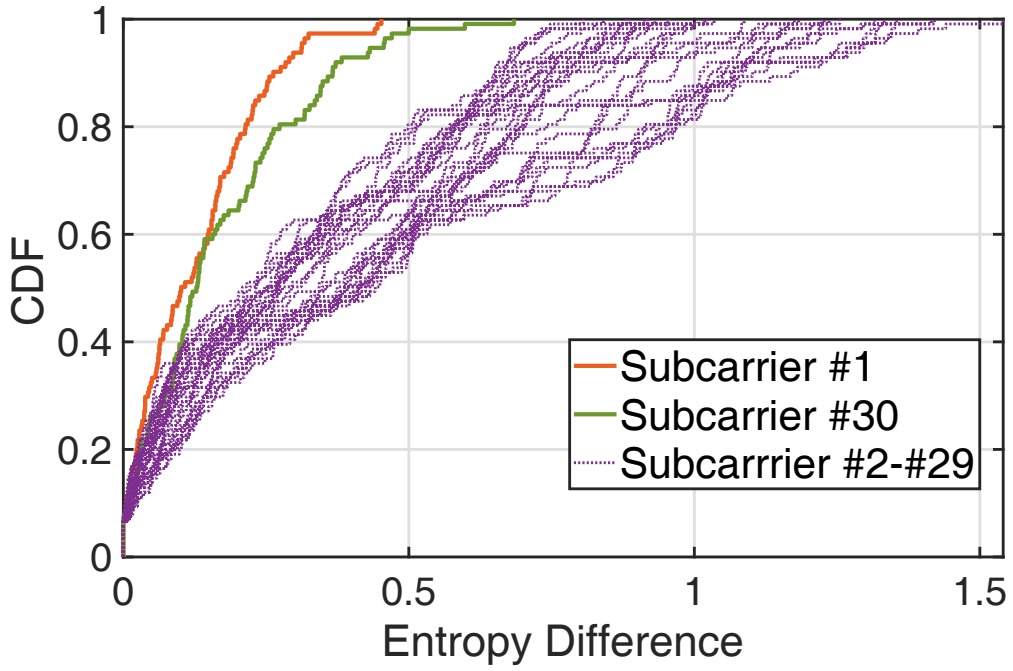

Figure 3.9: Ambiguity test for all 30 available subcarriers.

Therefore, we propose in this work to remove the two null endpoint subcarriers from the estimated AR entropies, which also serves as a dimension reduction strategy to further improve the execution efficiency of our AR entropy approach. Recall that we combine the CFR measurements of the total R subcarriers from all N_r receiving antennas, the estimated AR entropy fingerprint in the offline stage can be hereby represented as

$$\widehat{\mathbf{\Phi}}_{\mathbf{H}_m^s} = [\widehat{\phi}^1_{\mathbf{H}_m^s}, \ldots, \widehat{\phi}^{r'}_{\mathbf{H}_m^s}, \ldots, \widehat{\phi}^{R'}_{\mathbf{H}_m^s}], r' \in [1, R'] \tag{3.13}$$

where $R' = R - 2 \cdot N_r$ is the reduced number of subcarriers in this case. Likewise, the online estimated AR entropy is denoted by $\widehat{\mathbf{\Phi}}_{\mathbf{G}_o^s} = [\widehat{\phi}^1_{\mathbf{G}_o^s}, \ldots, \widehat{\phi}^{r'}_{\mathbf{G}_o^s}, \ldots, \widehat{\phi}^{R'}_{\mathbf{G}_o^s}], r' \in [1, R']$.

3.2.3 Online Location Estimation

As the final task of EntLoc, the online location estimation consists of two functional part: the distance based proximity comparison and the kernel regression based location inference. We lay out the details of both parts in the following.

3.2.3.1 Distance-based Proximity Comparison

For the online location determination, the mobile target is required to be accurately mapped to the pre-designed radio map. To quantitatively measure the similarity between the stored entropy fingerprints and the estimated online CFR entropies, we employ Manhattan distance [103] which is also known as taxicab metric, capable of measuring the gap between two points through the summation of the absolute differences of their corresponding components.

Given the offline and online entropy fingerprints $\widehat{\mathbf{\Phi}}_{\mathbf{H}_m^s}$ and $\widehat{\mathbf{\Phi}}_{\mathbf{G}_o^s}$, we define the Manhattan distance between them as

$$\mathscr{D}_m^s = \|\widehat{\mathbf{\Phi}}_{\mathbf{H}_m^s} - \widehat{\mathbf{\Phi}}_{\mathbf{G}_o^s}\|_1 = \sum_{i=1}^{R'} \left|\widehat{\phi}_{\mathbf{H}_m^s}^i - \widehat{\phi}_{\mathbf{G}_o^s}^i\right| \tag{3.14}$$

where $\|\cdot\|_1$ denotes the ℓ_1 norm. It concisely reveals the physical similarity between the online fingerprints at an unknown position and the offline dataset at the m^{th} RP location, both of which are measured from the s^{th} AP. Moreover, by using the chain rule for Shannon entropy [94], it can be proved that the Manhattan distance of a joint entropy of independent variables is equal to the sum of the distance for each variable's entropy. Under S independent AP assumption, we therefore have the Manhattan distance for all available APs as follows.

$$\mathscr{D}_m = \sum_{s=1}^{S} \mathscr{D}_m^s \tag{3.15}$$

3.2.3.2 Kernel Regression

In order to properly obtain the location estimation of the target, the weighted kernel regression is further adopted by employing the distance based kernel function $\mathcal{K}$ and the whole set of known reference points [33]. The estimated location can be derived from the following equation.

$$\widehat{\boldsymbol{\ell}_o} = \frac{\sum_{m=1}^{M} \mathcal{K}_m \boldsymbol{\ell}_m}{\sum_{m=1}^{M} \mathcal{K}_m} \tag{3.16}$$

Here $\mathcal{K}_m$ is defined as the probability kernel of the m^{th} RP position by exponentiating its corresponding Manhattan distance, which is presented as follows:

$$\mathcal{K}_m = \exp(-\rho \mathscr{D}_m) \tag{3.17}$$

where ρ is the kernel coefficient which is determined to optimally minimize the fingerprinting error by leave-one-out cross-validation in the offline phase [79].

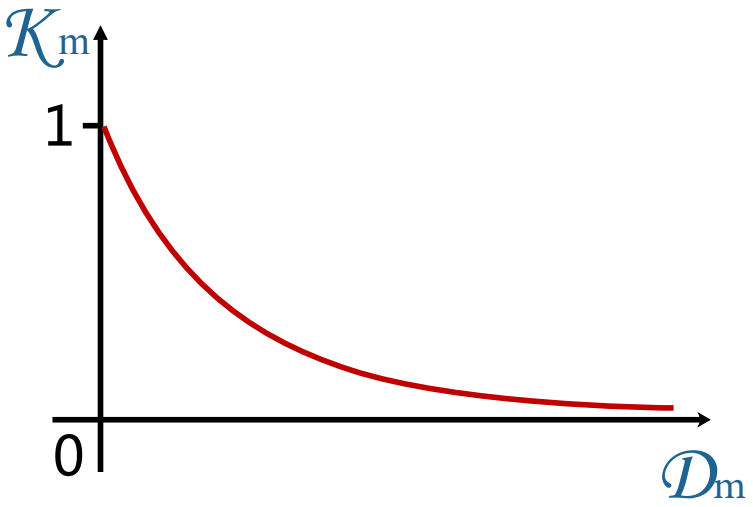

Figure 3.10: A simple example of the kernel function with $\rho = 2$.

Figure 3.10 displays a simple kernel function which changes with distance. It is notable that the kernel $\mathcal{K}_m$ is equal to one if the distributions of the given two fingerprints are identical (i.e., $\mathscr{D}_m = 0$) and decays to zero as the dissimilarity of the two fingerprints increases. In other words, this probability kernel provides a flexible way to naturally

handle the CFR data and hence takes full advantage of our probabilistic AR entropy model, thus leading to an improved localization performance.

The performance of aforementioned fingerprinting approaches will be evaluated in the follow-up section.

3.3 Performance Evaluation

In this section, we present the experimental evaluation of our proposed localization system. First of all, we start by introducing the experimental setup and the detailed implementation methodology. Then, the results of localization performance will be discussed in the sequel.

3.3.1 Experimental Setup

3.3.1.1 Experimental Presentation

(a) **Environment**: The entire experiments are conducted in the CEDRIC laboratory of CNAM (a typical office environment in a multistorey building as shown in Figure 3.11). This lab office is a large room with an area of over $200m^2$. The indoor space is partitioned into several office and meeting rooms with many desks, chairs, computers, shelves furnished inside, which forms a complex radio propagation environment. The whole CSI database was collected during the working time in February, 2019.

(b) **Configuration**: We conduct our real experiments on commodity-ready off-the-shelf Wi-Fi devices [25]. Specifically, by working in the 5GHz band of IEEE 802.11n monitor mode, we use an HP Elitebook 8530w laptop as the signal transmitter (TX) and an HummingBoard Pro (HMB) as the mobile receiver (RX), which are exhibited in Figure 3.12 and Figure 3.13. Both devices are equipped with Intel Wi-Fi Link (IWL) 5300 NIC and run 64-bit Ubuntu 14.04 OS and Debian 8.0 OS, respectively. Additionally, for our antenna settings, each Wi-Fi device is equipped with three omni-directional antennas to support 3×3 MIMO configuration.

Figure 3.11: CNAM laboratory scenario.

(c) **Implementation**: As mentioned above, we implement the CSI data collection in our lab scenario. Figure 3.14 shows the floor plan of this $15m \times 15m$ laboratory with a main corridor alongside several office and meeting rooms. The HP laptop serving as signal transmitter is fixed on the table of the central office room. Under injection mode, it is designed to intermittently transmit at the rate of 100 packets per second using only one transmitting antenna. It is worth mentioning that one transmitter setting is highly sufficient and well-performed in this lab scenario. If necessary, we may resort to multiple transmitters for the future larger testbed. The blue dots shown in Figure 3.14 denote the 70 training reference points with one meter spacing and the 30 testing locations are marked as red stars. In the offline training phase, the CSI measurements are collected by the lightweight HMB at these reference points to build up the raw radio map. At each point, around 5000 CSI packets are stored as

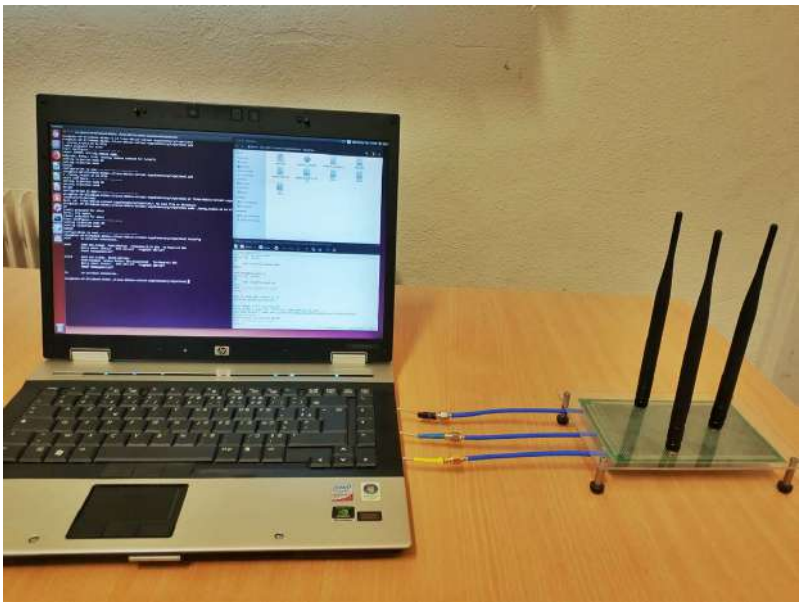

Figure 3.12: The laptop with Intel 5300 NIC as signal transmitter.

Figure 3.13: The HummingBoard Pro as mobile receiver.

RF signatures in the firmware. In the online phase, we then move the HMB receiver among 30 testing locations to obtain the same size of CSI packets. In addition, all receiver ends are placed at the same height, constructing a simple 2-D platform for the precise indoor position estimation.

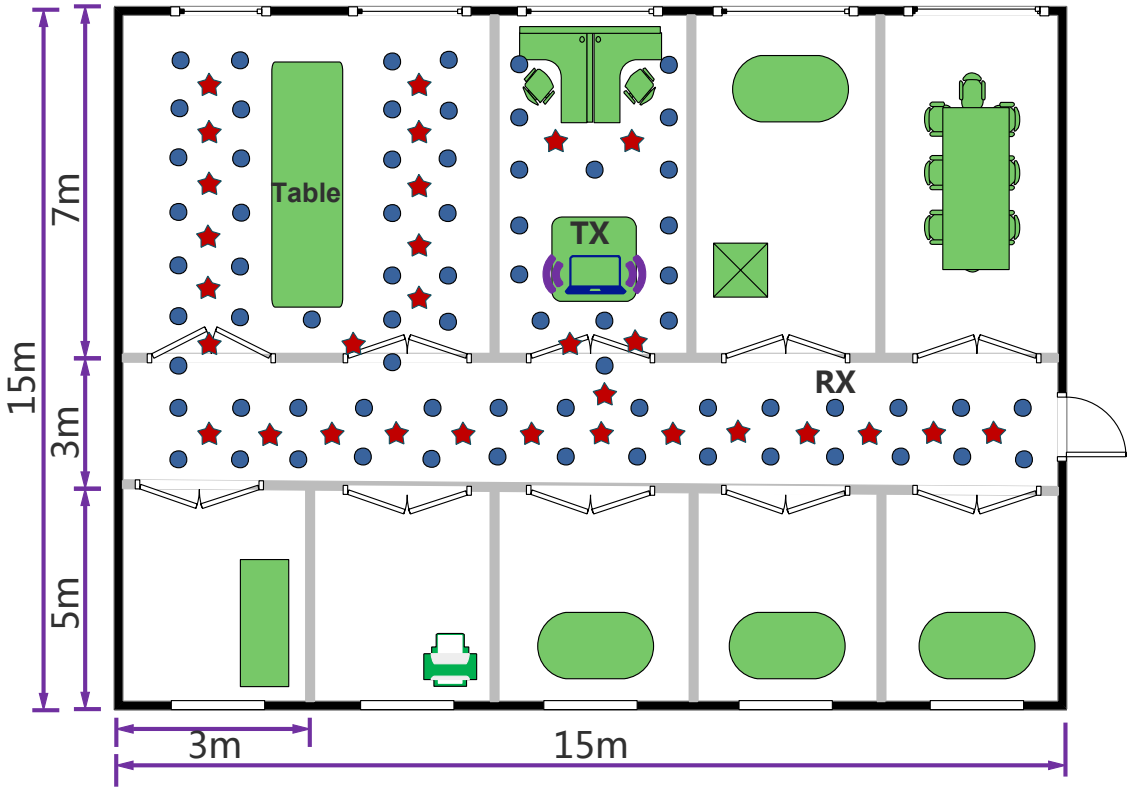

Figure 3.14: The floor plan of our laboratory.

3.3.1.2 Benchmarks and Performance Metrics

In this part, we evaluate three existing probabilistic fingerprint positioning systems for the comparison purpose. As discussed in the literature review section, these include Horus [28], FIFS [29] and PinLoc [30]. Considering that the original PinLoc system conducted war-driving procedure in a set of predefined $1m \times 1m$ grids, known as spots, in order to provide a fair comparison, we modify PinLoc to use the same training set that we use in the proposed EntLoc system.

As for performance metrics, we define the localization error as Euclidean distance between the estimated location and the mobile user's actual position, which is presented as $\|\widehat{\boldsymbol{\ell}}_o - \boldsymbol{\ell}_o\| = \sqrt{(\widehat{x}_o - x_o)^2 + (\widehat{y}_o - y_o)^2}$. When there are N_a testing locations, we evaluate the localization performance by using Mean Error (ME) metric which can be calculated

as

$$ME = \frac{1}{N_a} \sum_{i=1}^{N_a} \sqrt{(\widehat{x}_i - x_i)^2 + (\widehat{y}_i - y_i)^2} \tag{3.18}$$

where (x_i, y_i) and $(\widehat{x}_i, \widehat{y}_i)$ are the actual and estimated coordinates at the i^{th} testing location, respectively.

3.3.2 Numerical Results

In this section, we evaluate the experimental performance and provide numerical results with relevant discussions.

3.3.2.1 AR Entropy Property Study

Since AR modeling based CFR amplitude entropy is the cornerstone of our fingerprint localization system, prior to accuracy analysis, we first evaluate the following two key characteristics of our proposed AR entropy fingerprint in location fingerprinting.

Temporal Stability Practically, the channel response fluctuate frequently as the indoor environment varies over time. To investigate the robustness of our AR entropy based fingerprinting system, we design and implement a daytime measurement test in our lab. Specifically, the HummingBoard Pro was configured to periodically record CFR measurements at a fixed position from a transmitter placed in the next-door room from 9 a.m. to 5 p.m. during a busy working day. About 500 CFR packets were collected every 10 minutes. Indoor furniture remained static with several personnel in the vicinity moving around. Next, we divide the whole measurements into 100 groups and compute the AR entropy, averaged CFR amplitude and the corresponding RSS mean value, respectively. For the purpose of fair comparison, we normalize the three metrics in the same range. As shown in Figure 3.15, our AR entropy based fingerprint displays the lowest variance while the coarse-grained MAC layer RSS suffers the most severe fluctuations. It is reasonable that the environment changes do impact the time-varying channel response but cause less influence over its statistical entropy derivate.

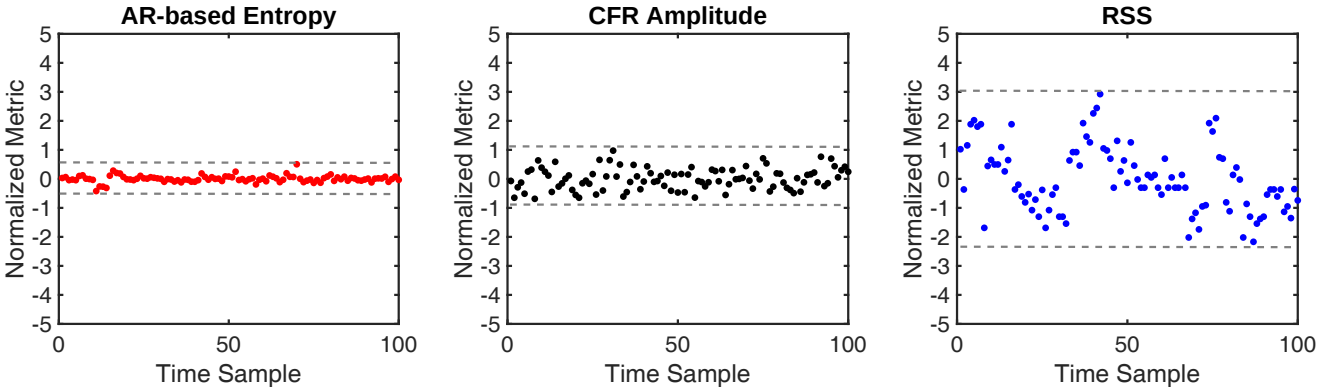

Figure 3.15: Temporal stability for three fingerprint signatures during the entire working times of one day (8 hours).

Spatial Proximity For indoor fingerprinting localization system, a good online signature is deemed to be qualified when it is capable of presenting similar trait with the offline signatures from the neighboring reference points. Based on the realistic testbed shown in Figure 3.14, we experimentally chose two testing locations which are under LoS and NLoS condition, respectively. At each location, the multi-dimensional estimated AR entropy from all three RX antennas is compared with the entropy vectors of the corresponding four neighboring RP positions. Results illustrated in Figure 3.16 demonstrate that for LoS test location #1, our AR modeling based entropy shows good spatial proximity with the fingerprints in the vicinity. For most subcarrier indices, the entropy value fits well in the center of its four neighbors. Especially for NLoS test location #2 in Figure 3.17, even though the neighboring entropies are relatively inconsistent (differ from different RX antennas), the overall multi-dimensional entropies at the center location can still capture the local minimal differences (Manhattan distance in our case) from its neighbors. This robust spatial property enables our AR modeling based entropy to be a strong candidate as fingerprint for most existing indoor positioning systems.

3.3.2.2 Localization Accuracy

This section provides a variety of numerical results in respect of localization accuracy, which firmly validates the superiority of our proposed localization system over other indoor geolocation schemes.

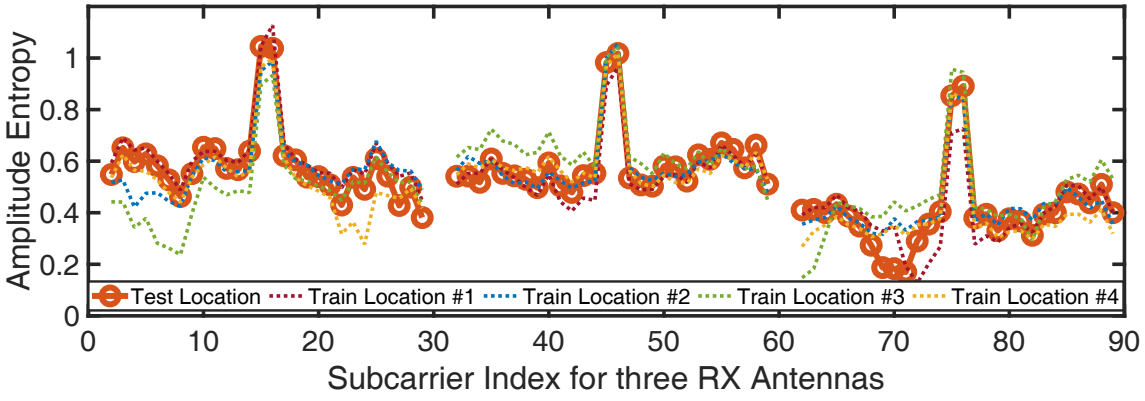

Figure 3.16: Proximity test under LoS condition.

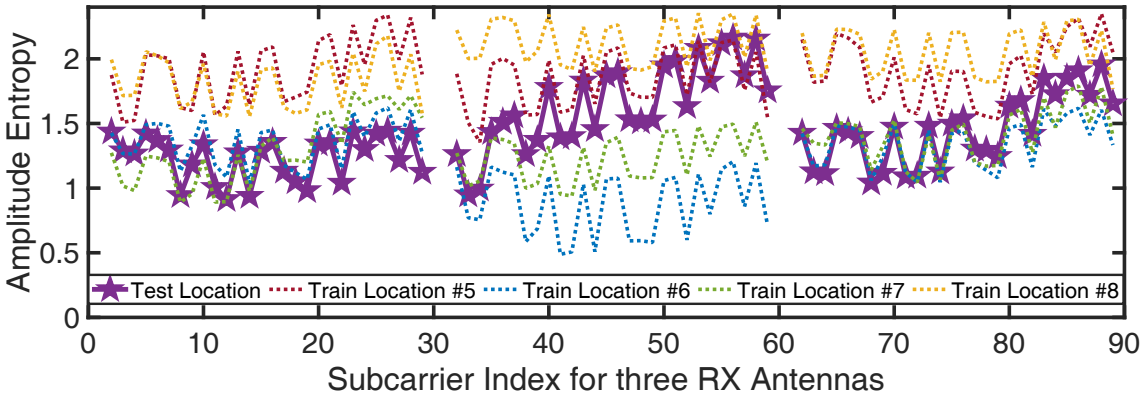

Figure 3.17: Proximity test under NLoS condition.

Comparison with CFR We begin the localization accuracy evaluation by comparing our proposed AR entropy fingerprint with its original CFR amplitude. It is worth mentioning that these two fingerprint schemes follow the same online protocol (i.e., using Manhattan distance as similarity metric and kernel regression to figure out user location). Figure 3.18 shows the CDF of localization errors for AR based entropy fingerprint and its original CFR amplitude. Specifically, our AR entropy approach shows a better performance with 90% positioning errors less than $2.69m$ while CFR amplitude signature can only reach the level of 50th percentile. The $1.84m$ ME of our proposed entropy scheme also precedes CFR amplitude based method whose mean sum error rises to $2.92m$. Since AR modeling based entropy accurately reflects the statistical distribution of the given CFR amplitudes, which unfortunately endure much more channel fluctuations, it can thus achieve better localization performance.

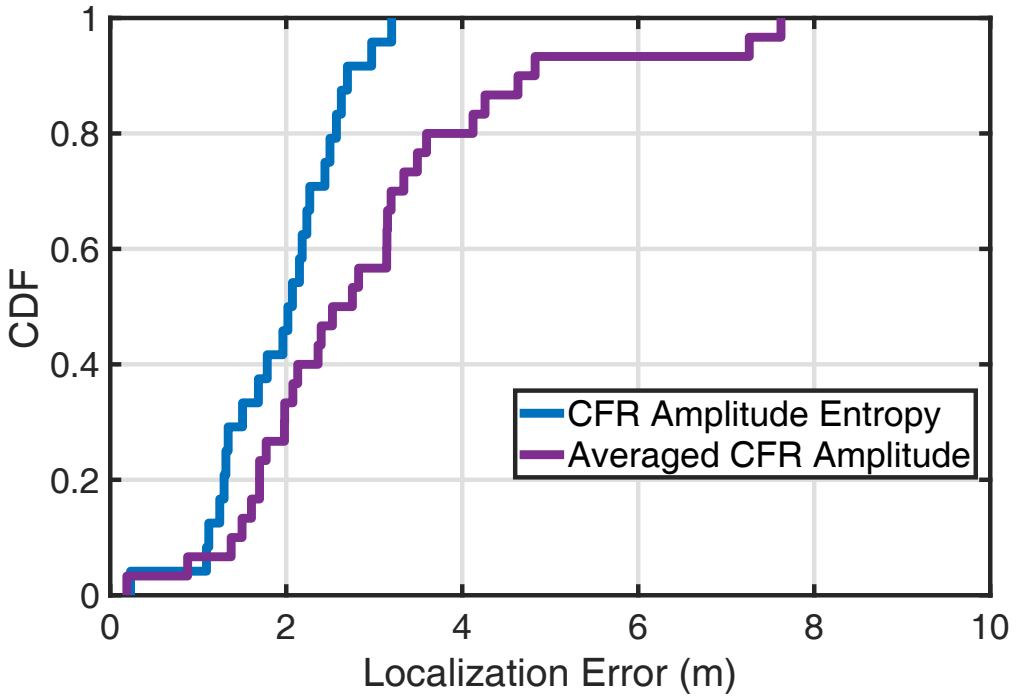

Figure 3.18: Localization accuracy of AR entropy against its original CFR amplitude.

Comparison with CIR Given that CIR is the inverse Fourier version of CFR, both of them should convey equivalent physical information. One may anticipate similar localization performance for these two channel response signatures. However, as shown in Figure 3.19, our AR entropy based scheme maintains less than 2.69 meters localization error with the probability of 0.9, which outperforms CIR amplitude based entropy with only 63% percentage of the same positioning error. Meanwhile, the mean error of the proposed CFR amplitude entropy scheme is $1.84m$, which is also superior over CIR entropy approach with the mean error of $2.64m$. A possible explanation would be that most variations of CIR distribute within only a few time indices (i.e., first 10 taps), while the frequency diversity spans the entire range of CFR subcarrier indices, making the structures of CFR more distinguishable with each other [18]. Moreover, as expected, CIR entropy based fingerprint has better location estimation precision than its original CIR amplitude signature. The former precedes around $1.2m$ localization error of the 90th percentile accuracy.

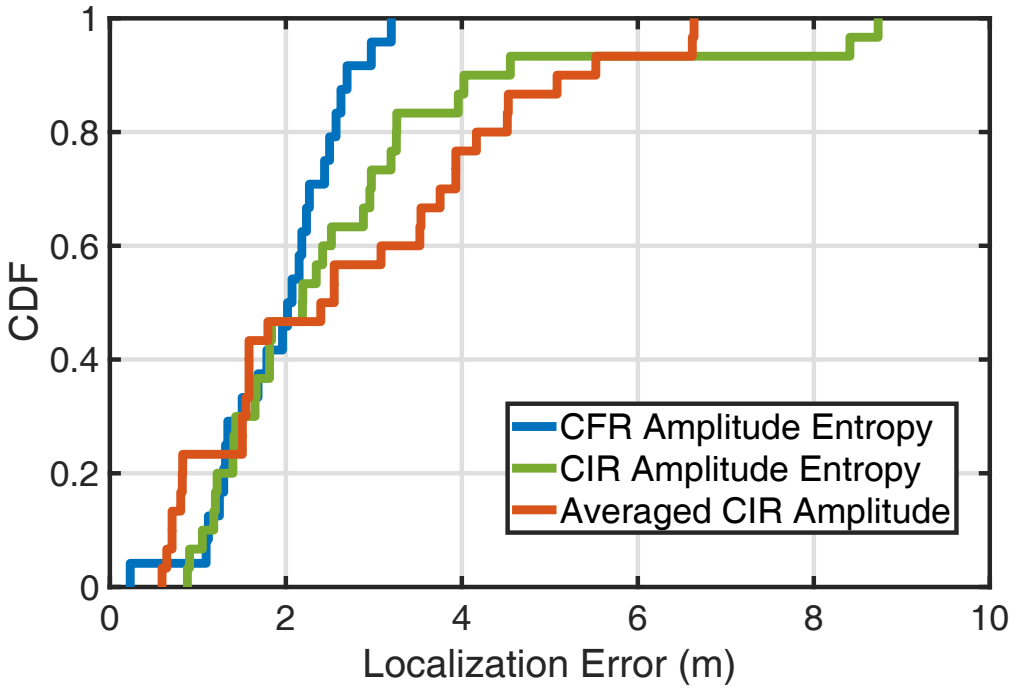

Figure 3.19: Localization accuracy of AR entropy against its time domain CIR.

Comparison with State-of-the-Art After comparing with the two most potential competitors, namely CFR and CIR amplitude schemes, our EntLoc system is then readily set to challenge other existing location fingerprinting systems. More specifically, as mentioned in previous section, we design a fair framework to compare our proposed AR entropy based localization approach with PinLoc-like, FIFS and Horus systems, respectively. As can be observed in Figure 3.20, our proposed system achieves the 90th percentile error of 2.69m, which outperforms PinLoc-like approach, FIFS and Horus with the same error level of 63%, 57% and 28%, respectively.

Additionally, in order to provide an in-depth and comprehensive comparison for these localization systems, we enumerate the respective maximum error (Max. err.), minimum error (Min. err.), mean error (Mean err.) and the 90th percentile accuracy (Acc. at 90%) in Table 3.1. Apart from the 90th percentile accuracy, our EntLoc system is able to achieve the lowest mean error of 1.84m compared with PinLoc-like, FIFS and Horus systems, improving the localization precision by 27.3%, 34.9% and 47.4%, respectively. As for maximum and minimum errors, EntLoc can still dominate the general accuracy

evaluation. It only falls behind FIFS with $0.08m$ in terms of minimum error, which can be neglected in realistic indoor environment.

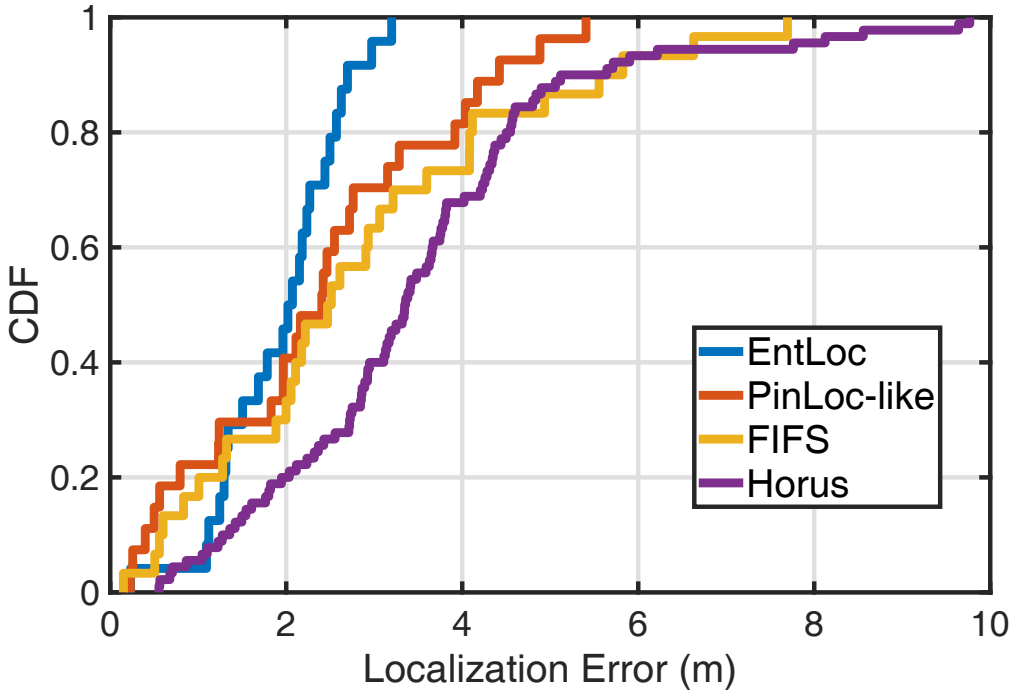

Figure 3.20: Localization accuracy of proposed EntLoc against state-of-the-art.

Table 3.1: Detailed localization accuracy of all different methods

Methods	Max. err.	Min. err.	Mean err.	Acc. at 90%
EntLoc	**3.20m**	0.23m	**1.84m**	**2.69m**
PinLoc-like	5.85m	0.46m	2.53m	4.15m
FIFS	7.70m	**0.15m**	2.83m	5.56m
Horus	9.77m	0.55m	3.50m	5.64m

3.3.2.3 Impact of Preprocessing Technique

Recall that we present a tap filtering based pre-processing technique before conducting location fingerprinting. Firstly the raw CFR measurements are converted into its time domain CIR by IFFT. Once removing irrelevant noise component in CIR, we can subsequently obtain a smoothed and finer version of CFR by applying FFT. It is interesting to study the impact of this approach to see how it can improve our localization performance.

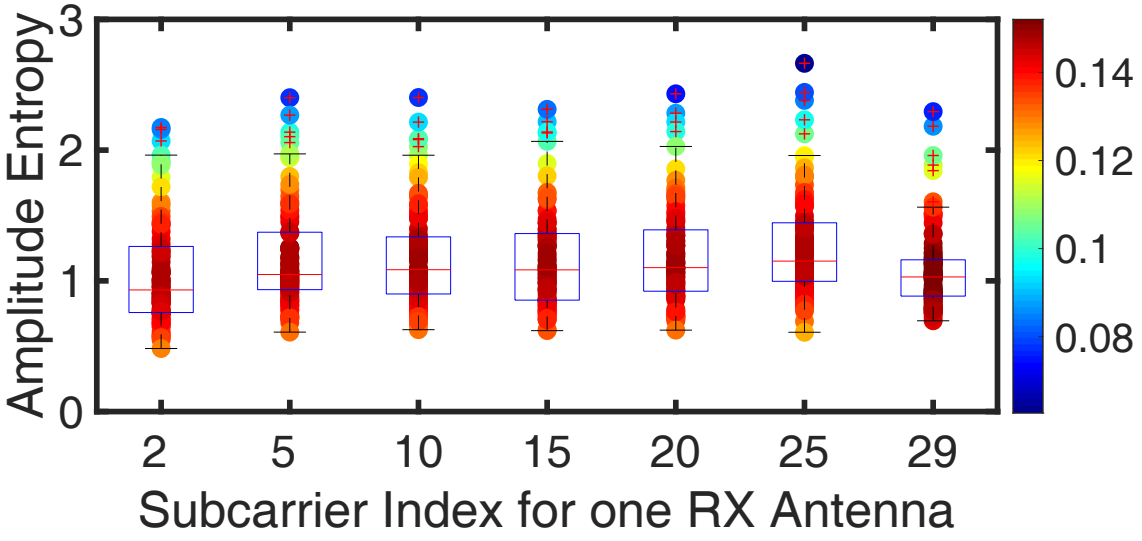

Figure 3.21: AR entropy box plot for raw CFR.

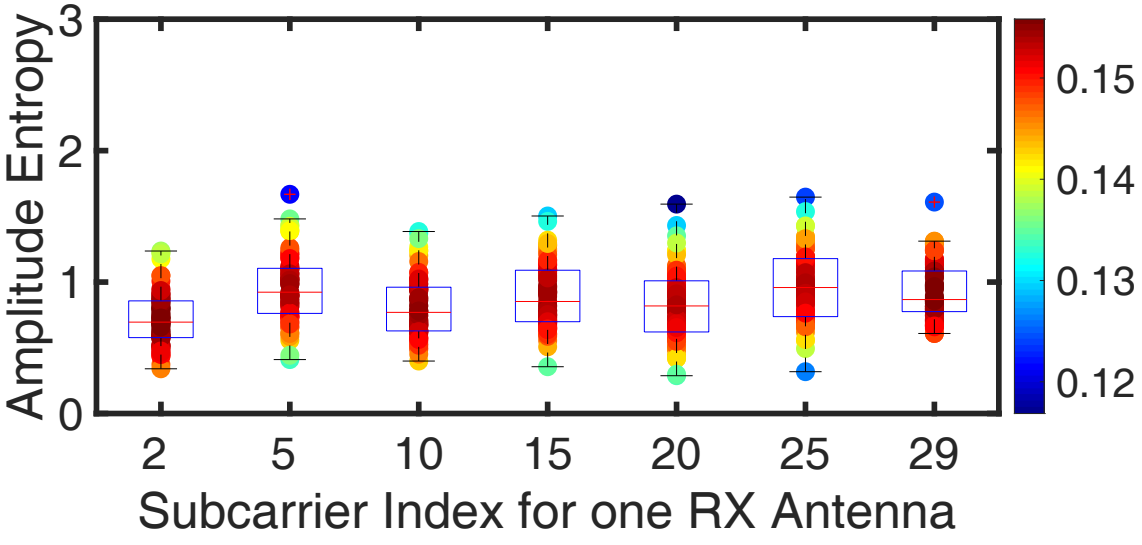

Figure 3.22: AR entropy box plot for filtered CFR.

To this end, we design a fingerprint robustness based evaluation scheme. In particular, we manually record 10000 raw CFR measurements at one predefined location. By taking into account three RX antennas, we divide these CFRs into 100 subgroups and calculate the AR entropy of their amplitudes for each subgroup. Afterwards, we conduct the same procedures on the filtered CFR measurements and lay out the differences. As displayed in Figure 3.21 and Figure 3.22, we show the AR entropy box plot of selected subcarriers from one RX antenna out of visual clarity. Specifically, the filtered CFR entropy achieves less variation and reduces the statistical outliers to a great extent.

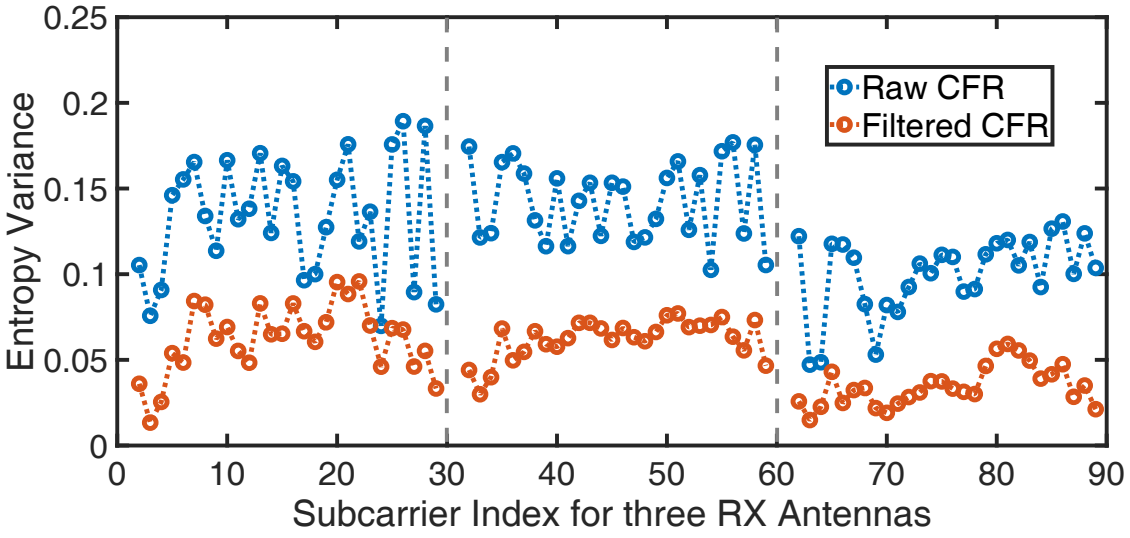

Figure 3.23: AR entropy variances for raw CFR and filtered CFR.

Furthermore, we can also observe from Figure 3.23 that for considering all three RX antennas, the filtered CFR entropy has an overall lower variance than its original raw CFRs. The above observations reveal that our pre-processing technique makes AR entropy based fingerprint more robust and can thus guarantee a preferable localization performance in the online location estimation phase.

3.3.2.4 Impact of Packet Number for Entropy Estimation

Since AR entropy estimation process requires sufficient CFR samples, larger number of samples can provide more accurate entropy estimation while increasing computational

complexity. How to determinate the CFR packet number for entropy calculation becomes a trade-off problem which needs to be balanced in our localization system. Here we devise an AR entropy variance based scheme to select the optimal number of CFR packets. The motive lies in the fact that if the entropy variance is small enough, which can already guarantee a good accuracy, there is no need to import more CFR samples to increase computational burden. To be more specific, by testing the packet number ranging from 10 to 5000, we observe in Figure 3.24 that 50 CFR packets can provide stable enough AR entropy estimates, which can further promote robust fingerprinting performance. So we choose and fix this packet number for all entropy estimation processes in our indoor positioning implementations.

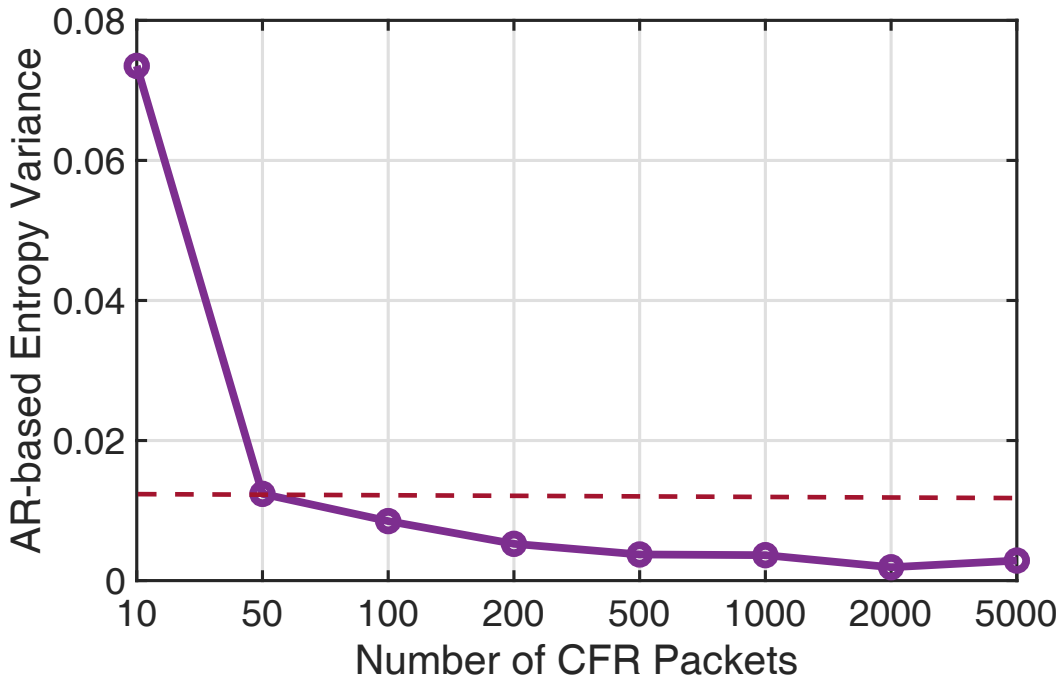

Figure 3.24: AR entropy variance changes with different CFR packet number selections.

3.3.2.5 Impact of RX Antenna Numbers

In this part, we study the impact of RX antenna number on the localization performance. Intuitively, using more antennas at receiver end brings about more diverse channel response measurements, thus containing more location-specific information. We then study

the localization accuracy differences for three RX antennas to deepen the understanding of our proposed localization system. As exhibited in Figure 3.25, our AR entropy based localization system with three RX antennas is able to obtain superior estimation error precision over the same platforms with less antennas. Numerically, the three-antenna configuration can achieve less than $2.69m$ localization error within the probability of 0.9, while the two and single antenna structures can only reach the same percentage level with the larger error of $4.1m$ and $5.2m$, respectively. It validates the aforementioned assumption and encourages us to make full use of all three RX antennas in our indoor location fingerprinting system.

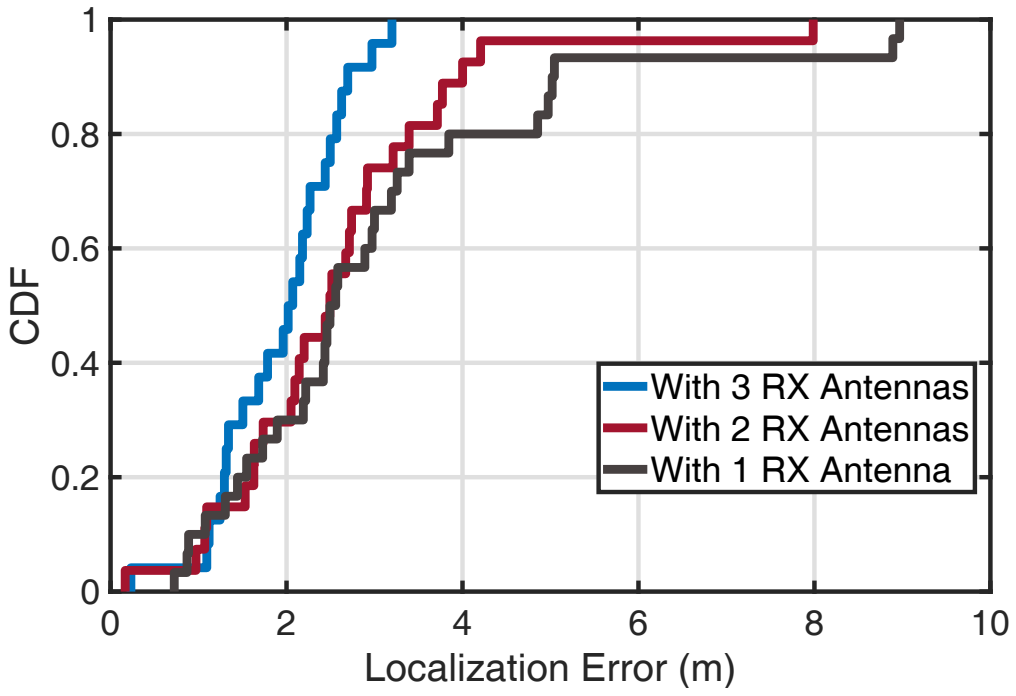

Figure 3.25: Localization accuracy under three different RX antenna configurations.

3.4 Summary

In this chapter, we presented EntLoc, an AR entropy based indoor location fingerprinting system using CSI amplitude information. In EntLoc, a tap filtering scheme was first utilized to remove the noisy component in raw CFR measurements. To capture the most informative statistical information of CFR while maintaining a simple structure, we adopted AR modeling based entropy as the fingerprint to construct a robust offline radio map. In the online phase, we proposed to use Manhattan distance as similarity metric and resorted to kernel regression scheme to infer the target's location. Experimental results from the lightweight HummingBoard device showed a superior localization performance of our proposed EntLoc system with an average accuracy improvement of 27.3%, 34.9% and 47.4%, in comparison with prominent PinLoc, FIFS and Horus system, respectively. In addition, we also examined the impacts of several different parameters on EntLoc's performance, which enables us with deepening insights to efficiently and productively implement our proposed localization system.

Chapter 4

Enhanced AoA-aware Fingerprint Localization involving CSI Phase

Contents

4.1 Introduction

As an updated version of the previous EntLoc system, in this chapter, we bring out AngLoc, an enhanced AR entropy based indoor location fingerprinting system involving an additional AoA fingerprint. The resulting localization accuracy has been elevated in comparison with EntLoc.

Likewise, after reviewing the state-of-the-art, we put forward the in-depth localization methodology of proposed AngLoc. We also add more experimental testbeds for the performance evaluation and provide some visionary perspectives in order to further improve AngLoc's localization performance in the future works.

4.1.1 State-of-the-Art

Since the biggest design highlight of the AngLoc localization system is that the geometric concept of AoA-aware directional RP refining further enhances the positioning accuracy. We ought to involve some geometric mapping based techniques in the state-of-the-art presentation. Additionally, given that we have conducted comprehensive literature review of the current location fingerprinting schemes in Chapter 3, in this chapter, we will further supplement some recent advancements to the current literature framework.

Geometric Mapping based Techniques: The geometric modeling of the RF propagation is fundamental to the ranging or direction based positioning systems. Wu et al. explored the frequency diversity of PHY layer CSI information to refine distance estimation and pinpoint the target's location through trilateration in FILA system [104], which achieved median accuracy of 1.2 m in the multi-room environment. Alternatively, ArrayTrack [105] embraced the trend of MIMO technology and exploited increased number of antennas at commodity access points (APs) to obtain high-resolution AoAs, which were further aggregated to infer the client location within 23 centimeters median accuracy. Unlike ArrayTrack which requires dedicated hardware modifications, Kotaru et al. designed SpotFi [20], an accurate indoor localization system capable of identifying direct path AoAs with only three physical RX antennas. Moreover, after incorporating the observed RSS infor-

mation for an optimization processing, SpotFi was able to achieve the median accuracy of 40 cm. More recently, the researchers of Chronos [106] leveraged a novel Chinese remainder theorem based algorithm to compute sub-nanosecond ToF with a single Wi-Fi access point. This distance-related metric was then formulated into a quadratic optimization problem for accurately locating clients within tens of centimeters.

Recent Fingerprinting based Techniques: Regardless of measurements' geometric relation, the pattern-matching based fingerprinting techniques have attracted a large body of research interests for the last decades. Wang et al. designed DeepFi [107], a deep learning based indoor location fingerprinting system using CSI amplitude information. In the offline phase, DeepFi enabled a deep network to train all the weights as location fingerprints, and harnessed the Radial Basis Function (RBF) based probabilistic scheme to accomplish the position estimation in the online phase. It outperformed FIFS system with 20% accuracy improvement.

4.1.2 Contributions

Prior to listing the relevant contributions of this chapter, in comparison with the aforementioned EntLoc system, we first elaborate the core concept and the major upgrade of our proposed AngLoc positioning system.

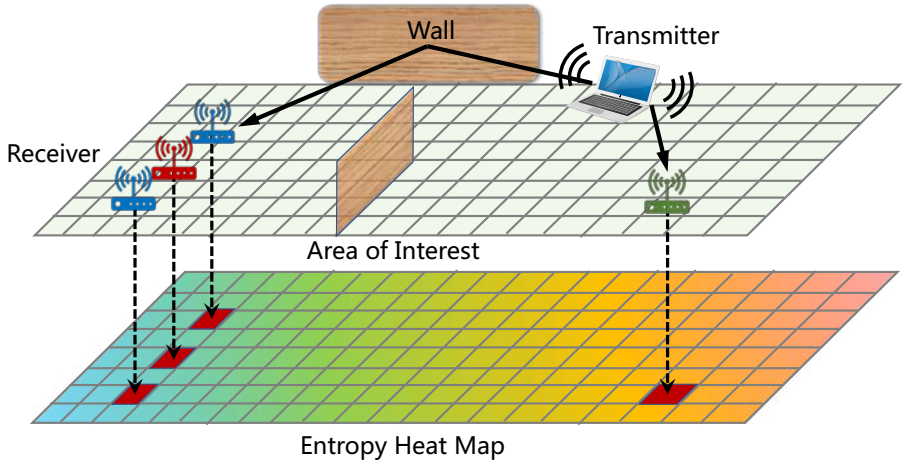

Figure 4.1: An illustrative example of the AngLoc system mechanism.

As illustrated in Figure 4.1, our AoA embedded solution adopts the methodological concept of the well-known k-Nearest Neighbors (kNN) technique and unveils two heuristic insights:

(i) For some offline surveying receivers at the corresponding RP positions, whether they are in the vicinity (blue ones) of the online receiver (red one) or in the distance (green one), their CSI measurements may share the similar entropy values.

(ii) These neighboring receivers also record the similar AoAs from parallel incident paths with this online receiver, whether it is for direct paths in LoS scenario or reflected paths in NLoS condition. Hence, the remote receiver can be selectively ruled out in accordance with the distinct AoA difference, which further improves the location estimation accuracy.

Accordingly, by adopting the above AoA aided RP refining approach, our inherited AngLoc positioning system is capable of achieving superior localization performance over its predecessor EntLoc system.

In a nutshell, the main contributions of this chapter can be laid out as follows:

- To the best of our knowledge, this is the first work to constructively incorporate angular signature in CSI entropy based indoor location fingerprinting system, fertilizing the opportunity to achieve a decimeter-level accuracy.
- We propose a power-based tap-filtering program alongside several phase calibration pre-processing techniques to effectively mitigate CSI noisy component and sanitize CSI phase errors, respectively.
- We design a feasible bivariate kernel regression scheme for the online location estimation stage, which organically combines the weighting factors for both amplitude based entropy and phase-based AoA fingerprints.
- Compared with EntLoc's performance evaluation, we further build and implement extensive experiments on the lightweight Hummingboard device for different testbeds.

In addition to the superior performance, our mobile prototype remarkably enhances the fingerprinting efficiency.

4.1.3 Chapter Organization

The remainder of this chapter is organized as follows. The overall architecture design of our proposed system is elaborated in Section 4.2. We provide experimental results and the corresponding analyses in Section 4.3 and dive into some insightful perspectives in Section 4.4. Conclusions are drawn in Section 4.5.

4.2 Localization Methodology

In this section, we proceed to lay out the detailed design of our proposed AngLoc fingerprint localization system.

4.2.1 AngLoc System Architecture

As illustrated in Figure 4.2, the overall architecture of our proposed AngLoc system has a block-wise design. To be specific, in the offline radio map construction block, once recording the raw CSI measurements through war-driving, we first introduce a tap filtering scheme to extract the most informative location-specific component from noisy CSIs. For the purpose of accurate AoA estimation, several phase calibration techniques are then leveraged to compensate the corresponding phase offsets, which exist in prevalent commodity WiFi devices. Subsequently, for CSI amplitudes, we statistically model them as the simply structural AR entropy metric. The JADE-MUSIC algorithm is then adopted for CSI phases to infer the angular estimates. Hence, the entire offline database can be fully embodied by the integration of entropy and AoA fingerprints, making full use of both CSI amplitude and phase information. For the online location estimation block, when a mobile target enters the area of interest, it executes the same pre-processing protocols to obtain the entropy and AoA estimates. The following location estimation task then consists of two major steps:

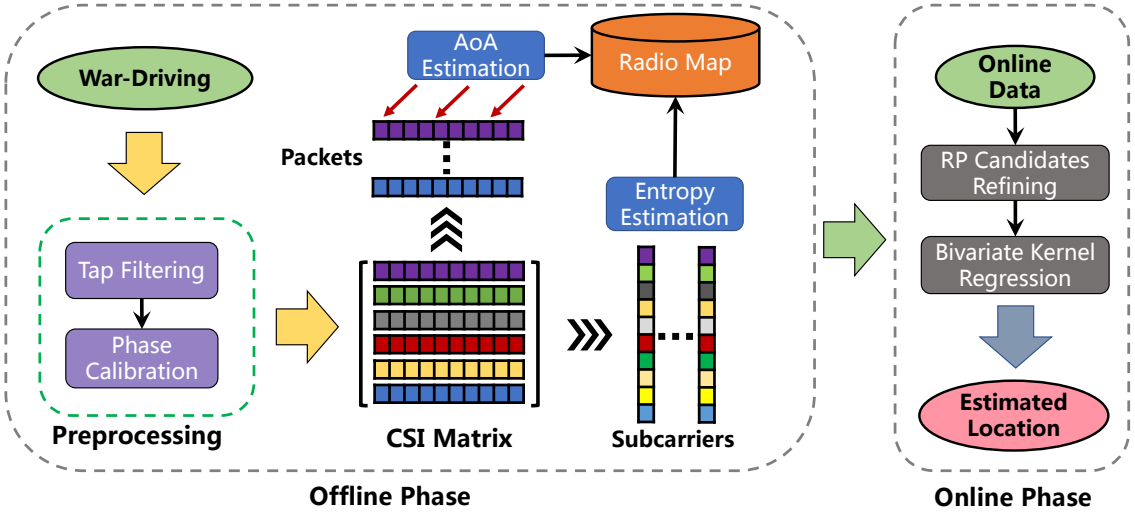

Figure 4.2: The overall AngLoc system architecture.

(i) The online entropy vector is first matched with offline database to find the most likely candidates from nearest RP positions.

(ii) Among these candidate locations, a novel bivariate kernel regression scheme is proposed to further narrow down the number of error-prone RPs, thus tackling the target's location determination with an improved accuracy.

In the sequel, we will take an in-depth structural dissection for each block of our proposed AngLoc system.

4.2.2 Offline Fingerprint Database Generation

For the offline training phase, we adopt the same problem formulation as presented in Chapter 3. Specifically, after acquiring the respective offline and online fingerprint data sets $\{\boldsymbol{\mathcal{H}}_m\}_{1\leq m\leq M}$ and $\boldsymbol{\mathcal{G}}_o$, the mobile target's position can be then determined as $\widehat{\boldsymbol{\ell}_o}$ by exploiting these online CSIs and the stored offline database.

4.2.2.1 CSI Phase Calibration

In this part, we focus on some technical details of CSI pre-processing techniques which serve as the precondition to attain superior localization performance.

Due to the inherent OFDM baseband operations and the hardware's imperfect signal processing, the CSI obtained from the commodity Wi-Fi devices is distorted with various errors [19, 9, 108], rendering the accurate AoA and ToF estimation much more challenging. For a transmission chain, the phase measurement $\angle\widehat{H}_{f_k}$ for subcarrier k with carrier frequency f_k can be presented as

$$\angle\widehat{H}_{f_k} = \angle H_{f_k} + 2\pi f_\delta k(\zeta_{\mathbf{csd}} + \xi_{\mathbf{sfo}}) + \varphi_{\mathbf{sto}} + \varphi_{\mathbf{cfo}} + \varphi_{\mathbf{cpo}} + Z \tag{4.1}$$

where $\angle H_{f_k}$ denotes the true phase from wireless propagation. f_δ is the OFDM subcarrier spacing. $\zeta_{\mathbf{csd}}$, $\xi_{\mathbf{sfo}}$, $\varphi_{\mathbf{sto}}$, $\varphi_{\mathbf{cfo}}$ and $\varphi_{\mathbf{cpo}}$ are the phase errors caused by Cyclic Shift Diversity (CSD), Sampling Frequency Offset (SFO), Symbol Timing Offset (STO), Carrier Frequency Offset (CFO) and Carrier Phase Offset (CPO), respectively. Z signifies the additive measurement noise. In the following, we will address these deep-rooted CSI phase issues in a divide-and-conquer manner.

- CSD: As described in Chapter 2, CSD is operated by sending cyclically shifted OFDM symbols over different TX antennas so that unintended beamforming is avoided. But this incurs an additive phase shift for each TX antenna in CSI matrix which potentially degrades the localization performance. SignFi [109] compensated the CSD errors by applying a multiple linear regression scheme. However, as a easier alternative suggested in [19], CSD can always be removed by the receiver when direct mapping takes place, under which the SMM equals an unitary matrix. Hence, in our data acquisition process, we can configure the Intel 5300 shipset to make $N_{ss} = N_t$, thus yielding the CSD-free CSIs.

- SFO: In OFDM transceiver system, SFO occurs when the receiver's ADC sampling rate differs from the transmitter's synthesization rate. Consequently, SFO manifests itself as an additive phase shift proportional to the subcarrier index, which gives rise to the first-order channel linearity (e.g. Figure 4.3). We then resort to a simple linear regression method to remove the residual SFO. It can be mathematically expressed as follows.

$$\widehat{\xi}_{\mathbf{sfo}} = \arg\min_{\rho} \sum_{k,n_t,n_r} (\varphi^k_{n_t,n_r} + 2\pi f_\delta k\rho + \omega)^2 \tag{4.2}$$

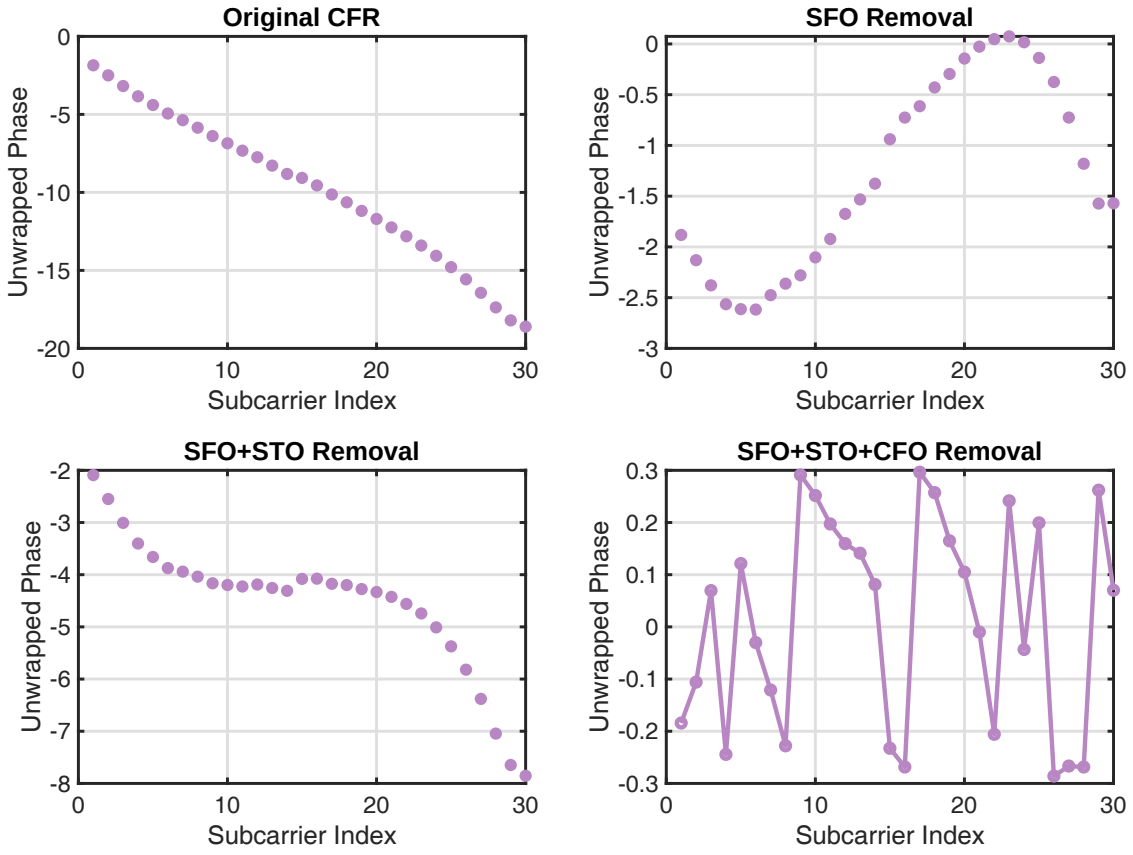

Figure 4.3: CFR phase changes after SFO, STO and CFO removal.

where ρ and ω are curve fitting variables and $\varphi^{k}_{n_t,n_r}$ denotes the unwrapped CSI phase for one packet at the k^{th} subcarrier from n_t^{th} TX antenna to n_r^{th} RX antenna, $n_t \in [1, N_t]$ and $n_r \in [1, N_r]$.

- STO: In general, the receiver utilizes the auto/cross-correlator to capture and detect the presence of the OFDM symbol header, which starts with short training fields. However, the length limitation of these STFs brings great uncertainty to determine the symbol boundary. This results in the irreversible STO. Fortunately, given that any frequency domain phase shift due to STO leads to the same amount of circular rotation in time domain, STO can be embodied as peaks at the far end of Power Delay Profile (PDP) owing to the CIR's cyclic-shifting property (e.g. Figure 4.4). On this basis, in order to estimate STO, we first derive the PDP from the CIR vector, i.e. $\{h_k(n)\}_{1\leq k\leq K}$ of the n^{th} packet. The corresponding tap index $N_{sto}(n)$

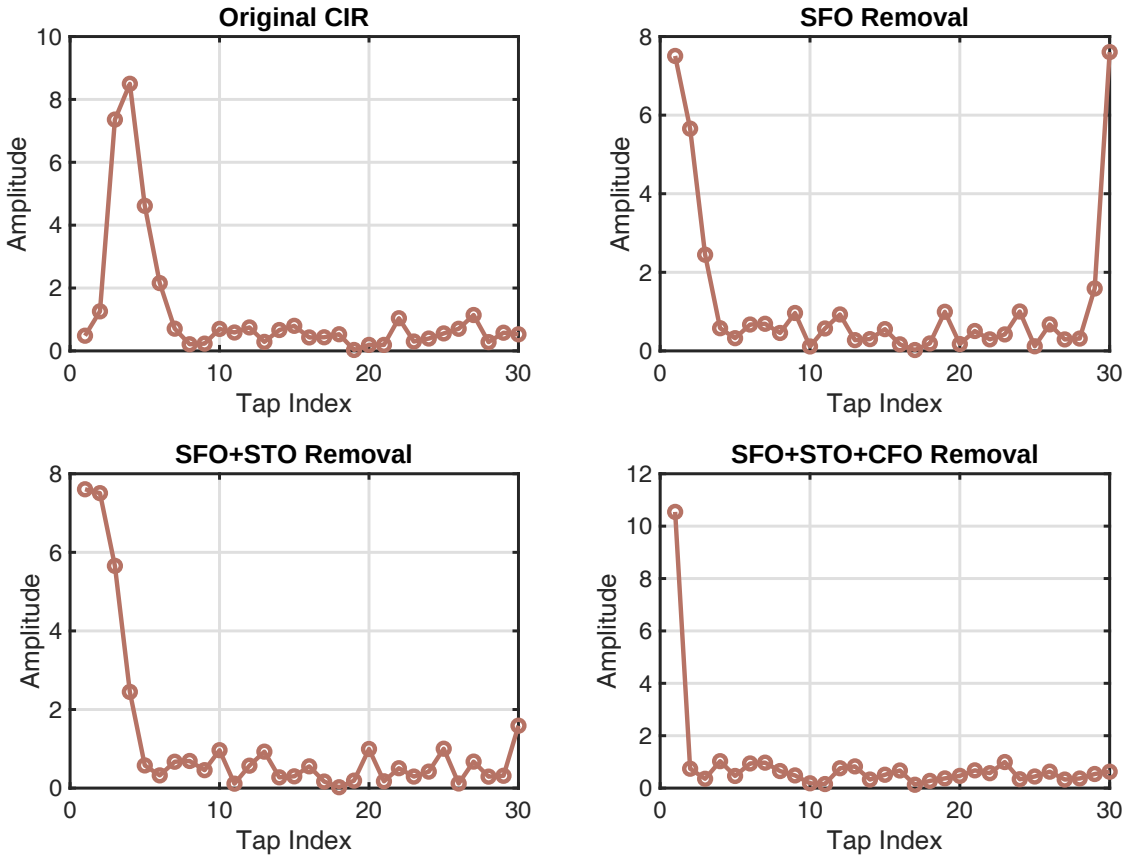

Figure 4.4: CIR amplitude changes after SFO, STO and CFO removal.

of the shifted PDP peak due to STO can be identified as

$$N_{sto}(n) = \arg\max_{k} |h_k(n)|^2, 1 < k \leq K \tag{4.3}$$

After applying (4.3) for multiple packets, the most frequent value of N_{sto} is then determined to finally shape the estimated STO as $\widehat{\varphi}_{\mathbf{sto}} = -2\pi k N_{sto}/K$.

- CFO/CPO: Due to the residual errors in receiver's Phase Locked Loop (PLL), CFO emerges when the receiver's carrier frequency for down-conversion mismatches with the transmitted carrier frequency. Meanwhile, since each time when the synthesizer restarts, a random initial phase will be generated by the receiver's voltage controlled oscillator and PLL cannot fully compensate for this phase difference, CPO is then experienced. According to [19], after the PDP-based STO removal, the ToF estimation becomes naturally immune to CPO. Additionally, during our site survey, we

only initiate the transceiver devices for once, which makes CPO negligible in our fingerprinting system. As CFO is also an accumulative error that has to be compensated by the receiver, we then employ a non-overlapping moving window with length N_p for geometric averaging to further smooth out CFO. Specifically, we first obtain K-dimensional $\bar{\mathbf{H}}$ by conducting element-wise multiplication for N_p packets.

$$\bar{\mathbf{H}} = \mathbf{H}(1) \circ \cdots \mathbf{H}(n_p) \cdots \mathbf{H}(N_p), n_p \in [1, N_p] \tag{4.4}$$

where $\circ$ denotes the Hadamard product operator and $\mathbf{H}(n_p)$ is the n_p^{th} CFR packet. The sanitized CFR can be then acquired by $\widehat{\mathbf{H}} = \{(\bar{H}_k)^{\frac{1}{N_p}}\}_{1 \leq k \leq K}$.

As illustrated in Figure 4.3 and Figure 4.4, the above adopted phase calibration techniques have effectively compensated CSI phase errors after the respective SFO, STO and CFO removal.

4.2.2.2 Enhanced AoA Fingerprint Estimation

After the noise removal and phase sanitization, the pre-processed CSIs then proceed readily to establish a self-contained fingerprint database which involves both amplitude and phase information.

For considerable wireless location-aware applications, accurate AoA measurement is non-trivial on commodity devices. In view of the super-resolution advantage, the classical subspace-based MUSIC algorithm is of the greatest appeal. The basic idea of standard MUSIC algorithm is that incident signals from different bearings give rise to different phase changes on each antenna at the receiver [42].

Assume that there are L incoming signals $\gamma_1, \ldots, \gamma_L$ arriving from directions $\theta_1, \ldots, \theta_L$ at N_r RX antennas of a linear array. The RX antennas are evenly-spaced with a distance d, which is about half of the signal's wavelength. As shown in Figure 4.5, for the l^{th} signal ($l \in [1, L]$), a phase difference of $-2\pi f d sin(\theta_l)/c$ is introduced at two adjacent antennas, where f is the signal frequency and c denotes the speed of light. For the whole antenna array, we can thereby define these phase shifts relative to the first antenna as the following

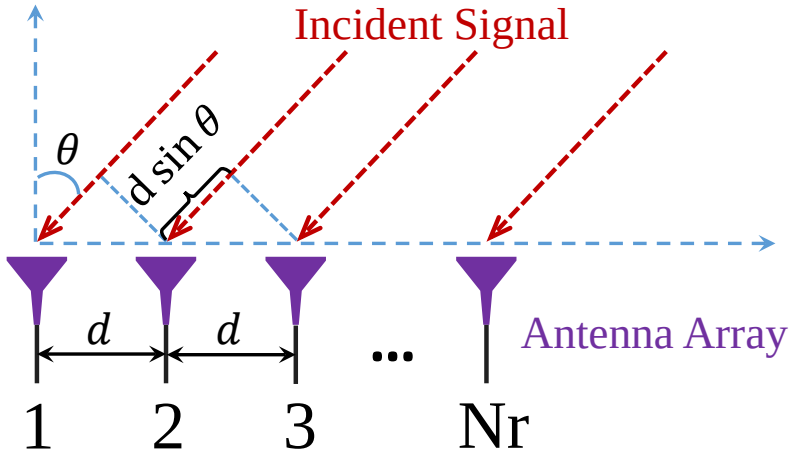

Figure 4.5: An incident signal arrives at an antenna array with an angle θ.

steering vector.

$$\mathbf{\Psi}(\theta_l) = [1, e^{-j2\pi f d \sin(\theta_l)/c}, \ldots, e^{-j2\pi(N_r-1) f d \sin(\theta_l)/c}]^\top \tag{4.5}$$

where $(\cdot)^\top$ is the transpose operator. Given all L incident signal paths, the $N_r \times L$ steering matrix is then constructed by $\mathbf{Q} = [\mathbf{\Psi}(\theta_1), \mathbf{\Psi}(\theta_2), \ldots, \mathbf{\Psi}(\theta_L)]$. Thus, the received signal x at each RX antenna can be expressed as the superposition of all L signal paths.

$$[x_1, x_2, \ldots, x_{N_r}]^\top = \mathbf{Q}[\gamma_1, \gamma_2, \ldots, \gamma_L]^\top + \mathbf{W}$$

or

$$\mathbf{X} = \mathbf{Q\Gamma} + \mathbf{W} \tag{4.6}$$

where $\mathbf{W}$ is the noise vector.

Note that there is an inherent constraint when applying the conventional MUSIC algorithm to Equation (4.6), which requires array antennas should outnumber the resolvable incident multipaths (i.e. $N_r > L$). However, in typical indoor environments, there are about 5-10 dominant multipath clusters [110] while our commodity Intel 5300 NIC only supports up to $N_r = 3$ antennas. This means it can merely capture 2 incident paths through MUSIC, thus largely limiting the AoA resolution and severely deteriorating the fidelity of the MUSIC outcome. To overcome this bottleneck, we leverage the fact that alongside AoA-related phase shifts across physical antennas, the incoming signals also invite phase differences across equispaced OFDM subcarriers due to ToF [20, 43]. Therefore,

we further extend the N_r-antenna physical array to a virtual sensor array with the size of $K \cdot N_r$, by which JADE-MUSIC algorithm can be readily employed to exploit CSI phase information in two dimensions. Specifically, the second steering vector which contains phase shifts relative to the first subcarrier can be defined as follows.

$$\mathbf{\Omega}(\tau_l) = [1, e^{-j2\pi f_\delta \tau_l}, \ldots, e^{-j2\pi(K-1) f_\delta \tau_l}]^\top \tag{4.7}$$

where τ_l is the time delay of the l^{th} path and f_δ is the two adjacent subcarrier spacing. Accordingly, the combined AoA-ToF steering vector can be updated by

$$\mathbf{a}(\theta_l, \tau_l) = \mathbf{\Psi}(\theta_l) \otimes \mathbf{\Omega}(\tau_l) \tag{4.8}$$

where $\otimes$ denotes the Kronecker product. After aggregating all L signal multipaths, the corresponding $KN_r \times L$ steering matrix is thereby presented as

$$\mathbf{A} = [\mathbf{a}(\theta_1, \tau_1), \ldots, \mathbf{a}(\theta_l, \tau_l), \ldots, \mathbf{a}(\theta_L, \tau_L)] \tag{4.9}$$

Hence, the received signals at RX antennas in Equation (4.6) can be rewritten by

$$\bar{\mathbf{X}} = \mathbf{A}\mathbf{\Gamma} + \bar{\mathbf{W}} \tag{4.10}$$

Next, we then move to apply JADE-MUSIC by first deriving the covariance matrix $\mathbf{R}_X$ of the received signal, which is calculated as

$$\mathbf{R}_X = \mathbb{E}\{\bar{\mathbf{X}}\bar{\mathbf{X}}^H\} = \mathbf{A}\mathbf{R}_S\mathbf{A}^H + \sigma_W^2\mathbf{I} \tag{4.11}$$

where $(\cdot)^H$ and $\mathbb{E}\{\cdot\}$ demotes the Hermitian transpose and expectation operator, respectively. $\mathbf{R}_S$ is the noise-free covariance matrix of the complex signal vector and σ_W^2 indicates the noise variance. Among $K \cdot N_r$ eigenvalues of $\mathbf{R}_X$, the smallest $(KN_r - L)$ eigenvalues represent the noise and the remaining L eigenvalues correspond to L incident signals. The eigenvectors corresponding to these smallest eigenvalues then form the noise subspace $\mathbf{E}_N$. Since the signal subspace and noise subspace are orthogonal, the spatial pseudo-spectrum function can be expressed as follows.

$$P(\theta, \tau) = \frac{\mathbf{a}^H(\theta, \tau)\mathbf{a}(\theta, \tau)}{\mathbf{a}^H(\theta, \tau)\mathbf{E}_N\mathbf{E}_N^H\mathbf{a}(\theta, \tau)} \tag{4.12}$$

By searching on the 2-D angle and delay continua, the sharp peaks in $P(\theta, \tau)$ will occur at the bearings of incident signals with their corresponding time delays.

Forward-Backward Spatial Smoothing In practice, subspace techniques like MUSIC also require the signal covariance matrix $\mathbf{R}_S$ has full rank. However, our stacked CSI measurements $\bar{\mathbf{X}}$ from all the subcarriers at all RX antennas is just a single column unit rank matrix. Due to the coherence of multiple signals, all subspace based methods suffer complete failure from the rank deficiency of $\mathbf{R}_S$. To address this issue, we propose to apply forward-backward spatial smoothing to mitigate the random noise and further improve the joint AoA-ToF estimation performance [111].

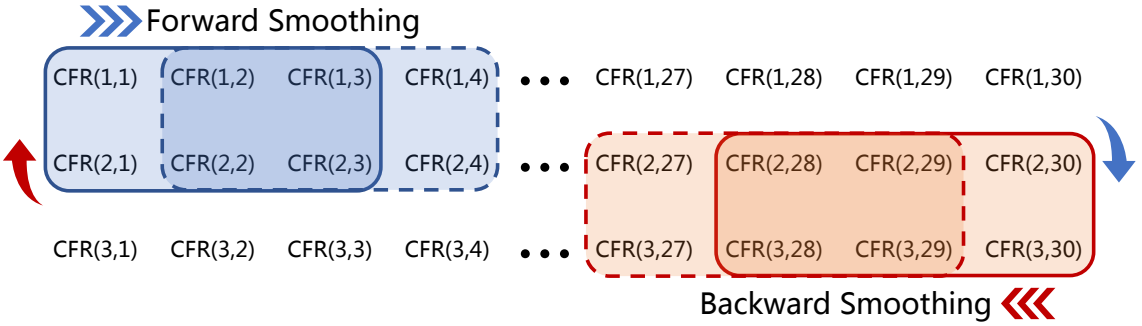

Figure 4.6: The mechanism of forward-backward spatial smoothing.

As shown in Figure 4.6, after reshaping the single measurement vector to the $N_r \times K$ CSI matrix, we first partition the CSI matrix into uniformly overlapping subarrays with the size of $K'N'_r$, where K' and N'_r are the number of subcarriers and antennas in the subarray, respectively. To ensure measurable phase shifts across RX antennas, here N'_r is fixed as 2 in our case. The total number of overlapping subarrays is then $T_K T_N$, where $T_K = K - K' + 1$ and $T_N = N_r - N'_r + 1$. In the sequel, a hardened spatially smoothed covariance matrix can be derived by averaging across those subarrays' covariance matrices with a forward direction (blue arrow). It is defined as follows.

$$\mathbf{R}_f = \frac{1}{T_K T_N} \sum_{i=1}^{T_K T_N} \mathbf{R}_s^i \tag{4.13}$$

where $\mathbf{R}_s^i$ is the covariance matrix of the i^{th} subarray. This covariance hardening processing achieves an improved rank, thus closer to the true source covariance matrix. Moreover, the invariant structure of CSI also enables a backward directional smoothing (red arrow) to further enhance the accuracy of MUSIC estimator. This averaged forward-backward

covariance matrix can be expressed as

$$\mathbf{R}_{fb} = \frac{1}{2}(\mathbf{R}_f + \mathbf{J}\mathbf{R}_f^*\mathbf{J}) = \frac{1}{2}(\mathbf{R}_f + \mathbf{R}_b) \tag{4.14}$$

where $\mathbf{J}$ is the $K' \times K'$ exchange matrix with only ones on its anti-diagonal and $\mathbf{R}_b$ denotes the backward covariance matrix.

Optimal Smoothing Length Selection Note that SpotFi only treats smoothed CSI matrix with a fixed smoothing length of $K'N'_r = 30$, which fails to dive deeper into the optimal selection of the smoothing length. As the smoothing length decreases, the noise level in estimated AoA spectrum gets lower, which helps to narrow the peak and improve the accuracy. But in the meantime, this also reduces the effective antenna sensors, which increases the risk of eliminating the peak from the direct path.

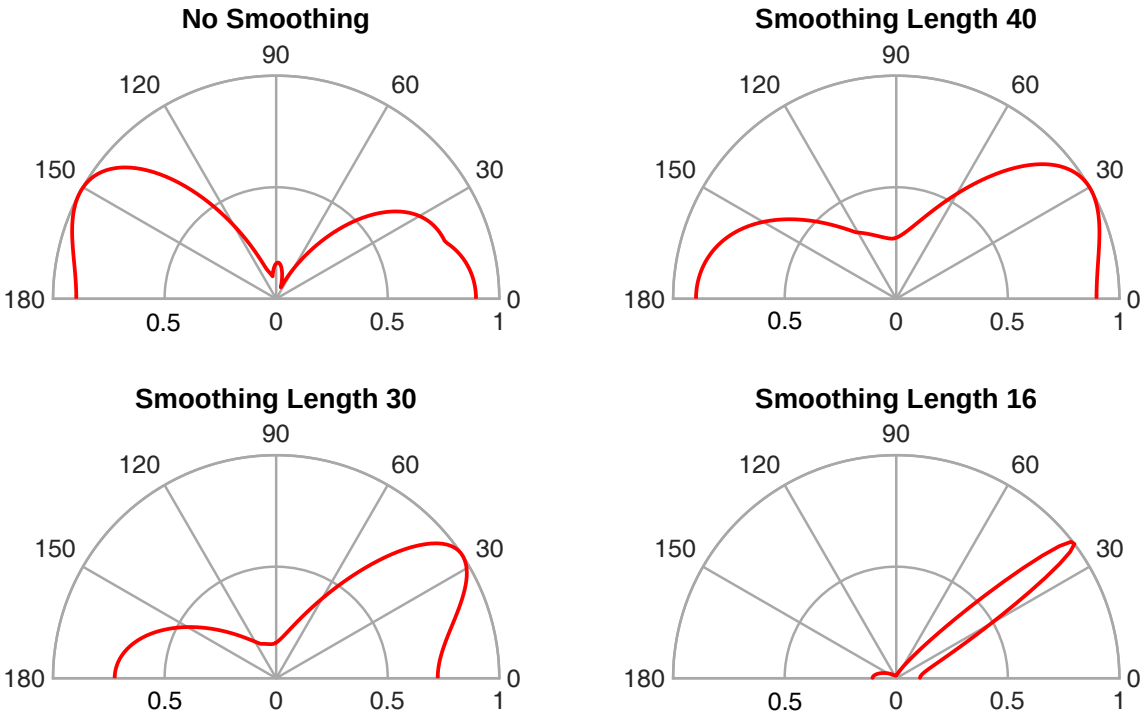

Figure 4.7: Optimal smoothing length selection through AoA spectrum.

To carefully cope with this trade-off problem, we perform a micro-benchmark which computes AoA spectra in a near LoS scenario (so the direct path bearing dominates)

with different smoothing lengths. As observed in Figure 4.7, the smoothing length of 16 ($K' = 8$) shows a good compromise during our experiments and thus is chosen for the performance evaluation section. It is also worth noting that since subcarrier index $k = 0$ is null due to the large direct current (DC), in addition to making smoothing length larger than the number of multipaths indoors (say 10 [110]), we also need to ensure that no partitioned subarray contains $k = 0$ subcarrier, which avoids $2f_\delta$ error for AoA estimation.

Augmented Multi-Packet Smoothing Considering that we only perform the forward-backward smoothing in the frequency domain, to fully acquire the empirical covariance matrix, different packet snapshots are also needed to implement the time-domain averaging, which can be denoted by

$$\mathbf{R}_{mp} = \frac{1}{N_{mp}} \sum_{i=1}^{N_{mp}} \mathbf{R}_{fb}^{i} \tag{4.15}$$

where N_{mp} is the number of multiple CSI packets for sample smoothing. We can observe in Figure 4.8 that the joint AoA and ToF estimation is further refined (the red dots are more centralized than the blue stars) after the process of multi-packet sample smoothing, which is conductive to provide better performance for location fingerprinting.

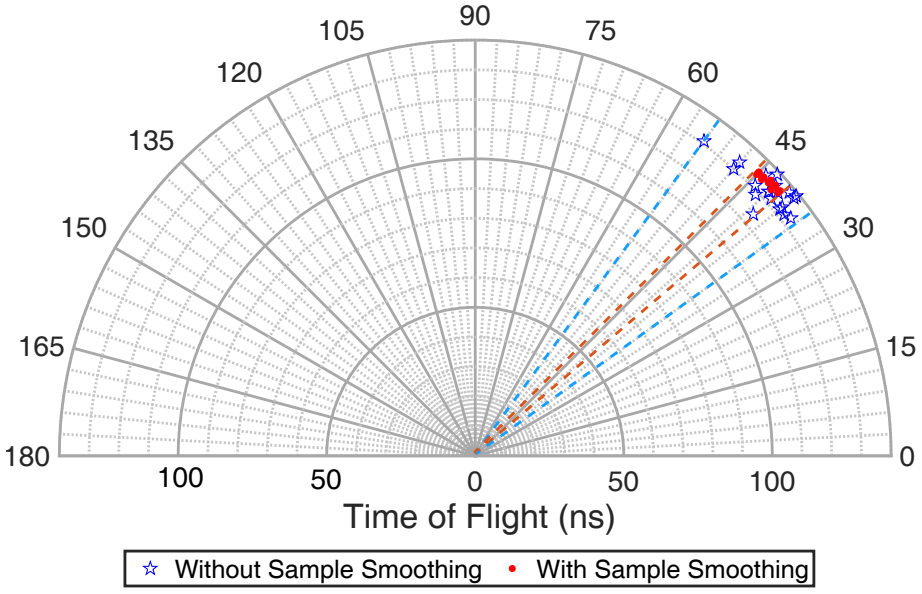

Figure 4.8: The comparison of AoA estimation with and without multi-packet smoothing.

As a result, along with AR entropy fingerprints which are introduced in Section 3.2, the final estimated AoA with the smallest ToF at the m^{th} RP location from the s^{th} AP can be also determined and stored as $(\widehat{\theta}_m^s, \widehat{\tau}_m^s)$ for the following online position estimation. Likewise, the online acquired AoA-ToF fingerprint can be expressed by $(\widehat{\theta}_o^s, \widehat{\tau}_o^s)$.

4.2.3 Online Position Determination

Unlike the previous EntLoc positioning system, the online location determination phase for AngLoc involves additional AoA element. The corresponding similarity metric calculation and final location estimation have been enriched and enhanced, which will be systematically discussed in the sequel.

4.2.3.1 Similarity Metric Calculation

In the online location estimation phase, the mobile target is required to be accurately mapped with the pre-defined fingerprint database. In order to quantify the similarity between the offline stored fingerprints and the online measured CSIs, we manage to independently adopt two simple distance metrics for the respective AR entropy and AoA fingerprints. For amplitude based AR entropy, the Manhattan distance is employed to measure the gap between two vectors through the summation of the absolute differences of their corresponding components. Given the offline and online entropy fingerprints $\widehat{\mathbf{\Phi}}_{\mathbf{H}_m^s}$ and $\widehat{\mathbf{\Phi}}_{\mathbf{G}_o^s}$, the Manhattan distance between them is represented as

$$\mathscr{D}_m^s = \|\widehat{\mathbf{\Phi}}_{\mathbf{H}_m^s} - \widehat{\mathbf{\Phi}}_{\mathbf{G}_o^s}\|_1 = \sum_{i=1}^{R'} \left|\widehat{\phi}_{\mathbf{H}_m^s}^i - \widehat{\phi}_{\mathbf{G}_o^s}^i\right| \tag{4.16}$$

where $\|\cdot\|_1$ denotes the ℓ_1 norm. Moreover, by following the chain rule for Shannon entropy [94], it can be proved that a joint entropy difference for multiple independent variables is equal to the sum of all these variable's entropy differences. Under the S independent AP assumption, we therefore have the Manhattan distance for all available APs as follows.

$$\mathscr{D}_m = \sum_{s=1}^{S} \mathscr{D}_m^s \tag{4.17}$$

For the estimated 2-D AoA and ToF fingerprints, we naturally resort to the simple

Euclidean distance to capture the discrepancy between the offline $(\widehat{\theta}_m^s, \widehat{\tau}_m^s)$ and online $(\widehat{\theta}_o^s, \widehat{\tau}_o^s)$ from all S APs. It can be then defined as

$$\mathcal{D}_m = \sqrt{\sum_{s=1}^{S}((\widehat{\theta}_m^s - \widehat{\theta}_o^s)^2 + (\widehat{\tau}_m^s - \widehat{\tau}_o^s)^2)} \tag{4.18}$$

Thus, the dissimilarities of both AR entropy fingerprint $\mathscr{D}_m$ and AoA fingerprint $\mathcal{D}_m$ for the m^{th} RP location are further obtained for the following target's position determination.

4.2.3.2 Bivariate Kernel Regression

In general, both of the two metrics are fully capable of concisely reflecting the spatial proximity between the offline learned traits at the m^{th} RP and the online measurements from an uncharted position. For the design of AngLoc, the remaining location estimation process consists of two main steps. First, by adopting the classical kNN theory, we can claim M_c out of M RP locations which signify M_c smallest AR entropy differences among $\{\mathscr{D}_m\}_{1\leq m\leq M}$. Then, a novel bivariate kernel regression scheme is further proposed to infer the final target's location by exploiting the distance based kernel function and the selected set of M_c reference points. The estimated location $\widehat{\boldsymbol{\ell}}_o$ is expressed by

$$\widehat{\boldsymbol{\ell}}_o = \frac{\sum_{m_c=1}^{M_c} \mathcal{K}_{m_c} \boldsymbol{\ell}_{m_c}}{\sum_{m_c=1}^{M_c} \mathcal{K}_{m_c}} \tag{4.19}$$

where $m_c \in [1, M_c]$ and $\mathcal{K}_{m_c}$ denotes the probability kernel of the m_c^{th} RP location which is obtained by exponentiating and weighting its corresponding entropy and AoA based distances. It can be mathematically presented as follows:

$$\mathcal{K}_{m_c} = w_e \exp(-\rho_e \mathscr{D}_{m_c}) + w_a \exp(-\rho_a \mathcal{D}_{m_c}) \tag{4.20}$$

Here w_e and w_a are the weighting factors for the respective AR entropy and AoA based kernel function and $w_e + w_a = 1$. ρ_e and ρ_a are their corresponding kernel coefficients which are chosen to optimally minimize the fingerprinting error by leave-one-out cross-validation in the offline phase. It is noteworthy that this bivariate kernel $\mathcal{K}_{m_c}$ equals to one if the given two fingerprints are identical and decays to zero as the dissimilarity of two fingerprints increases. Simply put, this bivariate kernel provides a flexible way to naturally

harness the CSI data and therefore makes full use of our probabilistic AR entropy and AoA information, thus leading to an improved localization performance.

The overall performance of our AngLoc fingerprinting system will be evaluated in the following section.

4.3 Performance Evaluation

In this section, we carry out the experimental evaluation of our proposed localization system. We will begin with the experimental setup introduction and the detailed results of localization performance will be discussed in the sequel.

4.3.1 Experimental Setup

1) *Additional Test Environment*: To evaluate the performance of our AngLoc system, the entire experiments are implemented at two different indoor testbeds in CNAM. As exhibited in Figure 3.11, the first testbed is a $15m \times 15m$ laboratory office in a multistorey building, which is comprised of a main corridor alongside several office and meeting rooms. Many desks, chairs, computers and shelves are furnished inside to form a complex indoor radio propagation environment. The second testbed in Figure 4.9 is an ample classroom scenario with an area of around 100 m^2. It lays out less obstacles within the fingerprinting area which presents a relative LoS scenario. It can then serve as a supplementary contrast with testbed #1. As for the implementation time, the CSI databases for these two testbeds were collected and stored in February and July of 2019, respectively.

2) *Hardware Descriptions*: For both testbeds, all the real experiments are conducted on the same commodity-ready off-the-shelf Wi-Fi devices with that used in the previous EntLoc system. To be specific, recall that in Figure 3.12 and Figure 3.13, by tuning into the IEEE 802.11n monitor mode with 5 GHz band, we deploy an HP Elitebook 8530w laptop as the signal transmitter and an Hummingboard Pro (HMB) device as the mobile receiver, both of which are equipped with Intel Wi-Fi Link (IWL) 5300

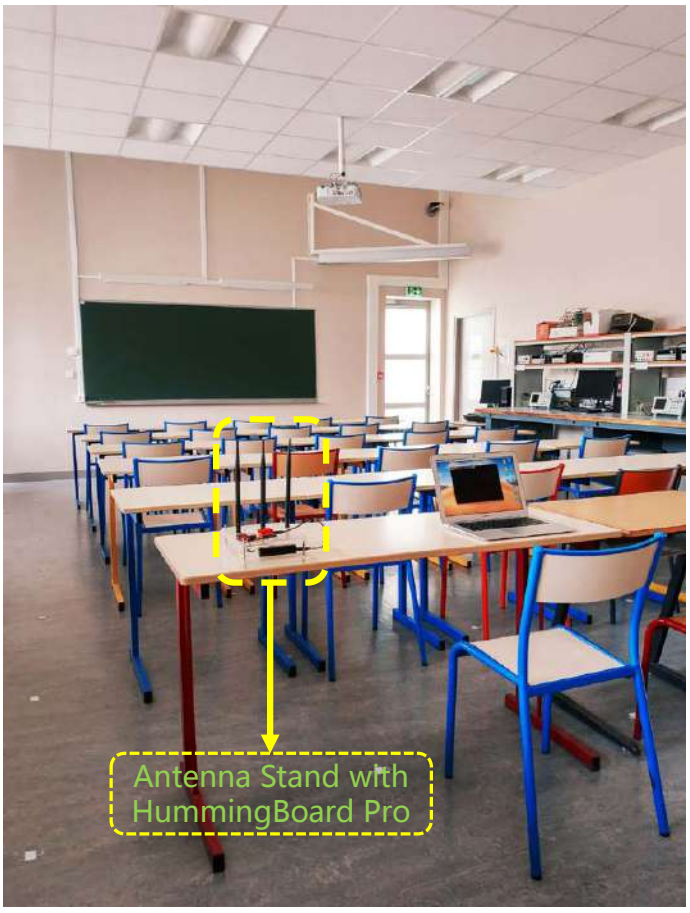

Figure 4.9: CNAM classroom scenario.

NIC and run 64-bit Ubuntu 14.04 OS and Debian 8.0 OS, respectively. In addition, as for the antenna settings, each wireless NIC-compatible device is also capable of installing up to three omni-directional antennas so that the 3×3 MIMO configuration can be supported.

3) *Data Acquisition*: As aforementioned in the beginning, we implement the CSI data collections in both laboratory and classroom environments. Figure 3.14 and Fig. 4.10 display the detailed floor plans and experimental layouts for our laboratory and classroom testbeds, respectively. First of all, for both testbeds, the laptop serves as signal transmitter whose placement is fixed on the table and known a priori. Under packet injection mode, it is designated to intermittently send at the rate of 100 packets per second using only one transmitting antenna. It is notable that such

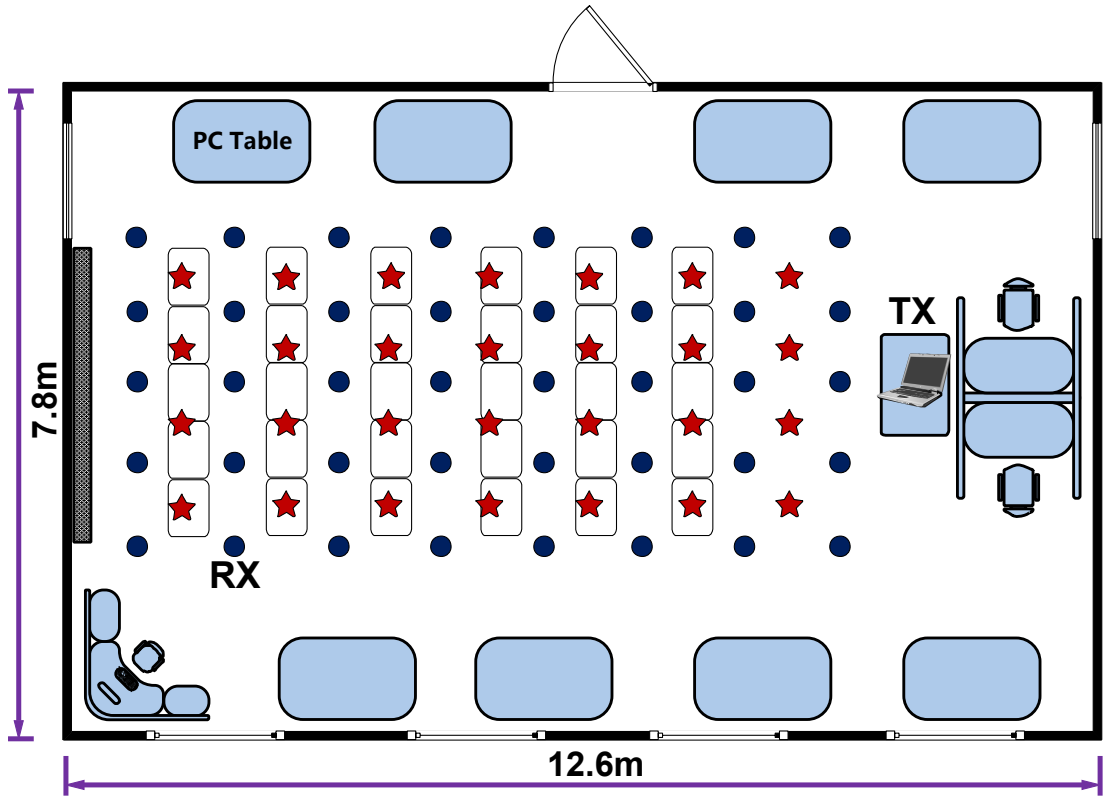

Figure 4.10: The floor plan of our classroom.

antenna setting means to meet the requirement of direct spatial mapping, which can yield CSD-free CSI data. Meanwhile, the localization accuracy can be also guaranteed with the lowest computational cost. For the two experimental layouts, the blue dots shown in Figure 3.14 and Figure 4.10 denote the 70(40) training RP locations with one meter spacing and the 30(28) testing positions are marked as red stars. During the offline training phase, roughly 5000 CSI packets are collected and stored by the lightweight HMB at each reference point to build up the raw CSI radio map. In the online phase, we proceed to move this HMB receiver among all the testing locations to acquire the same size of CSI packets for the localization purpose. Moreover, every receiver end is operated at the same height, constructing a simple 2-D platform for the precise indoor position estimation.

4) *Benchmarks and Performance Metrics*: In this section, we establish the whole benchmark program for the performance evaluation of our AngLoc system, which is com-

pared with aforementioned systems like Horus [28], FIFS [29] and PinLoc [30]. We also compare it with our previously proposed EntLoc system [34], which only exploits the CSI amplitude based entropy metric for indoor fingerprint localization. Besides, considering that the original PinLoc system conduct the war-driving procedure in a set of predefined $1m \times 1m$ grids, known as spots, in order to provide a fair comparison, we modify PinLoc to use the same training set that we use in the proposed AngLoc system. Particularly, for AoA accuracy evaluation, we take SpotFi [20] as the comparative rival due to its representativeness among recent AoA based indoor positioning systems.

As for the performance metrics, we define the localization error as Euclidean distance between the estimated location and the mobile user's actual position, which is presented as $\|\widehat{\boldsymbol{\ell}}_o - \boldsymbol{\ell}_o\| = \sqrt{(\widehat{x}_o - x_o)^2 + (\widehat{y}_o - y_o)^2}$. When there are N_a testing locations, we evaluate the localization performance by using the Mean Error (ME) metric which can be calculated as

$$ME = \frac{1}{N_a} \sum_{i=1}^{N_a} \sqrt{(\widehat{x}_i - x_i)^2 + (\widehat{y}_i - y_i)^2} \tag{4.21}$$

where (x_i, y_i) and $(\widehat{x}_i, \widehat{y}_i)$ are the actual and estimated coordinates at the i^{th} testing location, respectively.

4.3.2 Numerical Results

Prior to exhibiting the localization results of our proposed system, we first reveal the effects of different system parameters which play a defining role for our AngLoc's performance. In addition, some other experimental factors will also be evaluated at the end of this section.

4.3.2.1 Impact of Packet Number Selection for Entropy Estimate

For the sake of efficiently implementing our AngLoc positioning system in the practical testbeds, a reasonable number of CSI packets should be first determined to ensure a desired localization performance while maintaining a low computational cost. Since AngLoc

inherits the AR entropy fingerprint from the previous EntLoc system, we then adopt the same scheme of the packet number selection for AR entropy estimation, which is also chosen in the EntLoc system. As shown in Figure 3.24, we hereby choose 50 and fix this packet number for all entropy estimation processes in our AngLoc positioning implementations.

4.3.2.2 Impact of Packet Number Selection for AoA Estimate

Due to the spatial-temporal diversity of CSI measurements, one CSI packet is able to derive the AoA estimate at one time. Likewise, the excess usage of CSI packets increases the unnecessary computational complexity while fewer number of CSIs risks generating more error-prone AoA estimations.

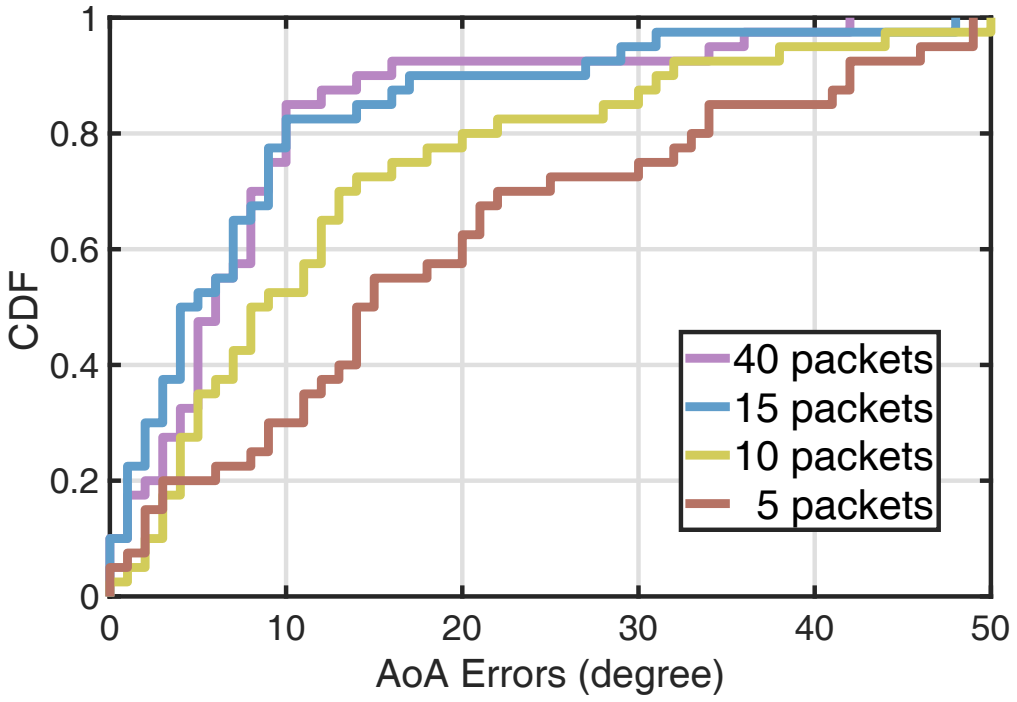

Figure 4.11: AoA estimation errors by using different number of CSI packets.

To address this issue, we devise an accuracy based packet number selection scheme to efficiently conduct AoA calculation. Considering that the multi-packet smoothing is required in our AngLoc system, we begin the testing packet number from 5 packets and extend it to 10, 15 and 40 packets, respectively. In addition, since the LoS-friendly class-

room is more convenient and can provide a clear ground truth (direct path) to compare the AoA estimation errors. It is thus chosen as the experimental environment in this part. As shown in Figure 4.11, we can observe that even with 15 packets, our AngLoc system works well and accurately identifies the true AoA with a mean error of 5 degrees, which shares the similar performance with 40 packets. The underlying explanation lies in the fact that once we determine the first arrival path through the smallest ToF, more CSI packets will not bring further improvement with regard to the AoA estimation accuracy.

4.3.2.3 Impact of Kernel Regression Parameters

Recall that in the online location estimation phase, we first find M_c closest RP locations in accordance with the amplitude's AR entropy. Then, a weighted bivariate kernel regression scheme is proposed to accurately calculate the target's location by exploiting both entropy and AoA informations. As a result, a proper selection of the relevant kernel regression parameters in the offline phase is of great importance in the final localization outcome. As listed in Table 4.1, by leveraging leave-one-out cross-validation, we optimally choose the M_c, weighting factors w_e, w_a and kernel coefficients ρ_e, ρ_a for both testbeds. It is interesting to observe that in the larger and more NLoS laboratory scenario, the AoA-driven RP refining scheme outweighs the AR entropy factor (i.e. $w_a > w_e$), which indicates the fact that the entropy metric tends to bring more ambiguities in more complex environment. On the contrary, the more LoS classroom testbed renders the AR entropy competent enough to differentiate locations since the channel property in such case appears to be more stable.

Table 4.1: Summary of parameters for both testbeds

Parameters	M_c	w_a	w_e	ρ_a	ρ_e
Testbed #1	12	0.57	0.43	0.14	0.23
Testbed #2	8	0.38	0.62	0.33	0.17

Furthermore, we also lay out the training results for choosing parameter M_c in Figure 4.12 and Figure 4.13 from both laboratory and classroom environments. Given a respective

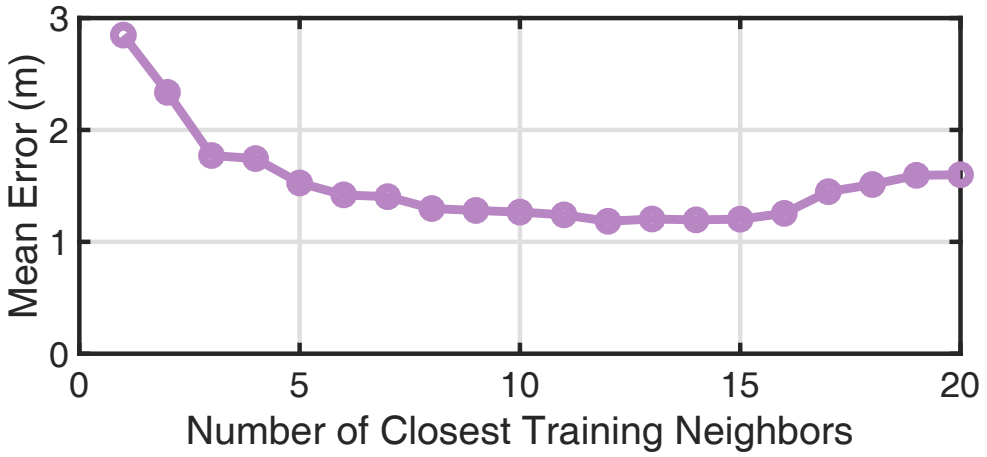

Figure 4.12: Optimal neighbor number selection for laboratory testbed.

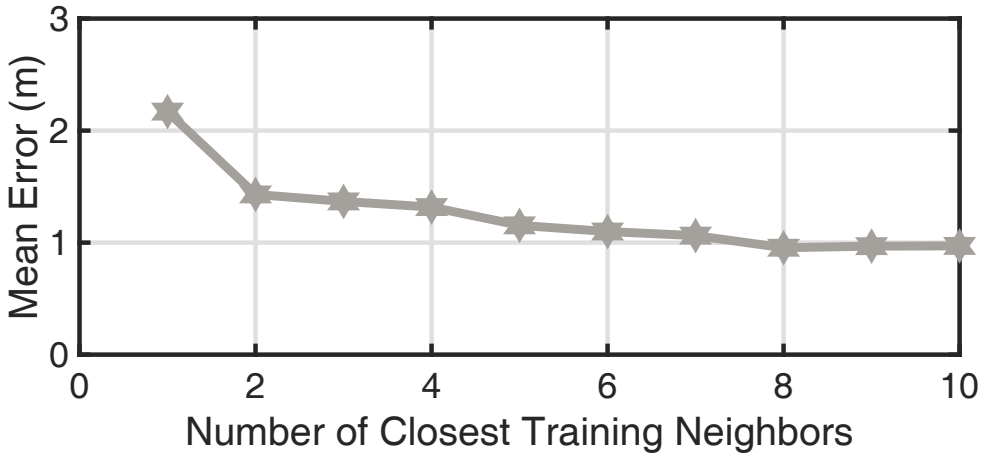

Figure 4.13: Optimal neighbor number selection for classroom testbeds.

range of $[1, 20]$ and $[1, 10]$, we can identify the optimal selection of M_c for both testbeds as 12 and 8, under which the localization mean errors reach minimum. It is fair to state that for the larger and multipath-richer room, a greater number of RP candidates should be required in order to well perform the position determination.

4.3.2.4 Localization Accuracy

In this part, by using the same parameters for all competing IPSs, we then move forward to evaluate the localization performance and present numerical results with relevant discussions.

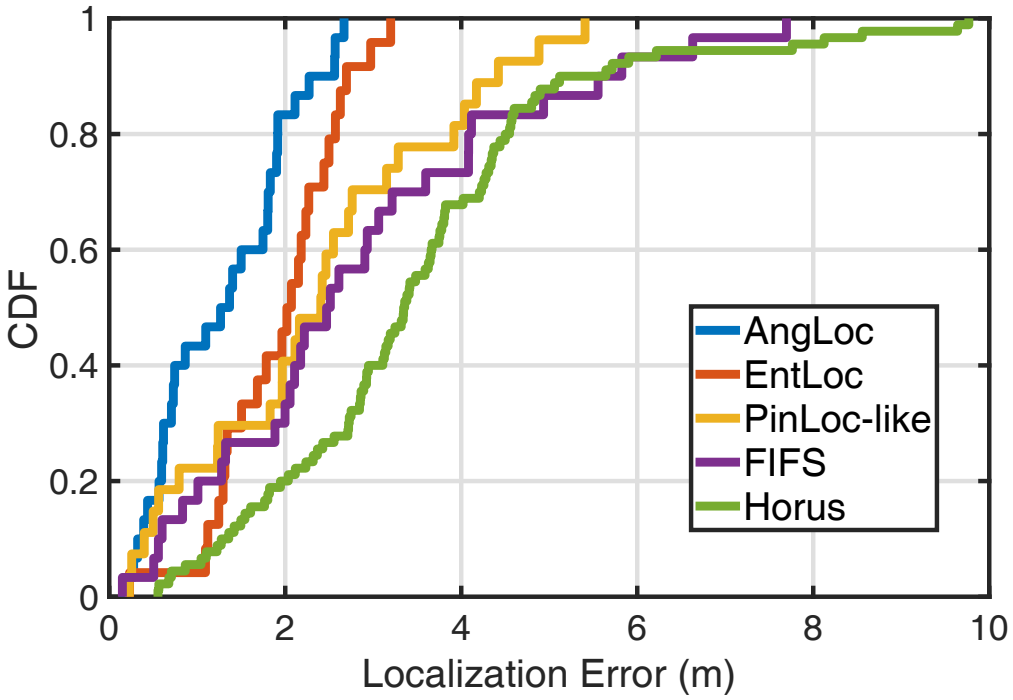

Figure 4.14: Localization accuracy for the laboratory.

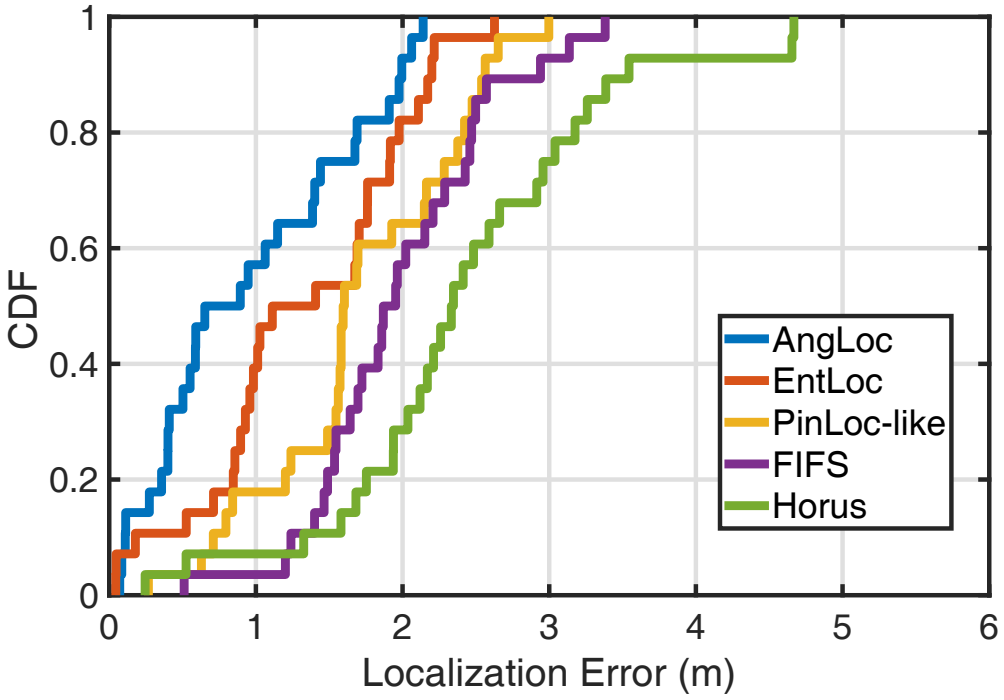

Figure 4.15: Localization accuracy for the classroom.

By virtue of Cumulative Distribution Function (CDF), we first evaluate the localization accuracy of our proposed AngLoc system in comparison with the state-of-the-art. As can be observed in Figure 4.14, for the laboratory environment, our proposed system is able to achieve the 90th percentile error of 2.27m, which outperforms EntLoc, PinLoc-like, FIFS and Horus systems with the same error level of 2.69m, 4.15m, 5.56m and 5.64m, respectively. Similarly, in the classroom scenario, we can notice in Figure 4.15 that AngLoc still precedes other rivals in terms of 90th percentile error. Concretely, it can ensure 90% of test locations have a positioning error under 1.99m, surpassing EntLoc, PinLoc-like, FIFS and Horus systems with the same error percentage of 82.1%, 64.3%, 57.1% and 28.6%, respectively.

Moreover, since the classroom environment is relatively smaller and exposes more LoS radio propagation than the laboratory testbed, a superior localization performance is expected under the same conditions. We further display the mean error bar plot in Figure 4.16 to provide an intuitive comparison within the five candidate systems. As expected,

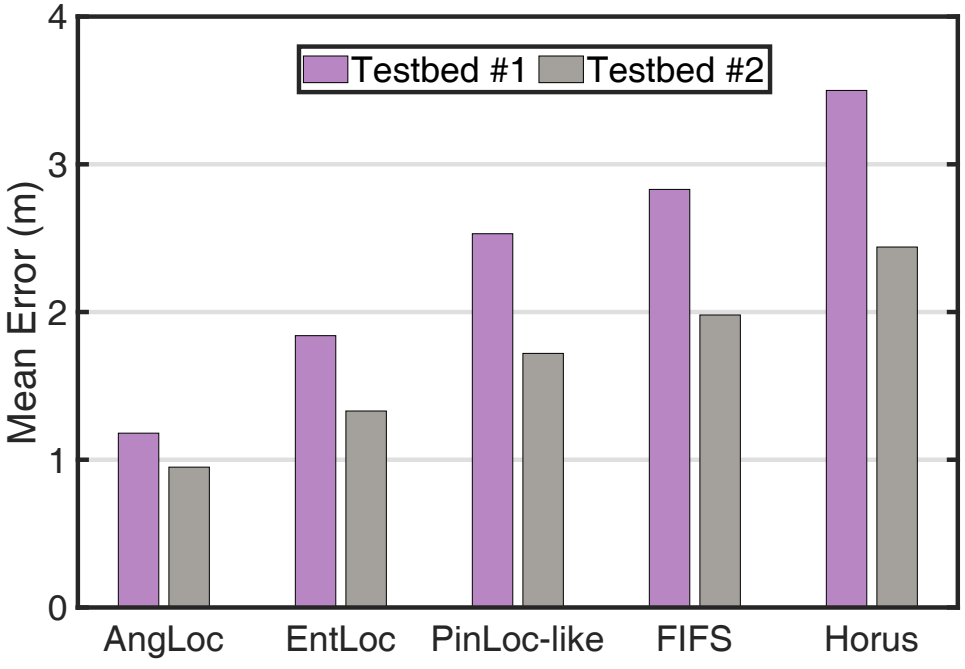

Figure 4.16: Bar plot of localization mean error comparison for both testbeds.

our proposed AngLoc system shows a mean error of 1.18m in the lab and 0.95m in the classroom, which even achieves the decimeter-level localization accuracy, outperforming other counterparts in both testbeds. Meanwhile, for all the competing IPSs, we can also observe that the mean error performance in the classroom is generally better than that in the laboratory scenario, which further validates our previous assumption.

Table 4.2: Localization accuracy for the laboratory scenario

Methods	Max. err.	Min. err.	Mean err.	Acc. at 90%
AngLoc	2.67m	0.16m	1.18m	2.27m
EntLoc	3.20m	0.23m	1.84m	2.69m
PinLoc-like	5.85m	0.46m	2.53m	4.15m
FIFS	7.70m	0.15m	2.83m	5.56m
Horus	9.77m	0.55m	3.50m	5.64m

Table 4.3: Localization accuracy for the classroom scenario

Methods	Max. err.	Min. err.	Mean err.	Acc. at 90%
AngLoc	2.14m	0.07m	0.95m	1.99m
EntLoc	2.62m	0.04m	1.33m	2.20m
PinLoc-like	2.99m	0.27m	1.72m	2.56m
FIFS	3.38m	0.51m	1.98m	2.94m
Horus	4.67m	0.24m	2.44m	3.54m

In order to provide an in-depth and comprehensive comparison for these localization systems, we also enumerate the respective maximum error (Max. err.), minimum error (Min. err.), mean error (Mean err.) and the 90th percentile accuracy (Acc. at 90%) in Table 4.2 and Table 4.3 for the laboratory and classroom, respectively. As can be observed, apart from the minimum error, our AngLoc system broadly dominates the general accuracy evaluation for the maximum error, mean error and 90th percentile accuracy. When it comes to the particular minimum error, AngLoc only falls behind FIFS and EntLoc with 0.01m and 0.03m in the respective testbed #1 and #2, which can be reasonably neglected in

both realistic indoor environments.

4.3.2.5 AoA Estimation Accuracy in LoS Condition

In comparison with our previous EntLoc system, the most productive advancement for AngLoc is that CSI phase based AoA information is organically combined to facilitate the improvement of localization performance. Since one of SpotFi's key insights is to identify the direct path AoA for geometric mapping, even in strong NLoS case, it still needs multiple APs to achieve this through a likelihood scheme. In contrast, the inherent difference of our AngLoc is that the physical direct path AoA is not necessary for fingerprinting as long as the test target's AoA reading (i.e. the first arrival path) is similar with those of its neighboring RP locations. In order to create a fair competition, we only compare the AoA estimation errors with SpotFi under the LoS condition. For the NLoS scenario, we design a different evaluation mechanism for the comparison purpose, which will be discussed in the next part.

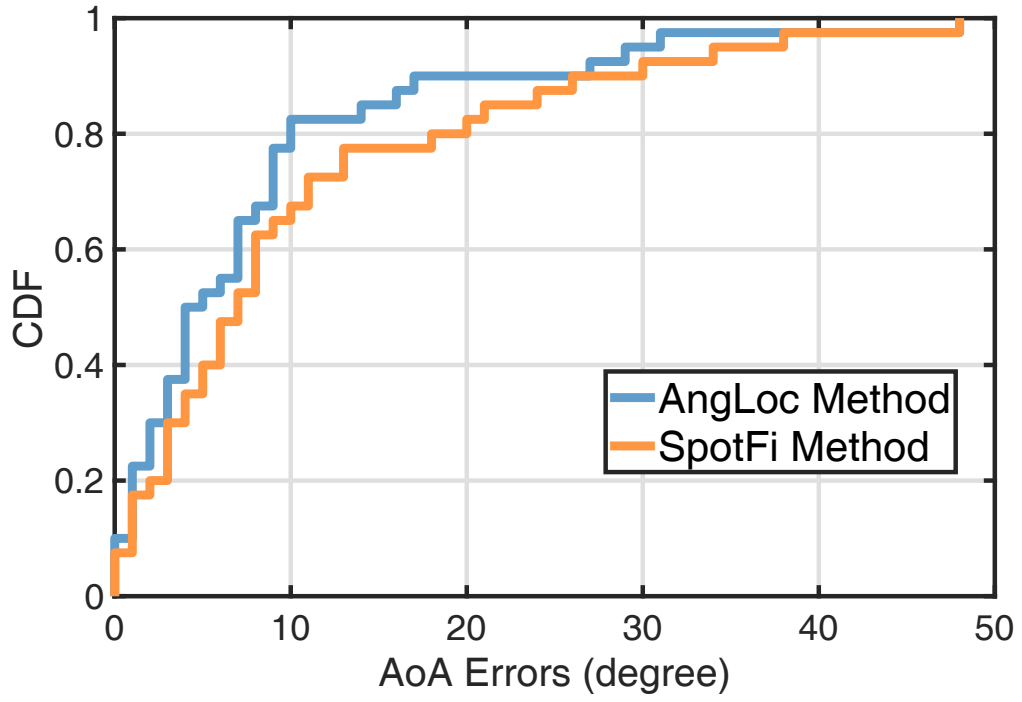

Figure 4.17: AoA estimation errors in LoS condition.

In practice, for the LoS classroom illustrated in Figure 4.10, by applying our AngLoc's enhanced AoA estimation approach as well as the SpotFi's method, we record the AoA readings at all 40 RP locations and compare them with their corresponding ground truth. Here it is worth mentioning that after obtaining several AoA-ToF estimates (clusters) from multiple CSI packets, SpotFi declares the direct path AoA from the cluster with the highest likelihood value. For a fair comparison, we modify the last part of SpotFi to determine the AoA from the first arrival path, which is exactly what we adopt in the AngLoc system. As shown in Figure 4.17, our AngLoc's AoA estimation method can yield the 90th percentile error of 17 degrees, outperforming SpotFi's 26 degrees error in the LoS condition. The total gain of nearly 10 degrees validates the superior performance of our super-resolution JADE-MUSIC algorithm.

4.3.2.6 Impact of AoA Proximity in NLoS Condition

For NLoS environment such as the laboratory shown in Figure 3.14, we design and implement a dedicated experiment to manifest the AoA based fingerprinting feasibility of our AngLoc system. Specifically, we first choose 20 test locations which are in the obvious NLoS conditions from the transmitter. Each of them is surrounded by four predefined RPs. After acquiring the AoA estimates from all these test positions and their neighboring RP locations, we then calculate the AoA differences between each test location and its corresponding four RPs in the vicinity. As displayed in Figure 4.18, compared with SpotFi's method, the box plot shows that our AngLoc's AoA estimation method is capable of deriving the overall lower level of AoA differences with the four RP neighbors, which nicely indicates the similar AoA estimations around the neighboring locations. This advantage further promotes our AngLoc-derived AoA to be a well-qualified position fingerprint for the accurate indoor location determination.

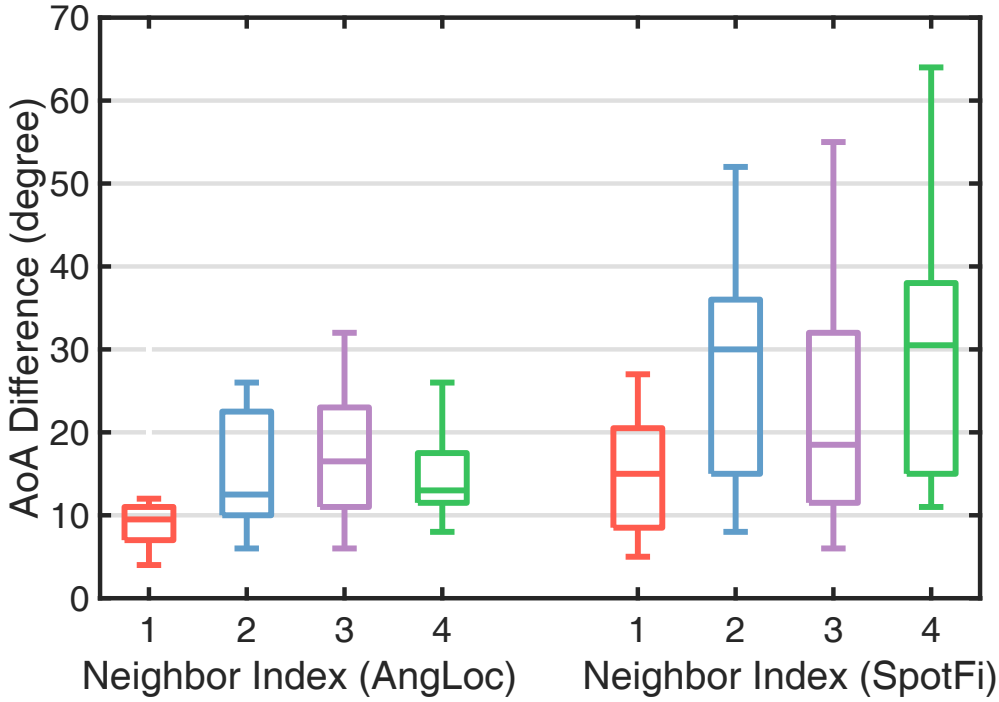

Figure 4.18: The box plot for AoA differences between 20 test locations and their corresponding 4 neighboring RP locations.

4.4 Discussions

In this section, we discuss several unsolved issues in this chapter and propose some possible solutions, which could further enhance the performance of our proposed AngLoc localization system.

4.4.1 Device Orientation Calibration

During the fingerprint site survey, we frequently move the HummingBoard embedded antenna stand among all the RP locations to collect CSI data. In principle, to achieve preferable AoA estimations, one should always maintain the same device orientation when moving the antenna stand from place to place. Otherwise, it may incur additional manual operational error for AoA estimates. To address this potential problem, the commodity smart robot can be leveraged in our future work, by which we can plan the moving path in

advance and fix the device orientation automatically, thus further improving AoA based location fingerprinting accuracy.

4.4.2 Alternative Hardware Implementation

As aforementioned in last Section, our entire experimental framework is established on the basis of commodity wireless IWL 5300 NIC chipset, which provides IEEE 802.11n CSI in a format of 30 subcarrier groups for both 20 MHz and 40 MHz bandwidth. In practice, this sets the limitation for some CSI based applications which demand higher resolution of CSI subcarriers. Such examples include human activity recognition [112], indoor distance ranging [113] and so forth. Recently, some other CSI tools like Atheros CSI tool [26] is getting prevalent in the academic domain due to its non-grouping and non-compressed CSI reporting. Unlike Intel's 5300 NIC, the Qualcomm Atheros NIC chipset is able to report CSI value for each subcarrier, i.e., 56 subcarriers for 20MHz channel and 114 subcarriers for a 40MHz channel. Furthermore, it can also display detailed payload records and retrieve rich status information about the received packet. These additional CSI information can be of great value to help further enhance the localization performance of our AngLoc fingerprinting system.

4.5 Summary

In this chapter, we presented AngLoc, an AoA-aware probabilistic indoor location fingerprinting system using CSI information. In AngLoc, a tap filtering scheme was first proposed to remove the noisy component in raw CSI measurements. Meanwhile, for achieving accurate AoA estimation, we employed several phase calibration techniques to further compensate CSI phase errors. In the offline phase, we adopted AR modeling entropy as the amplitude based fingerprint since it captures the most informative statistical information of CSI amplitude while maintaining a simple structure. In addition, an enhanced JADE-MUSIC algorithm was leveraged to derive AoA estimates as the CSI phase based fingerprint. A robust radio map containing both CSI amplitude and phase information is then readily constructed. In the online phase, for a mobile target, we first narrowed

down the candidate RP locations by finding RPs with the smallest AR entropy differences. A novel bivariate kernel regression method was then adopted to precisely infer the target's location. In comparison with our previous EntLoc system, experimental results from the lightweight HummingBoard device showed a superior localization performance of our proposed AngLoc system with an average accuracy improvement of 35.9% and 28.6% in both laboratory and classroom testbeds. Additionally, we also examined the impacts of several parameters on AngLoc's performance in different indoor scenarios, which empowers us with deepening insights to efficiently and productively conduct our indoor location fingerprinting.

Chapter 5

Conclusions and Future Works

Contents

5.1 Dissertation Conclusions

Due to the economical deployment beyond existing networks and superior adaptivity to the sophisticated indoor environment, fingerprint based localization, represented by Wi-Fi fingerprinting, has attracted much attention in recent academic and industrial trials. In this dissertation, we demonstrate the feasibility of exploiting the PHY layer channel state information available on commodity Wi-Fi infrastructure to boost the capabilities of accurate indoor position determination. On the ground of designing effective location fingerprinting systems, we summarize this thesis in the following.

First, due to the presence of channel bandwidth limitation and unintentional device noise, we design a power based tap filtering scheme to largely mitigate the CSI measurement noise. Specifically, we seek the solution in the more intuitive time domain channel impulse response by converting CFR via IFFT and analyze the resolvable time taps. Through a power based thresholding scheme, we experimentally unveil the most multipath-informative, or location-dependent CIR taps. By removing the irrelevant noisy components, we are able to achieve a more robust probabilistic fingerprint performance while retaining the desired accuracy. Additionally, we also dive into some deep-rooted CSI phase error issues. As the sanitized or compensated CSI phase information is of critical importance for the accurate ranging and direction estimation, we manage to leverage several phase calibration techniques to acquire adequate and reliable CSI measurements, which lays a solid foundation for the upcoming location fingerprinting implementation.

Second, in order to exploit the probabilistic inference of the complex indoor wireless channel properties, we experimentally validate the infeasibility of traditional channel statistic based on the Gaussian assumption and resort to the AR modeling based entropy metric, which shares the structural simplicity with RSS while embodying the rich statistical channel information. On this basis, we proposed EntLoc, an AR entropy of CSI amplitude based fingerprint localization system using commercial off-the-shelf Wi-Fi device. Through extensive experiments conducted in a typical laboratory office scenario, EntLoc demonstrated a superior localization performance with an average accuracy improvement of 27.3%, 34.9% and 47.4%, when compared with the state-of-the-art PinLoc,

FIFS and Horus system, respectively. We envision this work as an early step towards a generic, pervasive and finer-grained CSI location fingerprinting framework in the complex indoor environments.

Third, on top of the amenable EntLoc positioning system, which only harnesses the CSI amplitude information, we further prototype AngLoc, an upgraded location fingerprinting system involving CSI phase information. It is capable of unleashing the complete location-aware potentials by employing additional AoA based fingerprint. To be specific, since the intricate indoor environments can breed similar AR entropy based signatures among certain predefined reference points, which may be randomly distributed in the area of interest. It may mightily tamper the location estimation accuracy when some of the remote RP candidates are falsely involved. The geometric nature of AoA based fingerprint, from another perspective, complementarily helps to rule out these error-prone RPs and further improve the location fingerprinting accuracy. In comparison with EntLoc, the experimental results of our proposed AngLoc from both laboratory and classroom testbeds validate its improved positioning performance with the mean error reduction of 35.9% and 28.6%, respectively.

Last but not least, the pursuit towards the easy fingerprinting implementation never gets tired. Throughout the entire practical study of the CSI based indoor positioning, we gradually manage to develop the more lightweight and feasible CSI data acquisition platform based on the HummingBoard Pro embedded system. It tremendously facilitates our location site survey process and enables us with insightful and bold visions to shed light on some more complex indoor wireless sensing applications in the future research.

5.2 Perspectives for Future Works

Despite the increasing research interest in recent years, wireless indoor location fingerprinting is still in its infancy. This thesis mainly focuses on leveraging channels state information on the commodity Wi-Fi infrastructure to improve the accuracy of the probabilistic localization systems. Herein we also point out some possible future research directions.

- *Machine Learning based Feature Extraction*: Depending on the indoor area of interest, the amount and size of measurements recorded at all the reference points could be incredibly huge. Traditional signal processing approaches turn to be highly ineligible. Under such circumstance, we may resort to the prevalent data-driven machine learning techniques such as Convolutional Neural Network (CNN) [114, 107]. Some representative features hidden in the acquired CSI measurements can be extracted and exploited to match against the stored fingerprint database and finally infer the target's physical position.

- *Crowdsourcing based Radio Map Updating*: In fingerprint based localization systems, the offline database is often obtained through site survey, where a professional surveyor walks around the site to measure signal signatures at all RP positions. Since signals may evolve over time, this survey has to be conducted frequently to maintain a desired performance. This is laborious, time-consuming and costly [115]. Therefore, we can also consider CSI based fingerprinting crowdsourcing scheme by using Bayesian Compressive Sensing (BCS) [116] or sparse Bayesian learning [117, 118] to efficiently update the database and further reduce the labor work for the process of the fingerprint database construction.

- *CSI Temporal Variation Exploitation*: Different from the last perspective which addresses the signal temporal dynamics by crowdsourcing based updating, a promising alternative for the location fingerprinting can treat this issue from two aspects. For small-scale time variations (normally in one day), a threshold based decision-making scheme [119] can be leveraged to decide whether the dissimilarity of two signatures are due to the location difference or just the normal temporal dynamics at the same site. For the large-scale temporal dynamics (e.g. days or weeks), channel response-based signatures tend to be in distinct states. Therefore, these large-scale temporal dynamics can be modeled as a Markov chain in practice [120], which can be properly exploited to pinpoint the target's location.

- *Multi-target Simultaneous Localization*: One major limitation of fingerprint-based techniques is that the training phase consumes a significant amount of time and

effort. This situation is particularly true when we scale our system to simultaneously identifying multiple targets, since the training overhead increases exponentially with the combination of all subjects. In the context of device-based localization system, RF propagation tool [121] and the approach in [122] can be applied to ease the effort of radio map construction, thus promoting the commercial practicability of the promising indoor location-aware industry.

Bibliography

[1] A. Küpper, *Location-Based Services: Fundamentals and Operation.* John Wiley & Sons, 2005.

[2] J. Schiller and A. Voisard, *Location-Based Services.* Elsevier, 2004.

[3] B. Rao and L. Minakakis, "Evolution of Mobile Location-Based Services," *Communications of the ACM*, vol. 46, no. 12, pp. 61–65, 2003.

[4] F. Zafari, A. Gkelias, and K. K. Leung, "A Survey of Indoor Localization Systems and Technologies," *IEEE Communications Surveys and Tutorials*, 2019.

[5] J. Xiao, Z. Zhou, Y. Yi, and L. M. Ni, "A Survey on Wireless Indoor Localization from the Device Perspective," *ACM Computing Surveys (CSUR)*, vol. 49, no. 2, p. 25, 2016.

[6] D. Dardari, P. Closas, and P. M. Djurić, "Indoor Tracking: Theory, Methods, and Technologies," *IEEE Transactions on Vehicular Technology*, vol. 64, no. 4, pp. 1263–1278, 2015.

[7] C. Yang and H.-R. Shao, "WiFi-based Indoor Positioning," *IEEE Communications Magazine*, vol. 53, no. 3, pp. 150–157, 2015.

[8] S. He and S.-H. G. Chan, "Wi-Fi Fingerprint-based Indoor Positioning: Recent Advances and Comparisons," *IEEE Communications Surveys and Tutorials*, vol. 18, no. 1, pp. 466–490, 2015.

[9] Y. Ma, G. Zhou, and S. Wang, "WiFi Sensing with Channel State Information: A Survey," *ACM Computing Surveys (CSUR)*, vol. 52, no. 3, p. 46, 2019.

[10] S. Liu, Y. Jiang, and A. Striegel, "Face-to-Face Proximity Estimation using Bluetooth on Smart Phones," *IEEE Transactions on Mobile Computing*, vol. 13, no. 4, pp. 811–823, 2013.

[11] L. M. Ni, Y. Liu, Y. C. Lau, and A. P. Patil, "LANDMARC: Indoor Location Sensing using Active RFID," in *Proceedings of the First IEEE International Conference on Pervasive Computing and Communications (PerCom)*, 2003, pp. 407–415.

[12] B. Kempke, P. Pannuto, B. Campbell, and P. Dutta, "SurePoint: Exploiting Ultra Wideband Flooding and Diversity to Provide Robust, Scalable, High-fidelity Indoor Localization," in *Proceedings of the 14th ACM Conference on Embedded Network Sensor Systems CD-ROM*, 2016, pp. 137–149.

[13] R. Want, A. Hopper, V. Falcao, and J. Gibbons, "The Active Badge Location System," *ACM Transactions on Information Systems (TOIS)*, vol. 10, no. 1, pp. 91–102, 1992.

[14] P. H. Pathak, X. Feng, P. Hu, and P. Mohapatra, "Visible Light Communication, Networking and Sensing: A Survey, Potential and Challenges," *IEEE Communications Surveys and Tutorials*, vol. 17, no. 4, pp. 2047–2077, 2015.

[15] S. S. Torkestani, S. Sahuguede, A. Julien-Vergonjanne, and J.-P. Cances, "Indoor Optical Wireless System Dedicated to Healthcare Application in A Hospital," *IET Communications*, vol. 6, no. 5, pp. 541–547, 2012.

[16] A. Ward, A. Jones, and A. Hopper, "A New Location Technique for the Active Office," *IEEE Personal Communications*, vol. 4, no. 5, pp. 42–47, 1997.

[17] Y. Shu, C. Bo, G. Shen, C. Zhao, L. Li, and F. Zhao, "Magicol: Indoor Localization using Pervasive Magnetic Field and Opportunistic WiFi Sensing," *IEEE Journal on Selected Areas in Communications*, vol. 33, no. 7, pp. 1443–1457, 2015.

[18] Z. Yang, Z. Zhou, and Y. Liu, "From RSSI to CSI: Indoor Localization via Channel Response," *ACM Computing Surveys (CSUR)*, vol. 46, no. 2, p. 25, 2013.

[19] N. Tadayon, M. T. Rahman, S. Han, S. Valaee, and W. Yu, "Decimeter Ranging with Channel State Information," *IEEE Transactions on Wireless Communications*, 2019.

[20] M. Kotaru, K. Joshi, D. Bharadia, and S. Katti, "Spotfi: Decimeter Level Localization using WiFi," *ACM SIGCOMM Computer Communication Review*, vol. 45, no. 4, pp. 269–282, 2015.

[21] B. Wang, Q. Xu, C. Chen, F. Zhang, and K. R. Liu, "The Promise of Radio Analytics: A Future Paradigm of Wireless Positioning, Tracking, and Sensing," *IEEE Signal Processing Magazine*, vol. 35, no. 3, pp. 59–80, 2018.

[22] A. M. Haimovich, R. S. Blum, and L. J. Cimini, "MIMO Radar with Widely Separated Antennas," *IEEE Signal Processing Magazine*, vol. 25, no. 1, pp. 116–129, 2007.

[23] R. Boyer, "Performance Bounds and Angular Resolution Limit for the Moving Colocated MIMO Radar," *IEEE Transactions on Signal Processing*, vol. 59, no. 4, pp. 1539–1552, 2010.

[24] S. B. Weinstein, "The History of Orthogonal Frequency Division Multiplexing [History of Communications]," *IEEE Communications Magazine*, vol. 47, no. 11, pp. 26–35, 2009.

[25] D. Halperin, W. Hu, A. Sheth, and D. Wetherall, "Tool Release: Gathering 802.11 n Traces with Channel State Information," *ACM SIGCOMM Computer Communication Review*, vol. 41, no. 1, pp. 53–53, 2011.

[26] Y. Xie, Z. Li, and M. Li, "Precise Power Delay Profiling with Commodity Wi-Fi," *IEEE Transactions on Mobile Computing*, vol. 18, no. 6, pp. 1342–1355, 2018.

[27] N. Alsindi, Z. Chaloupka, N. AlKhanbashi, and J. Aweya, "An Empirical Evaluation of A Probabilistic RF Signature for WLAN Location Fingerprinting," *IEEE Transactions on Wireless Communications*, vol. 13, no. 6, pp. 3257–3268, 2014.

[28] M. Youssef and A. Agrawala, "The Horus WLAN Location Determination System," in *Proceedings of the 3rd International Conference on Mobile Systems, Applications and Services.* ACM, 2005, pp. 205–218.

[29] J. Xiao, K. Wu, Y. Yi, and L. M. Ni, "FIFS: Fine-grained Indoor Fingerprinting System," in *Proceedings of the 21st International Conference on Computer Communications and Networks (ICCCN).* IEEE, 2012, pp. 1–7.

[30] S. Sen, B. Radunovic, R. R. Choudhury, and T. Minka, "You are Facing the Mona Lisa: Spot Localization using PHY Layer Information," in *Proceedings of the 10th International Conference on Mobile Systems, Applications and Services.* ACM, 2012, pp. 183–196.

[31] Z. Zhou, Z. Yang, C. Wu, L. Shangguan, and Y. Liu, "Omnidirectional Coverage for Device-free Passive Human Detection," *IEEE Transactions on Parallel and Distributed Systems*, vol. 25, no. 7, pp. 1819–1829, 2013.

[32] P. Mirowski, H. Steck, P. Whiting, R. Palaniappan, M. MacDonald, and T. K. Ho, "KL-Divergence Kernel Regression for Non-Gaussian Fingerprint based Localization," in *Proceedings of IEEE International Conference on Indoor Positioning and Indoor Navigation.* IEEE, 2011, pp. 1–10.

[33] L. Chen, I. Ahriz, D. Le Ruyet, and H. Sun, "Probabilistic Indoor Position Determination via Channel Impulse Response," in *Proceedings of the 29th Annual International Symposium on Personal, Indoor and Mobile Radio Communications (PIMRC).* IEEE, 2018, pp. 829–834.

[34] L. Chen, I. Ahriz, and D. Le Ruyet, "CSI-based Probabilistic Indoor Position Determination: An Entropy Solution," *IEEE Access*, 2019.

[35] C. E. Shannon, "A Mathematical Theory of Communication," *Bell System Technical Journal*, vol. 27, no. 3, pp. 379–423, 1948.

[36] J.-F. Bercher and C. Vignat, "Estimating the Entropy of A Signal with Applications," *IEEE Transactions on Signal Processing*, vol. 48, no. 6, pp. 1687–1694, 2000.

[37] P. Stoica, R. L. Moses *et al.*, *Spectral Analysis of Signals*. Pearson Prentice Hall Upper Saddle River, NJ, 2005.

[38] S. Kay, "Model-based Probability Density Function Estimation," *IEEE Signal Processing Letters*, vol. 5, no. 12, pp. 318–320, 1998.

[39] A. F. Molisch, *Wireless Communications*. John Wiley & Sons, 2012, vol. 34.

[40] P. Brémaud, *An Introduction to Probabilistic Modeling*. Springer Science & Business Media, 2012.

[41] L. Chen, I. Ahriz, and D. L. Ruyet, "AoA-aware Probabilistic Indoor Location Fingerprinting using Channel State Information," *arXiv preprint arXiv: 1912.10108*, 2019.

[42] R. Schmidt, "Multiple Emitter Location and Signal Parameter Estimation," *IEEE Transactions on Antennas and Propagation*, vol. 34, no. 3, pp. 276–280, 1986.

[43] M. C. Vanderveen, C. B. Papadias, and A. Paulraj, "Joint Angle and Delay Estimation (JADE) for Multipath Signals Arriving at An Antenna Array," *IEEE Communications Letters*, vol. 1, no. 1, pp. 12–14, 1997.

[44] R. Boyer and G. Bouleux, "Oblique Projections for Direction-of-Arrival Estimation with Prior Knowledge," *IEEE Transactions on Signal Processing*, vol. 56, no. 4, pp. 1374–1387, 2008.

[45] *HummingBoard Pro*. [Online]. Available: https://shop.solid-run.com/product-tag/hummingboard-pro/

[46] S. Farahani, *ZigBee Wireless Networks and Transceivers*. Newnes, 2011.

[47] W. C. Lee, *Mobile Cellular Telecommunications: Analog and Digital Systems*. McGraw-Hill Professional, 1995.

[48] D. Tse and P. Viswanath, *Fundamentals of Wireless Communication.* Cambridge University Press, 2005.

[49] A. Goldsmith, *Wireless Communications.* Cambridge University Press, 2005.

[50] T. S. Rappaport, *Wireless Communications: Principles and Practice.* Prentice Hall PTR, 1996.

[51] F. Wolf, C. Villien, S. de Rivaz, F. Dehmas, and J.-P. Cances, "Improved Multi-Channel Ranging Precision Bound for Narrowband LPWAN in Multipath Scenarios," in *Proceedings of IEEE Wireless Communications and Networking Conference (WCNC).* IEEE, 2018, pp. 1–6.

[52] S. Gezici, Z. Tian, G. B. Giannakis, H. Kobayashi, A. F. Molisch, H. V. Poor, and Z. Sahinoglu, "Localization via Ultra-Wideband Radios: A Look at Positioning Aspects for Future Sensor Networks," *IEEE Signal Processing Magazine*, vol. 22, no. 4, pp. 70–84, 2005.

[53] "IEEE Standard for Information Technology — Local and Metropolitan Area Networks-Specific Requirements — Part 11: Wireless LAN Medium Access Control (MAC) and Physical Layer (PHY) Specifications — Amendment 5: Enhancements for Higher Throughput," *IEEE 802.11n-2009.*

[54] "IEEE Standard for Information Technology — Telecommunications and Information Exchange Between Systems — Local and Metropolitan Area Networks — Specific Requirements — Part 11: Wireless LAN Medium Access Control (MAC) and Physical Layer (PHY) Specifications — Amendment 4: Enhancements for Very High Throughput for Operation in Bands Below 6 GHz," *IEEE 802.11ac-2013.*

[55] B. T. Fang, "Trilateration and Extension to Global Positioning System Navigation," *Journal of Guidance, Control and Dynamics*, vol. 9, no. 6, pp. 715–717, 1986.

[56] G. Han, J. Jiang, C. Zhang, T. Q. Duong, M. Guizani, and G. K. Karagiannidis, "A Survey on Mobile Anchor Node Assisted Localization in Wireless Sensor Networks," *IEEE Communications Surveys and Tutorials*, vol. 18, no. 3, pp. 2220–2243, 2016.

[57] X. Li, Y. Zhang, K. Xu, G. Fan, and H. Wu, "Research of Localization and Tracking Algorithms based on Wireless Sensor Network," *Journal of Information and Computational Science*, vol. 8, no. 4, pp. 708–715, 2011.

[58] F. Santos and I. Técnico, "Localization in Wireless Sensor Networks," *ACM Journal*, vol. 5, pp. 1–19, 2008.

[59] K. Qian, C. Wu, Z. Yang, Y. Liu, F. He, and T. Xing, "Enabling Contactless Detection of Moving Humans with Dynamic Speeds using CSI," *ACM Transactions on Embedded Computing Systems (TECS)*, vol. 17, no. 2, p. 52, 2018.

[60] H. Abdelnasser, K. A. Harras, and M. Youssef, "UbiBreathe: A Ubiquitous Non-invasive WiFi-based Breathing Estimator," in *Proceedings of the 16th ACM International Symposium on Mobile Ad Hoc Networking and Computing*. ACM, 2015, pp. 277–286.

[61] Y. Chen, W. Dong, Y. Gao, X. Liu, and T. Gu, "Rapid: A Multimodal and Device-free Approach using Noise Estimation for Robust Person Identification," *Proceedings of the ACM on Interactive, Mobile, Wearable and Ubiquitous Technologies*, vol. 1, no. 3, p. 41, 2017.

[62] N. Yu, W. Wang, A. X. Liu, and L. Kong, "QGesture: Quantifying Gesture Distance and Direction with WiFi Signals," *Proceedings of the ACM on Interactive, Mobile, Wearable and Ubiquitous Technologies*, vol. 2, no. 1, p. 51, 2018.

[63] S.-H. Fang, W.-H. Chang, Y. Tsao, H.-C. Shih, and C. Wang, "Channel State Reconstruction using Multilevel Discrete Wavelet Transform for Improved Fingerprinting-based Indoor Localization," *IEEE Sensors Journal*, vol. 16, no. 21, pp. 7784–7791, 2016.

[64] H. Abdelnasser, M. Youssef, and K. A. Harras, "WiGest: A Ubiquitous WiFi-based Gesture Recognition System," in *Proceedings of IEEE Conference on Computer Communications (INFOCOM)*. IEEE, 2015, pp. 1472–1480.

[65] S. Arshad, C. Feng, Y. Liu, Y. Hu, R. Yu, S. Zhou, and H. Li, "Wi-Chase: A WiFi based Human Activity Recognition System for Sensorless Environments," in

Proceedings of the 18th International Symposium on A World of Wireless, Mobile and Multimedia Networks (WoWMoM). IEEE, 2017, pp. 1–6.

[66] R. Zhou, J. Chen, X. Lu, and J. Wu, "CSI Fingerprinting with SVM Regression to Achieve Device-Free Passive Localization," in *Proceedings of the 18th International Symposium on A World of Wireless, Mobile and Multimedia Networks (WoWMoM)*. IEEE, 2017, pp. 1–9.

[67] D. Huang, R. Nandakumar, and S. Gollakota, "Feasibility and Limits of Wi-Fi Imaging," in *Proceedings of the 12th ACM Conference on Embedded Network Sensor Systems*. ACM, 2014, pp. 266–279.

[68] D. Han, S. Jung, M. Lee, and G. Yoon, "Building A Practical Wi-Fi-based Indoor Navigation System," *IEEE Pervasive Computing*, vol. 13, no. 2, pp. 72–79, 2014.

[69] C. Feng, W. S. A. Au, S. Valaee, and Z. Tan, "Received Signal Strength based Indoor Positioning using Compressive Sensing," *IEEE Transactions on Mobile Computing*, vol. 11, no. 12, pp. 1983–1993, 2011.

[70] S. He and S.-H. G. Chan, "SectJunction: Wi-Fi Indoor Localization based on Junction of Signal Sectors," in *Proceedings of IEEE International Conference on Communications (ICC)*. IEEE, 2014, pp. 2605–2610.

[71] C. Chen, Y. Han, Y. Chen, and K. R. Liu, "Indoor Global Positioning System with Centimeter Accuracy using Wi-Fi," *IEEE Signal Processing Magazine*, vol. 33, no. 6, pp. 128–134, 2016.

[72] X. Wang, Y. Liu, Z. Shi, X. Lu, and L. Sun, "A Privacy-Preserving Fuzzy Localization Scheme with CSI Fingerprint," in *Proceedings of IEEE Global Communications Conference (GLOBECOM)*. IEEE, 2015, pp. 1–6.

[73] V. Honkavirta, T. Perala, S. Ali-Loytty, and R. Piché, "A Comparative Survey of WLAN Location Fingerprinting Methods," in *Proceedings of the 6th IEEE Workshop on Positioning, Navigation and Communication*. IEEE, 2009, pp. 243–251.

[74] C.-L. Wu, L.-C. Fu, and F.-L. Lian, "WLAN Location Determination in E-Home via Support Vector Classification," in *Proceedings of IEEE International Conference on Networking, Sensing and Control*, vol. 2. IEEE, 2004, pp. 1026–1031.

[75] G. Nuño-Barrau and J. M. Páez-Borrallo, "A New Location Estimation System for Wireless Networks based on Linear Discriminant Functions and Hidden Markov Models," *EURASIP Journal on Advances in Signal Processing*, vol. 2006, no. 1, p. 068154, 2006.

[76] D. Madigan, E. Einahrawy, R. P. Martin, W.-H. Ju, P. Krishnan, and A. Krishnakumar, "Bayesian Indoor Positioning Systems," in *Proceedings of the 24th Annual Joint Conference of the IEEE Computer and Communications Societies*, vol. 2. IEEE, 2005, pp. 1217–1227.

[77] R. Nandakumar, K. K. Chintalapudi, and V. N. Padmanabhan, "Centaur: Locating Devices in An Office Environment," in *Proceedings of the 18th Annual International Conference on Mobile Computing and Networking*. ACM, 2012, pp. 281–292.

[78] R. W. Ouyang, A. K.-S. Wong, C.-T. Lea, and M. Chiang, "Indoor Location Estimation with Reduced Calibration Exploiting Unlabeled Data via Hybrid Generative/Discriminative Learning," *IEEE Transactions on Mobile Computing*, vol. 11, no. 11, pp. 1613–1626, 2011.

[79] P. Mirowski, P. Whiting, H. Steck, R. Palaniappan, M. MacDonald, D. Hartmann, and T. K. Ho, "Probability Kernel Regression for WiFi Localisation," *Journal of Location Based Services*, vol. 6, no. 2, pp. 81–100, 2012.

[80] B. Ferris, D. Fox, and N. D. Lawrence, "WiFi-SLAM using Gaussian Process Latent Variable Models," in *Proceedings of International Joint Conferences on Artificial Intelligence (IJCAI)*, vol. 7, no. 1, 2007, pp. 2480–2485.

[81] Z. Xiao, H. Wen, A. Markham, and N. Trigoni, "Lightweight Map Matching for Indoor Localisation using Conditional Random Fields," in *Proceedings of the 13th International Symposium on Information Processing in Sensor Networks*. IEEE, 2014, pp. 131–142.

[82] J. Jun, Y. Gu, L. Cheng, B. Lu, J. Sun, T. Zhu, and J. Niu, "Social-Loc: Improving Indoor Localization with Social Sensing," in *Proceedings of the 11th ACM Conference on Embedded Networked Sensor Systems*. ACM, 2013, p. 14.

[83] W. Sun, J. Liu, C. Wu, Z. Yang, X. Zhang, and Y. Liu, "MoLoc: On Distinguishing Fingerprint Twins," in *Proceedings of the 33rd International Conference on Distributed Computing Systems*. IEEE, 2013, pp. 226–235.

[84] P. Bahl and V. N. Padmanabhan, "RADAR: An In-building RF-based User Location and Tracking System," in *Proceedings of the 19th Annual Joint Conference of the IEEE Computer and Communications Societies (INFOCOM)*, vol. 2, March 2000, pp. 775–784 vol.2.

[85] Z. Yang, C. Wu, and Y. Liu, "Locating in Fingerprint Space: Wireless Indoor Localization with Little Human Intervention," in *Proceedings of the 18th Annual International Conference on Mobile Computing and Networking*. ACM, 2012, pp. 269–280.

[86] Z. E. Khatab, A. Hajihoseini, and S. A. Ghorashi, "A Fingerprint Method for Indoor Localization using Autoencoder based Deep Extreme Learning Machine," *IEEE Sensors Letters*, vol. 2, no. 1, pp. 1–4, 2017.

[87] C. Wu, Z. Yang, Z. Zhou, Y. Liu, and M. Liu, "Mitigating Large Errors in WiFi-based Indoor Localization for Smartphones," *IEEE Transactions on Vehicular Technology*, vol. 66, no. 7, pp. 6246–6257, 2016.

[88] Y. Jin, W.-S. Soh, and W.-C. Wong, "Indoor Localization with Channel Impulse Response based Fingerprint and Nonparametric Regression," *IEEE Transactions on Wireless Communications*, vol. 9, no. 3, pp. 1120–1127, 2010.

[89] C. Chen, Y. Chen, Y. Han, H.-Q. Lai, F. Zhang, and K. R. Liu, "Achieving Centimeter-Accuracy Indoor Localization on WiFi Platforms: A Multi-antenna Approach," *IEEE Internet of Things Journal*, vol. 4, no. 1, pp. 122–134, 2016.

[90] Z. Zhou, Z. Yang, C. Wu, L. Shangguan, H. Cai, Y. Liu, and L. M. Ni, "WiFi-based Indoor Line-of-Sight Identification," *IEEE Transactions on Wireless Communications*, vol. 14, no. 11, pp. 6125–6136, 2015.

[91] S. Shi, S. Sigg, L. Chen, and Y. Ji, "Accurate Location Tracking from CSI-based Passive Device-free Probabilistic Fingerprinting," *IEEE Transactions on Vehicular Technology*, vol. 67, no. 6, pp. 5217–5230, 2018.

[92] E. Homayounvala, M. Nabati, R. Shahbazian, S. A. Ghorashi, and V. Moghtadaiee, "A Novel Smartphone Application for Indoor Positioning of Users based on Machine Learning," in *Proceedings of the 2019 ACM International Joint Conference on Pervasive and Ubiquitous Computing and Proceedings of the 2019 ACM International Symposium on Wearable Computers*. ACM, 2019, pp. 430–437.

[93] X. Wang, L. Gao, and S. Mao, "BiLoc: Bi-modal Deep Learning for Indoor Localization with Commodity 5GHz WiFi," *IEEE Access*, vol. 5, pp. 4209–4220, 2017.

[94] T. M. Cover and J. A. Thomas, *Elements of Information Theory*. John Wiley & Sons, 2012.

[95] S. Kay, *Fundamentals of Statistical Signal Processing*. Prentice Hall PTR, 1993.

[96] R. Moddemeijer, "On Estimation of Entropy and Mutual Information of Continuous Distributions," *Signal Processing*, vol. 16, no. 3, pp. 233–248, 1989.

[97] J. C. Correa, "A New Estimator of Entropy," *Communications in Statistics-Theory and Methods*, vol. 24, no. 10, pp. 2439–2449, 1995.

[98] E. Parzen, "On Estimation of A Probability Density Function and Mode," *The Annals of Mathematical Statistics*, vol. 33, no. 3, pp. 1065–1076, 1962.

[99] S. Kay, *Fundamentals of Statistical Signal Processing: Practical Algorithm Development*. Pearson Education, 2013, vol. 3.

[100] Kay, Steven, "Exponentially Embedded Families-New Approaches to Model Order Estimation," *IEEE Transactions on Aerospace and Electronic Systems*, vol. 41, no. 1, pp. 333–345, 2005.

[101] G. U. Yule, "On a Method of Investigating Periodicities Disturbed Series, with Special Reference to Wolfer's Sunspot Numbers," *Philosophical Transactions of the Royal Society of London*, vol. 226, no. 636-646, pp. 267–298, 1927.

[102] G. T. Walker, "On Periodicity in Series of Related Terms," *Proceedings of the Royal Society of London*, vol. 131, no. 818, pp. 518–532, 1931.

[103] E. F. Krause, *Taxicab Geometry: An Adventure in Non-Euclidean Geometry*. Courier Corporation, 1986.

[104] K. Wu, J. Xiao, Y. Yi, M. Gao, and L. M. Ni, "FILA: Fine-Grained Indoor Localization," in *Proceedings of the 31st Annual IEEE International Conference on Computer Communications (INFOCOM)*. IEEE, 2012, pp. 2210–2218.

[105] J. Xiong and K. Jamieson, "ArrayTrack: A Fine-Grained Indoor Location System," in *Proceedings of the 10th USENIX Symposium on Networked Systems Design and Implementation (NSDI)*, 2013, pp. 71–84.

[106] D. Vasisht, S. Kumar, and D. Katabi, "Decimeter-Level Localization with a Single WiFi Access Point," in *Proceedings of the 13th USENIX Symposium on Networked Systems Design and Implementation (NSDI)*, 2016, pp. 165–178.

[107] X. Wang, L. Gao, S. Mao, and S. Pandey, "CSI-based Fingerprinting for Indoor Localization: A Deep Learning Approach," *IEEE Transactions on Vehicular Technology*, vol. 66, no. 1, pp. 763–776, 2016.

[108] Y. Zhuo, H. Zhu, H. Xue, and S. Chang, "Perceiving Accurate CSI Phases with Commodity WiFi Devices," in *Proceedings of IEEE Conference on Computer Communications (INFOCOM)*. IEEE, 2017, pp. 1–9.

[109] Y. Ma, G. Zhou, S. Wang, H. Zhao, and W. Jung, "SignFi: Sign Language Recognition using WiFi," *Proceedings of the ACM on Interactive, Mobile, Wearable and Ubiquitous Technologies*, vol. 2, no. 1, p. 23, 2018.

[110] N. Czink, M. Herdin, H. Özcelik, and E. Bonek, "Number of Multipath Clusters in Indoor MIMO Propagation Environments," *Electronics Letters*, vol. 40, no. 23, pp. 1498–1499, 2004.

[111] S. U. Pillai and B. H. Kwon, "Forward/Backward Spatial Smoothing Techniques for Coherent Signal Identification," *IEEE Transactions on Acoustics, Speech, and Signal Processing*, vol. 37, no. 1, pp. 8–15, 1989.

[112] J. Yang, H. Zou, H. Jiang, and L. Xie, "Device-free Occupant Activity Sensing using WiFi-enabled IoT Devices for Smart Homes," *IEEE Internet of Things Journal*, vol. 5, no. 5, pp. 3991–4002, 2018.

[113] H. Zhu, Y. Zhuo, Q. Liu, and S. Chang, "π-Splicer: Perceiving Accurate CSI Phases with Commodity WiFi Devices," *IEEE Transactions on Mobile Computing*, vol. 17, no. 9, pp. 2155–2165, 2018.

[114] K. P. Murphy, *Machine Learning: A Probabilistic Perspective*. MIT Press, 2012.

[115] B. Wang, Q. Chen, L. T. Yang, and H.-C. Chao, "Indoor Smartphone Localization via Fingerprint Crowdsourcing: Challenges and Approaches," *IEEE Wireless Communications*, vol. 23, no. 3, pp. 82–89, 2016.

[116] B. Yang, S. He, and S.-H. G. Chan, "Updating Wireless Signal Map with Bayesian Compressive Sensing," in *Proceedings of the 19th ACM International Conference on Modeling, Analysis and Simulation of Wireless and Mobile Systems*. ACM, 2016, pp. 310–317.

[117] Z. Zhang and B. D. Rao, "Extension of SBL Algorithms for the Recovery of Block Sparse Signals with Intra-block Correlation," *IEEE Transactions on Signal Processing*, vol. 61, no. 8, pp. 2009–2015, 2013.

[118] L. Chen, I. Ahriz, H. Sun, D. Le Ruyet, and D. Peng, "Source Position Estimation via Subspace based Joint Sparse Recovery," in *Proceedings of the 13th International Conference on Signal Processing (ICSP)*. IEEE, 2016, pp. 149–152.

[119] N. Patwari and S. K. Kasera, "Temporal Link Signature Measurements for Location Distinction," *IEEE Transactions on Mobile Computing*, vol. 10, no. 3, pp. 449–462, 2010.

[120] J. Zhang, M. H. Firooz, N. Patwari, and S. K. Kasera, "Advancing Wireless Link Signatures for Location Distinction," in *Proceedings of the 14th ACM International Conference on Mobile Computing and Networking*. ACM, 2008, pp. 26–37.

[121] M. Scholz, L. Kohout, M. Horne, M. Budde, M. Beigl, and M. A. Youssef, "Device-free Radio-based Low Overhead Identification of Subject Classes," in *Proceedings of the 2nd Workshop on Workshop on Physical Analytics*. ACM, 2015, pp. 1–6.

[122] H. Lim, L. . Kung, J. C. Hou, and H. Luo, "Zero-Configuration, Robust Indoor Localization: Theory and Experimentation," in *Proceedings of the 25th IEEE International Conference on Computer Communications (INFOCOM)*, April 2006, pp. 1–12.

le cnam

Luan CHEN

Enhancing Indoor Location Fingerprinting using Channel State Information

le cnam

Résumé: Grâce au développement rapide des communications sans fil, la localisation par empreinte digitale (LF) a favorisé des services géodépendants considérables dans le domaine de l'Internet des objets. Dans cette thèse, nous avons d'abord proposé le système EntLoc, qui adopte l'entropie de modélisation autorégressive (AR) de l'amplitude des informations d'état de canal (CSI) comme empreinte digitale de localisation. Il partage la simplicité structurelle de la force du signal reçu (RSS) tout en réservant les informations de canal statistique les plus spécifiques à l'emplacement. De plus, un système AngLoc amélioré est également conçu, dont l'empreinte digitale d'angle d'arrivée (AoA) supplémentaire peut être récupérée avec précision de la phase CSI grâce à un algorithme amélioré basé sur le sous-espace, qui sert à éliminer davantage les candidats au point de référence (RP) sujets aux erreurs. Dans la phase LF en ligne, en exploitant à la fois les informations d'amplitude et de phase CSI, un nouveau schéma de régression par noyau bivarié est proposé pour déduire précisément l'emplacement de la cible. Les résultats d'expériences approfondies en intérieur valident la performance de localisation supérieure de notre système proposé par rapport aux approches précédentes.

Mots clés: Localisation indoor, informations des canaux, entropie, traitement du signal du réseau, régression par noyaux.

Abstract: With expeditious development of wireless communications, Location Fingerprinting (LF) has nurtured considerable indoor location based services in the field of Internet of Things. In this thesis, we first proposed EntLoc system, which adopts Autoregressive (AR) modeling entropy of the Channel State Information (CSI) amplitude as location fingerprint. It shares the structural simplicity of the Received Signal Strength (RSS) while reserving the most location-specific statistical channel information. Moreover, an upgraded AngLoc system is further designed, whose additional angle of arrival (AoA) fingerprint can be accurately retrieved from CSI phase through an enhanced subspace based algorithm, which serves to further eliminate the error-prone Reference Point (RP) candidates. In the LF online phase, by exploiting both CSI amplitude and phase information, a novel bivariate kernel regression scheme is proposed to precisely infer the target's location. Results from extensive indoor experiments validate the superior localization performance of our proposed system over previous approaches.

Keywords: Indoor localization, channel state information, entropy, array signal processing, kernel regression.